The Tissue Biology of Inflammasomes

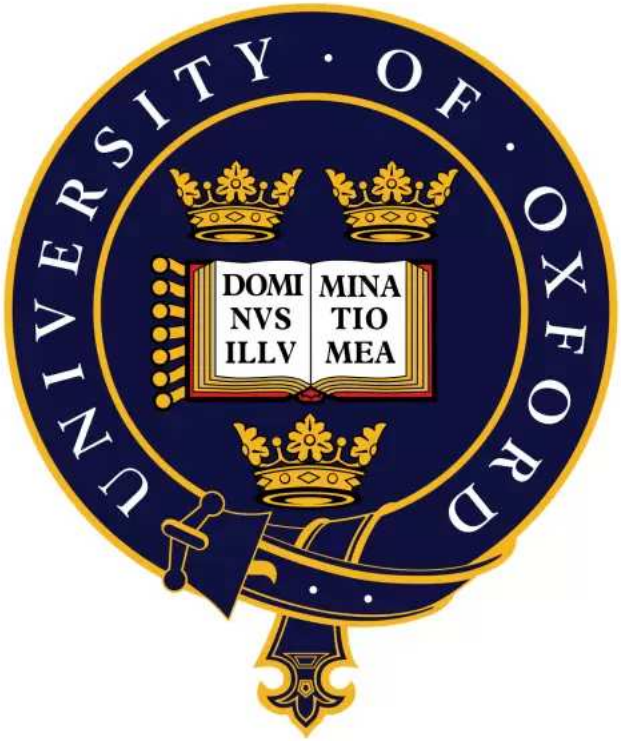

Gabrielle Rose Chappell
Reuben College
University of Oxford

A thesis submitted for the degree of
Doctor of Philosophy
Trinity Term 2025

Acknowledgements

I would like to express immense gratitude for my primary DPhil supervisor, newly minted Professor Jelena Bezbradica Mirkovic, for her unwavering support both academically, professionally, and personally. I feel incredibly fortunate to have been a member of your lab for four years. Under your supervision, I have blossomed as a young scientist and feel so grateful that you took a chance on me after a fateful Zoom call during the middle of COVID. Thank you for supporting me through difficult times and illness, even bringing home cooked food to my flat with Zelya. Thank you for holding space to let me explore different career options. Let's see where my love for science and business takes me next year.

I would like to extend my thanks and well wishes to all present and past members of the Bezbradica-Mirkovic lab. The wonderful people of this lab have shaped me and my DPhil for the better. Special mentions must go to Ada, for being the best partner in crime on the dance floor and in the lab anyone could ask for (special mention also for our rodent themed movie night); Su Qi, for loving coffee and climbing as much as I do and making both infinitely more enjoyable (cheers to more adventures and fewer injuries); Madelon, for being truly my guardian angel in so many ways. From comedy nights and screaming Sabrina Carpenter, to every low moment where you've sat in the trenches, held deep conversations, and looked after me and my family – thank you. Thank you to the beloved "Bezard" group for many silly lunches, pub trips, and the single most eclectic Spotify blend known to human existence. I will truly miss this group of people so much.

I would like to thank my co-supervisors, Professor Chris Buckley and Professor Mark Coles for their helpful discussions and career advice. I would like to thank Professor Kim Midwood and Professor Adam Croft for their support as members of my thesis committee.

To my parents, who have always prioritized my education – I love you both so much. You have inspired me to dream big and never give up. You taught me to always think for myself, to walk the uncharted paths, to be bold, independent, and forever curious. You are the most resilient people I know. So much has changed for our family during the past four

years but you both continue to be a North Star for me, Will and Cole. Thank you. To my brothers, Will and Cole, your joy, laughter, hugs, and zest for life have brightened me up on so many difficult days. You are both rays of sunshine and never fail to make me laugh. I am proud of the young gentlemen you are both becoming, and it is an honour to be your sister. To my third brother, Neo, you are the super glue that holds all of us together. Thank you for carrying the weight of our collective mental health on your furry little shoulders.

To my dear friends who have made life inside and outside the lab vibrant and full of laughter, thank you. Natasha and Sophia, we met on day one and here we are at the end. Our friendship will be one of the defining features of this DPhil. I will never forget crying on that piece of driftwood in Sardinia, being soppy, and being so thankful for our friendship and the trip that brought us together. I am so lucky to have such smart, funny, strong women in my life. It is only fitting in the last days of writing this we are together in the library, seeing it through to the very end. Thank you to Lakshanie and Sarah Hill, my coffee buddies and cheerleaders, you two are some of the sweetest, purest people I know. Thank you for your kindness, friendship, and heartfelt chats.

Thank you to the wonderful staff of the Kennedy Institute for silently ensuring everything is running smoothly behind the scenes – none of the incredible science we do is possible without you. Thank you to CommonGround and Alex Farrow for welcoming me into the comedy family; JC has been such a core part of my life in Oxford. Thank you to Gallery Bouldering for keeping me physically fit and mentally sane. Thank you to Liam, James, and Will; as the one year ‘bandiversary’ approaches, I am so excited to see what next year has in store – it has been a pleasure making music and getting to know you three. Thank you to the Immposters for the pure joy every rehearsal and performance has brought. There are too many people to individually name but thank you to everyone who has been part of the last four years. When I started this DPhil, we were just coming out of COVID, and the world was in a very different state. It is crazy to reflect how much life has changed both internally and externally throughout this program. Thank you to everyone who has been along for the ride.

Abstract

Inflammasomes are tissue damage and infection sensing pathways in immune cells which, when overactive, contribute to immunopathology in diseases such as inflammatory arthritis. Using time-resolved single-cell RNA sequencing analyses of mouse inflammatory arthritis compared with human rheumatoid arthritis, spatial transcriptomics, and functional studies, we provide a view into the tissue biology of NLRP3 using rheumatoid arthritis as an exemplar of sterile tissue inflammation. We report that NLRP3 inflammasome expression and activity are kept low in all tissue-resident macrophage subsets. Myeloid sensing of normal apoptotic cell turnover, via efferocytosis receptors such as MERTK, contributes to low inflammasome activity in health. In disease, GM-CSFR+ recruited monocyte-derived macrophages home to the lining layer, drive most of NLRP3 and pro-IL-1β expression and contribute to inflammatory pain, which can be controlled by blocking GM-CSF *in vivo*. Therefore, current technologies allow us to move inflammasome research into the tissue context and explore their link with pathology and pain.

Table of Contents

1. Abbreviations

ACPA	Anti-citrullinated protein antibodies
ActD	Actinomycin D
AIA	Antigen induced arthritis
AIM2	Absent In Melanoma 2
AKT kinase	AK strain Thymoma
AMP	Accelerating Medicines Partnership
ANOVA	Analysis of variance
ASC	Apoptosis-associated speck-like protein containing a CARD
ATP	Adenosine triphosphate
BM	Bone marrow
BMDM	Bone Marrow-Derived Macrophages
CAPS	Cryopyrin-associated periodic syndrome
CARD	Caspase recruitment domain
CARD8	Caspase Recruitment Domain Family Member 8
CASP1	Caspase-1
Caspase	Cysteine-Aspartic Proteases
CCL2	C-C Motif Chemokine Ligand 2
CCL7	C-C Motif Chemokine Ligand 7
CCR2	C-C chemokine receptor type 2
CD	Cluster of differentiation
CD14	Cluster of differentiation 14
CIA	Collagen-induced arthritis
CLIC5	Chloride intracellular channel protein 5
COVID	Coronavirus disease 2019
CRISPR	Clustered regularly interspaced short palindromic repeats
CSF2	Colony stimulating factor 2 (GM-CSF)
CytoD	Cytocholasin D
DAMP	Damage associated molecular pattern
DMARD	Disease-modifying anti-rheumatic drugs
DMSO	Dimethyl sulfoxide
DNA	Deoxyribonucleic Acid
ELISA	Enzyme-linked immunosorbent assay
ER	Endoplasmatic reticulum
FBS	Foetal Bovine Serum
FCAS	Familial cold autoinflammatory syndrome
FMF	Familial Mediterranean Fever
FOLR2	Folate Receptor Beta
GAPDH	Glyceraldehyde 3-Phosphate Dehydrogenase
GAS6	Growth Arrest Specific 6
GFP	Green fluorescent protein
GM-CSF	Granulocyte-macrophage colony-stimulating factor

GoF	Gain-of-function
GSDMD	Gasdermin D
GSDME	Gasdermin E
HBEGF	Heparin-binding EGF-like growth factor
HLA	Human leukocyte antigen
HMDM	Human monocyte derived macrophage
ICAM1	Intercellular Adhesion Molecule 1
IDH1	Isocitrate Dehydrogenase 1
ID2	DNA-binding protein inhibitor ID-2
IFN	Interferon
IgG	Immunoglobulin G
IL	Interleukin
IRF4	Interferon regulatory factor 4
IRF5	Interferon regulatory factor 5
ISG15	Interferon-stimulated gene 15
kDa	Kilodalton
KO	Knockout
LDH	Lactate dehydrogenase
LPS	Lipopolysaccharide
LRR	Leucine-rich repeats
M-CSF	Macrophage Colony-Stimulating Factor
MCC950	Matthew Cooper Compound 950
MEFV	Mediterranean fever
MSU	Monosodium urate
mtDNA	Mitochondrial DNA
MTOC	Microtubule Organisation Centre
mtROS	Mitochondrial reactive oxygen species
MWS	Muckle-wells syndrome
NEK7	NIMA Related Kinase 7
NINJ1	Ninjurin 1
NLRC4	NLR family CARD domain-containing protein 4
NLRP1	NACHT, LRR and PYD domains-containing Protein 1
NLRP3	NACHT, LRR and PYD domains-containing Protein 3
NOMID	Neonatal onset multisystem inflammatory disease
PAMP	Pathogen-associated molecular pattern
PBS	Phosphate-Buffered Saline
PI	Propidium Iodide
PMR	Plasma membrane rupture
PP2A	Protein Phosphatase 2A
PRR	Pattern Recognition Receptor
PTM	Posttranslational modification
PYD	Pyrin domain
RNA	Ribonucleic Acid

ROS	Reactive oxygen species
siRNA	Short-Interfering RNA
TBK1	TANK-Binding Kinase 1
TcdB	Clostridium Difficile Toxin B
Tet2	Tet methylcytosine dioxygenase 2
TGN	Trans-Golgi Network
TLR	Toll-Like Receptor
TNF	Tumour Necrosis Factor
TNFR	Tumour necrosis factor receptor
WT	Wildtype
VFI	Vaccine Formulation Institute

2. Authorship Declaration

I declare that this thesis has never been submitted, in same or different form, to this or any other university for a degree or qualification. All data presented in this thesis is the result of my own work with the following exceptions:

1) Publicly available single-cell RNA sequencing datasets were generated by others as described in Methods. In-house single-cell RNA sequencing of time-resolved murine arthritis was done at the University of Birmingham in Prof. Adam Croft's lab. All downstream bioinformatics analysis was done by me.
2) The spatial transcriptomic dataset of human RA and subsequent data analysis was conducted by Patricia Reis Nisa and Dr. Christopher Mahony at the University of Birmingham in Prof. Adam Croft's lab.
3) *In vivo* mBSA AIA models were conducted by Dr. Isu-Huang with my assistance.

The work contained in this thesis was carried out during my time as a DPhil student in Kennedy Institute of Rheumatology at the University of Oxford, under the supervision of Associate Prof. Jelena Bezbradica Mirkovic, Prof. Christopher Buckley, and Prof. Mark Coles.

My DPhil work, which forms the basis of this thesis, has been submitted as a first-authored article for peer-reviewed publication in 2025 and is currently in revision.

I was also involved in a collaboration regarding macrophage activation in response to vaccination adjuvants. This was published during my DPhil and is discussed in Appendix Data Chapter 5.

1. Reinke, S., Pantazi, E., **Chappell, GR**…. Bezbradica, JS., Milicic, A. Emulsion and liposome-based adjuvanted R21 vaccine formulations mediate protection

against malaria through distinct immune mechanisms. ***Cell Reports Medicine***, Volume 4, Issue 11, 101245 (2023).

2. Yow, SJ., … **Chappell, GR**… Bezbradica, JS., Boucher, D., Chen, KW. Threat assessment shapes neutrophil cell fate upon inflammasome activation. Manuscript prepared for submission.
3. **Chappell, GR.**, … Bezbradica, JS. Tissue-recruited inflammatory GM-CSFR+ macrophages drive inflammasome activity and pain in arthritis. In revision.

3. Introduction

3.1 Inflammasomes

Inflammasomes are multi-protein complexes expressed mostly in innate immune cells and epithelial barrier cells, functioning as intracellular pattern recognition receptors (PRRs) that detect pathogen-associated molecular patterns (PAMPs) and damage-associated molecular patterns (DAMPs)[1]. Inflammasome activity is protective in acute settings including infection and vaccination, as it drives maturation and secretion of IL-1β, a potent pro-inflammatory cytokine that promotes vascular activation and the acute phase response[2,3]. However, poor control and overactivation of inflammasomes are associated with immunopathology including genetic inflammasomopathies, acquired chronic inflammatory conditions, and inflammaging[4–6]. For example, gain-of-function mutations that lead to Nucleotide-Binding Domain, Leucine-Rich–Containing Family, Pyrin Domain–Containing-3 (NLRP3) hyperactivity result in cryopyrin-associated periodic inflammatory syndromes (CAPS) presenting with fever, severe arthritis, urticaria, and arthalgia[7]. Additionally, increased inflammasome activity has been associated with several autoimmune diseases, neurodegenerative disorders, and metabolic disorders[8,9]. These pathologies underscore the delicate balance between inflammasome-mediated host defence and pathology.

3.1.1 The NLRP3 inflammasome: structure, activation, and regulation

As inflammasomes are essential sentinels of homeostasis but contribute to several human diseases, studying inflammasome signalling and regulation has important translational implications for both acute and chronic inflammatory diseases.

The NLRP3 inflammasome is the most well-understood inflammasome and is the primary source of IL-1β and IL-18 in tissues[10,11].

3.1.1a Structure and composition

The NLRP3 inflammasome is a multi-protein complex composed of a sensor (NLRP3), an adaptor (apoptosis-associated speck-like protein containing a caspase activation and recruitment domain, ASC), and the effector enzyme (caspase-1)[10,11].

NLRP3 itself consists of three functionally distinct domains: an N-terminal pyrin domain (PYD) for protein-protein interactions, a central NACHT domain critical for ATP-dependent self-oligomerization, and a C-terminal leucine-rich repeat (LRR) domain implicated in ligand sensing and autoinhibition. This modular structure enables NLRP3 to integrate diverse danger signals into a coordinated inflammatory response[12–14].

3.1.1b Two-step activation mechanism

NLRP3 inflammasome activation requires two distinct signals (Figure 1). **Signal 1**, or priming, upregulates NLRP3 and pro-IL-1β expression via nuclear factor-κB (NF-κB) and hypoxia-inducible factor-1α (HIF-1α) nuclear translocation[15,16]. Priming is triggered downstream of PRR activation, through Toll-like receptor 4 (TLR4) ligation by PAMPs (such lipopolysaccharide, LPS) or DAMPs (including tumour necrosis factor-α (TNF-α) and tenascin C (TNC))[17]. PAMPs induce robust, transient NLRP3 priming, while sterile DAMP-mediated signals elicit weaker but more sustained responses[18]. Short-term priming insufficient for transcriptional activation can still prime NLRP3 activation through post-translational modifications (PTMs)[15,19,20]. Several post-translational modifications to NLRP3 have been identified by our group and others including phosphorylation of Ser5 (human) and Ser3 (mouse) by TBK1/IKKε and dephosphorylation by PP2A in the PYD domain[14,21].

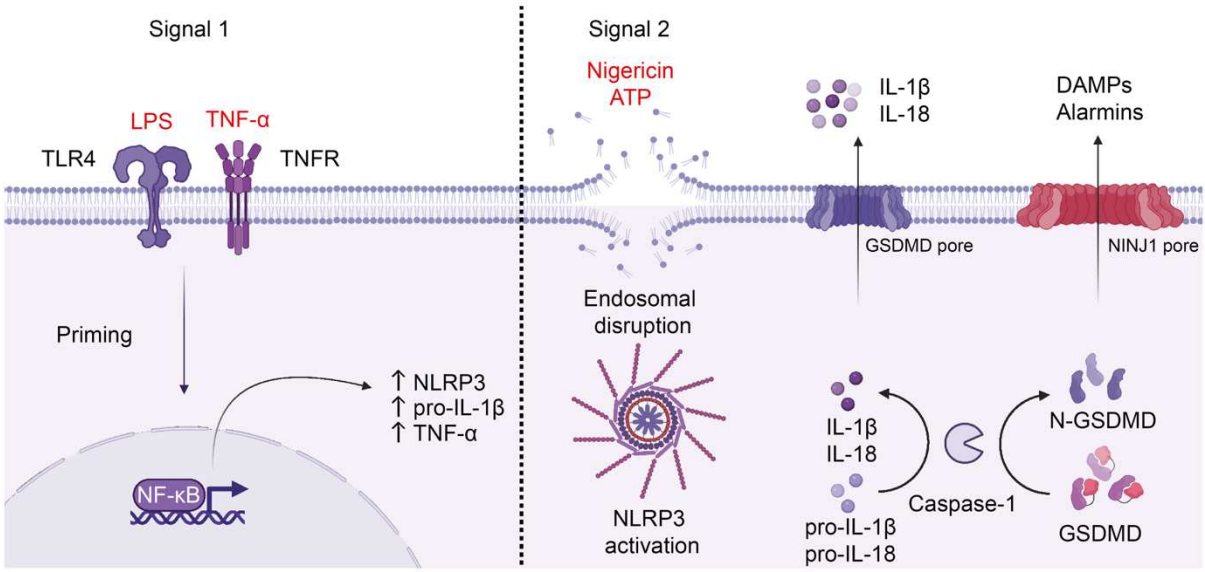

Figure 1 | The NLRP3 inflammasome requires two signals for activation.
The NLRP3 inflammasome, an intracellular sensor, detects disruptions in cellular homeostasis and requires two distinct signals for full activation: a priming signal and an activating signal. The priming step is triggered by pathogen-associated molecules, such as lipopolysaccharide (LPS), or sterile tissue damage-associated molecular patterns (DAMPs), like tenascin-C (TNC), which signal through Toll-like receptor 4 (TLR4). Tumour necrosis factor receptor (TNFR) signalling can also weakly prime NLRP3. Priming induces nuclear translocation of NF-κB, driving transcription and translation of *Nlrp3* (encoding NLRP3), *Il1b* (encoding pro-IL-1β), and *Tnf* (encoding TNF-α). The second signal, indicating cellular damage or invasion, is triggered by events such as potassium (K^+) or chloride (Cl^-) ion efflux, millimolar ATP concentrations, or nigericin, an ionophore that depletes K^+ ions. Upon activation, NLRP3 co-localizes with the disrupted TGN38+ endosomal network, self-oligomerizes, and recruits the adaptor protein ASC. ASC, in turn, recruits caspase-1, which undergoes self-activation and cleaves pro-IL-1β, pro-IL-18, and gasdermin D (GSDMD) into their mature, biologically active forms. The N-terminal fragment of GSDMD (N-GSDMD) forms pores in the plasma membrane, enabling selective release of IL-1β and IL-18. Subsequently, NINJ1 mediates plasma membrane rupture and alarmin release downstream of GSDMD pore formation. Figure was partially made in BioRender.

Signal 2, the activation step, is triggered by cellular perturbations indicating loss of membrane integrity, such as potassium (K^+) or chloride (Cl^-) ion efflux. Activating stimuli include ionophores (nigericin), millimolar extracellular ATP, pathological crystals (monosodium urate (MSU)), and organelle damage[11,22]. A convergent mechanism involves disruption of the endosomal network and endosomal cargo trafficking, which serves as a scaffold for NLRP3 recruitment and inflammasome

assembly[23]. This diversity of stimuli underscores NLRP3's role as a broad sensor of cellular stress.

3.1.1c Regulatory Mechanisms

NLRP3 activity is tightly regulated at transcriptional, post-translational, and structural levels to prevent aberrant inflammation. Beyond NF-κB-mediated transcriptional control and epigenetic modifications, PTMs such as phosphorylation and dephosphorylation fine-tune NLRP3 activation[14,21]. A critical regulatory partner, NIMA-related kinase 7 (NEK7), binds the LRR domain to facilitate inflammasome assembly, at least in mice, albeit in humans it is not always required[24,25]. Structurally, in resting cells, NLRP3 self-oligomerizes via LRR-LRR interactions, forming a protective "cage" that sequesters the PYD and NEK7-binding sites, thereby preventing premature activation[26].

3.1.1d Effector functions and outcomes

Upon activation, NLRP3 undergoes a conformational change, recruits ASC via PYD-PYD interactions, forming a macromolecular speck that activates caspase-1[27]. Caspase-1 proteolytically cleaves pro-IL-1β and pro-IL-18 into their biologically active, mature forms[28]. In addition to the maturation of IL-1β and IL-18, NLRP3 inflammasome activity processes GSDMD into its pore-forming N-terminal fragment, mediating the rapid secretion of IL-1β and IL-18[29,30]. The GSDMD pore is the primary route for IL-1β secretion; however, a slower GSDMD-independent process of IL-1β release has also been identified[31]. Prolonged GSDMD pore formation triggers plasma membrane rupture (PMR) and pyroptosis, driven by the second, larger pore made by oligomerisation of the membrane protein called Ninjurin1 (NINJ1), releasing alarmins and amplifying inflammation[32]. While pyroptosis eliminates pathogen reservoirs, excessive cell death exacerbates tissue damage and immunopathology[33].

3.1.2 The pathogenicity of NLRP3: insights from monogenic mutations

Monogenic mutations in the *NLRP3* gene underlie CAPS, a group of rare autoinflammatory disorders that exemplify how single-gene defects can elucidate the pathogenic role of NLRP3 in systemic inflammation.

3.1.2a CAPS: clinical spectrum and molecular basis

CAPS encompasses three clinically distinct disorders with a continuum of severity, all driven by gain-of-function mutations in NLRP3: Familial Cold Autoinflammatory Syndrome (FCAS), Muckle-Wells Syndrome (MWS), and Neonatal-Onset Multisystem Inflammatory Disease (NOMID)[34,35]. FCAS, the mildest form, is triggered by cold exposure and manifests as fever, urticaria-like rash, and arthralgia[34]. MWS presents with recurrent fever, urticarial rash, joint pain, and risks of sensorineural hearing loss and amyloidosis[34]. NOMID, the most severe, is characterised by chronic meningitis, developmental delays, persistent fever, rash, and destructive joint deformities[34,35]. Over fifty CAPS-associated mutations have been identified, predominantly within the NACHT and LRR domains of NLRP3[36]. These mutations often disrupt the regulatory constraints on NLRP3 activation, with some enabling constitutive inflammasome assembly and caspase-1 activation in the absence of a canonical second signal, relying solely on priming stimuli, and others allowing activation by signal 1 alone, in the absence of signal 2[37]. This results in spontaneous or exaggerated IL-1β and IL-18 production, driving systemic inflammation[37].

A common clinical feature of CAPS disorders is joint pain and stiffness (arthralgia), suggesting dysregulated NLRP3 drives systemic inflammation that manifests in the joint[7].

3.1.2b Validation of IL-1β as a key effector in CAPS

The critical role of IL-1β in CAPS pathogenesis, particularly in driving joint pain and systemic inflammation, has been validated through targeted biologic therapies. A pivotal multicentre, randomized, double-blind, placebo-controlled trial of canakinumab, a monoclonal antibody (mAb) neutralizing IL-1β, enrolled 35 CAPS patients in the treatment arm. Within one week, 34 patients achieved a complete clinical response, defined as resolution of rash, arthralgia, and fever, alongside normalization of C-reactive protein (CRP) levels[38]. This rapid and near-universal efficacy underscores IL-1β as the primary effector of NLRP3-mediated pathology in CAPS and highlights the therapeutic potential of IL-1β blockade in NLRP3-driven diseases.

3.1.3 The pyrin inflammasome: molecular mechanisms and pathogenic implications

Like NLRP3, the pyrin inflammasome senses disruptions in cellular homeostasis, but it has a narrower range of activating signals. Pyrin senses loss of homeostasis induced by bacterial toxins[41]. The pyrin inflammasome is encoded by the *MEFV* gene, and its mutations resulting in its overactivation give rise to Familial Mediterranean Fever (FMF)[39,40].

3.1.3a Molecular structure and activation

Pyrin, a tripartite protein comprising an N-terminal PYD, a B-box domain, and a C-terminal SPRY domain, detects modifications to RhoA GTPases, targeted by

toxins such as those from *Clostridium difficile* or *Vibrio parahaemolyticus*[41,42]. In its inactive state, pyrin is sequestered from ASC, by binding to 14-3-3 proteins[43]. Phosphorylation of pyrin at serine residues (Ser208, Ser242) by kinases PKN1 and PKN2 occurs downstream of active RhoA[43]. Dephosphorylation, triggered by toxin-mediated RhoA inactivation, releases pyrin from 14-3-3, enabling PYD-mediated homotypic interactions with ASC[43]. This facilitates the assembly of the inflammasome scaffold, recruiting and activating caspase-1, which processes pro-IL-1β and pro-IL-18 into their mature forms and cleaves GSDMD to initiate pyroptosis[41–43].

3.1.3b Clinical manifestations in FMF

Activating mutations in *MEFV* cause FMF, an autosomal recessive autoinflammatory disorder characterized by recurrent, self-limiting inflammatory episodes[39,40]. Clinical features include fever, abdominal pain, arthritis or arthralgia, and skin manifestations[39,40]. FMF shares phenotypic similarities with CAPS due to convergent downstream signalling via ASC, caspase-1, and IL-1β. However, FMF's distinct trigger, RhoA GTPase modification, underlies its unique epidemiology and pathophysiology. Notably, heterozygous carriers of *MEFV* mutations are typically asymptomatic, and the high prevalence of such carriers in Mediterranean populations suggests a historical selective advantage. Recent studies have demonstrated that pathogenic *MEFV* variants confer resistance to *Yersinia pestis*, the causative agent of the Black Death, which decimated 30–50% of Europe's population in the 14th century[44]. This evolutionary pressure likely drove the enrichment of *MEFV* variants in affected regions.

3.1.3c Pathogenic variants beyond FMF

While heterozygous *MEFV* mutations are generally subclinical, emerging evidence implicates single-copy variants in exacerbating inflammatory diseases.

Heterozygosity for *MEFV* mutations has been associated with very-early-onset inflammatory bowel disease (IBD) and systemic-onset juvenile idiopathic arthritis (soJIA), suggesting that pyrin dysregulation may amplify inflammatory responses in genetically predisposed individuals[45,46]. In rheumatoid arthritis (RA), cohort studies have identified a higher prevalence of *MEFV* mutations in patients with seronegative RA and an overrepresentation of heterozygous carriers among severe RA cases[47,48]. These findings indicate that pyrin variants may lower the threshold for inflammasome activation, intensifying tissue-specific inflammation, particularly in synovial joints.

3.1.4 Implications for joint inflammation and autoimmunity

The NLRP3 and pyrin inflammasomes exemplify the dual nature of innate immune sensors as both protectors and perpetrators of inflammation. Their shared upstream mode of activation (loss of cellular homeostasis) and shared downstream signalling via ASC, caspase-1, and IL-1β/IL-18 underscores a conserved mechanism driving chronic immunopathology. NLRP3's broad sensitivity to PAMPs and DAMPs positions it as a central player in diverse diseases, from monogenic CAPS to polygenic disorders like gout, atherosclerosis, and inflammaging[4–6]. Pyrin's specificity for RhoA modifications highlights its role in bacterial defence and FMF, with heterozygous variants amplifying autoimmune conditions like RA[47,48]. The joint-centric pathology in both CAPS and FMF, suggests convergent mechanisms in inflammatory arthropathies and necessitates a deep understanding of inflammasome tissue biology.

3.2 Current methods to study the inflammasome

Inflammasome signalling, critical to innate immunity, is primarily studied *in vitro* using macrophages due to their high expression of NLRP3 and other

inflammasomes[49]. This section reviews methodologies for investigating NLRP3 and pyrin inflammasomes, highlighting their strengths and limitations in elucidating molecular mechanisms.

3.2.1 *In vitro* models and activation protocols

The NLRP3 inflammasome is activated *in vitro* in primary macrophages such as bone marrow-derived macrophages (BMDMs) or human monocyte derived macrophages (HMDMs) using a two-signal activation protocol. Priming with LPS via TLR4 upregulates NLRP3 and pro-IL-1β, while nigericin induces K^+ efflux to trigger activation. Pyroptosis is quantified by lactate dehydrogenase (LDH) release into supernatants. Secreted IL-1β and IL-18 are detected via ELISA, and caspase-1 cleavage, GSDMD processing, and pro-IL-1β maturation are assessed by Western blotting to confirm inflammasome activity. The pyrin inflammasome, activated by *Clostridium difficile* Toxin B (TcdB) to inhibit RhoA GTPases, is studied similarly. LDH release and IL-18 secretion are measured, but IL-1β detection requires LPS priming to induce pro-IL-1β expression[41].

3.2.2 Experimental advantages

In vitro macrophage models enable precise mechanistic studies through genetic knockouts, pharmacological inhibitors like MCC950 for NLRP3, and high temporal resolution with imaging techniques such as ASC speck visualization. BMDMs, easily generated in large numbers allow for reproducible, high-throughput experiment.

3.2.3 Limitations and challenges

In vitro models fail to fully capture tissue-specific inflammasome biology, as cultured macrophages lack the complex microenvironmental cues present in tissue. The reliance on macrophages may overlook contributions from other cell types, such as neutrophils. Simplified stimuli like LPS and nigericin do not fully mimic complex *in vivo* triggers, and murine BMDMs may not reflect human responses due to species-specific differences. Complementary *in vivo* models, discussed in Chapter 4, are needed to address these gaps and enhance translational relevance.

3.3 Tissue macrophages and inflammasome biology

It is poorly understood how relevant the extensive *in vitro* knowledge of inflammasome signalling is to inflammasome tissue biology. Tissue macrophages comprise long-lived, self-renewing tissue-resident populations and short-lived, bone marrow-derived monocytes recruited during inflammation, each with distinct origins and roles in modulating inflammasome activity.

3.3.1 Tissue-resident macrophages

Tissue-resident macrophages originate from yolk sac, foetal liver, or primitive embryonic myelopoiesis, distinct from adult bone marrow-derived monocytes[50]. Tissue-resident macrophages are long-lived, often self-renewing, with minimal replacement from steady-state myelopoiesis, and occupy specialized niches dedicated to tissue surveillance and homeostasis[51]. Their homeostatic role is thought to suppress inflammatory programs to prevent tissue pathology[52]. For example, peritoneal tissue-resident macrophages, a well-studied population, produce IL-10 to

inhibit IL-1β expression and fail to upregulate IL-1β in response to TNF-α, suggesting unique mechanisms to restrain NLRP3 activity not recapitulated *in vitro*[53].

In the joint, seminal murine fate-mapping studies identified two synovial tissue-resident macrophage populations[54]. One forms the lining layer, a protective barrier adjacent to lining fibroblasts, while the other resides in the sub-lining, surveying the synovial space near vascular endothelium, self-renewing, and giving rise to the lining subset[54]. These macrophages suppress chronic inflammation, and their depletion in experimental arthritis models precedes arthritis onset and inflammatory monocyte infiltration[55]. Human single-cell RNA sequencing (scRNAseq) studies have identified analogous synovial macrophage populations expressing MerTK, an efferocytosis receptor linked to joint health and RA remission[56]. Loss of MerTK+ macrophages correlates with active RA and predicts poor treatment response[56]. MerTK, part of the TAM (Tyro3, Axl, MerTK) receptor family, recognizes apoptotic cells and promotes IL-10 synthesis, a negative regulator of NLRP3 expression[57–59]. In MerTK-deficient or TAM triple-knockout mice, severe and spontaneous polyarthritis develop, highlighting TAM signalling's protective role[60]. MerTK also limits NLRP3 activity in neuroinflammation models by inducing autophagy, a pathway that degrades active NLRP3 complexes[61]. Thus, synovial tissue-resident macrophages likely use efferocytosis and TAM-receptor signalling to suppress NLRP3 expression and activity during homeostasis and inflammation resolution, a mechanism explored further in Data Chapter 4.

3.3.2 Monocyte-derived macrophages

In contrast, monocyte-derived macrophages are recruited to tissues during inflammation, differentiating into inflammatory macrophages with enhanced NLRP3

expression and activity, unconstrained by tissue-resident homeostatic signals[62]. In serum-transfer-induced arthritis (STIA), monocyte depletion prevents disease development, underscoring their pathogenic role[63]. In human RA, a subset of recruited macrophages expressing HBEGF and IL-1β drives a destructive fibroblast gene signature *in vitro*[64]. Monocyte recruitment, mediated by monocyte-chemoattractant protein 1 (MCP-1/CCL2), correlates with synovial and serum CCL2 levels and inflammatory infiltrates in RA patients[65]. Genetic deletion of CCR2, the CCL2 receptor, protects against multiple murine autoimmune models[66,67]. CCR2+ monocyte-driven pathology involves IL-1β and iNOS production, regulated by GM-CSF, as discussed in Data Chapters 2 and 3[66,67].

We aimed to investigate the differential NLRP3 expression and activity of tissue-resident and recruited macrophages using RA as a model. Our findings suggest that recruited monocytes, rather than resident macrophages, may be the primary drivers of NLRP3-mediated inflammation in RA.

3.4 Rheumatoid arthritis (RA)

RA, a chronic autoimmune disease, affects approximately 1% of the population in developed countries, causing synovial inflammation, joint destruction, and systemic complications[68,69]. Seminal studies have elucidated RA's immunological and molecular mechanisms, identifying critical roles for T cells, B cells, macrophages, and cytokines such as TNF-α, IL-6, and GM-CSF, alongside pathways like NF-κB and JAK-STAT[62,70–72]. Foundational work by Professors M. Feldmann and R. Maini demonstrated TNF-α as a pivotal proinflammatory cytokine in RA, inducing IL-1 production by synovial cells[73]. Their experiments showed that TNF-α blockade reduced inflammation in *ex vivo* RA synovial cultures, providing the mechanistic basis

for anti-TNF therapies like infliximab and etanercept, which revolutionized RA treatment[70,73]. Subsequent studies by Professor J. Hamilton revealed that GM-CSF-deficient mice are resistant to collagen-induced arthritis (CIA), implicating GM-CSF in RA-like pathology, as explored further in Data Chapter 2/3[74]. Concurrently, NF-κB was identified as a central hub in RA, activated by TNF-α and IL-1 to drive proinflammatory cytokine and matrix metalloproteinase (MMP) expression in synoviocytes, perpetuating chronicity and tissue destruction[75]. Recent single-cell sequencing advances have further refined these insights, revealing cellular heterogeneity in RA synovium, as discussed in Data Chapter 1.

3.5 RA as a model to understand inflammasome tissue biology

This project leverages RA as a biologically relevant model to characterize inflammasome expression and regulation in tissues, utilizing the data-rich resources at the Kennedy Institute of Rheumatology.

Despite effective management with disease-modifying anti-rheumatic drugs (DMARDs) and anti-TNF therapies, approximately 50% of RA patients do not respond to standard treatments, underscoring the need to elucidate mechanisms driving RA's diverse pathotypes[76]. Aberrant inflammasome activity is implicated in RA and other chronic inflammatory diseases. A recent study in inflammatory bowel disease linked an IL-1β-activated fibroblast signature to poor treatment response, suggesting parallels in RA[77]. Single nucleotide polymorphisms (SNPs) in *NLRP3*, *MEFV*, and *CARD8*, a negative NLRP3 regulator, increase RA susceptibility and arthritis severity[78,79]. Specific *NLRP3* SNPs are associated with poor anti-TNF response, particularly in smokers, while anti-citrullinated peptide antibodies (ACPAs) enhance NLRP3 activity *in vitro*[80–82]. Peripheral blood mononuclear cells (PBMCs) from RA

patients show elevated *ASC*, *MEFV*, *NLRP3*, and *CASP1* expression, with reduced CARD8 compared to controls[79]. Serum IL-1β levels are higher in RA patients and correlate with disease severity[83], and IL-1β and IL-18 are elevated in RA synovial fluid, with higher IL-1β in inflamed joints compared to contralateral joints in asymmetric disease[84,85]. RA monocytes and macrophages also exhibit increased inflammatory cell death, with elevated GSDME and N-terminal GSDMD[86].

While human RA is a heterogenous disease and only a fraction of patients responded to IL-1 blockade in clinical trials (suggesting better patient stratification is needed), the experimental models of RA are largely inflammasome dependent. Specifically, NLRP3 inhibition with MCC950 ameliorates joint inflammation and destruction in CIA[87]. Dual IL-1α and IL-1β blockade reduces cartilage damage, bone erosion, and cellular infiltrates in CIA, while IL-18 blockade mitigates disease severity[88,89]. Synovial NLRP3 expression correlates with arthritis severity and radiographic scores in CIA, and myeloid-specific deletion of A20, an NLRP3 negative regulator, induces spontaneous arthritis, preventable by NLRP3 deletion[90,91]. Despite this evidence, anakinra, an IL-1R antagonist, is not clinically approved for RA, though meta-analyses suggest benefits in reducing disease activity and pain. RA's heterogeneity suggests NLRP3 and IL-1β drive only specific subsets, such as leukocyte-rich RA, where IL-1β+ myeloid cells predominate, as identified by scRNAseq and mass cytometry[93]. Other alarmins released during inflammasome-driven cell death, may also contribute to RA pathology, highlighting the need for pan-inflammasome inhibitors.

3.6 Knowledge gaps and research significance

Despite substantial evidence implicating NLRP3 in RA pathogenesis, no systematic study has characterized NLRP3 and other inflammasome sensors in human and murine joints across arthritis stages, including health, initiation, peak, resolution, remission, or persistence. The spatial distribution of inflammasome expression and activity within the joint's architecture remains unknown. Molecular mechanisms preventing premature NLRP3 activation in healthy joints are poorly defined, as are the signals promoting NLRP3 expression and activity during joint inflammation. Addressing these gaps is critical to understanding inflammasome contributions to RA, understanding tissue biology of inflammasomes in general, and developing targeted therapies for non-responsive patients.

3.7 Research hypothesis and objectives

We hypothesize that tissue-resident macrophages in healthy joints suppress inflammasome expression and activity via endogenous or tissue-specific signals to prevent immunopathology, while inflammatory myelopoiesis generates recruited macrophages with enhanced inflammasome expression and activity.

- Aim 1: Characterize inflammasome expression in tissues during health and disease using bioinformatic approaches
- Aim 2: Identify mechanisms driving inflammasome expression and activity in the synovium through *in vitro* and *in vivo* techniques
- Aim 3: Elucidate the role of apoptotic cell sensing in lowering inflammasome activity in homeostatic settings

3.8 Thesis structure

Data Chapter 1 demonstrates that NLRP3 expression is restricted to recruited, inflammatory monocyte-derived macrophages in the synovium and suppressed in tissue-resident macrophages, addressing the first objective.

Data Chapter 2 reveals that GM-CSF enhances and prolongs NLRP3 responses in vitro, facilitating IL-1β release in response to sterile priming signals, contributing to the second objective.

Data Chapter 3 shows that GM-CSF antagonism *in vivo* reduces synovial pro-IL-1β levels, neutrophil recruitment, and pain in antigen-induced arthritis, further addressing the second objective.

Data Chapter 4 establishes that apoptotic cell sensing via phosphatidylserine reduces NLRP3 activity *in vitro*, fulfilling the third objective.

Appendix Data Chapter 5 discusses RA patient stratification and proposes a cohort where GM-CSF blockade or NLRP3 inhibition may be beneficial, supported by preliminary *in vitro* evidence, aligning with the second objective.

Appendix Data Chapter 6 summarizes data from a second-author publication in *Cell Reports Medicine* (2023) on inflammasome activation in rational vaccine design, providing broader context.

3.9 References

1. Broz, P. & Dixit, V. M. Inflammasomes: mechanism of assembly, regulation and signalling. *Nature Reviews Immunology* **16**, 407–420 (2016).
2. von Moltke, J., Ayres, J. S., Kofoed, E. M., Chavarría-Smith, J. & Vance, R. E. Recognition of Bacteria by Inflammasomes. *Annu. Rev. Immunol.* **31**, 73–106 (2013).

3. Dinarello, C. A. The IL-1 family of cytokines and receptors in rheumatic diseases. *Nature Reviews Rheumatology* **15**, 612–632 (2019).
4. Mangan, M. S. J. *et al.* Targeting the NLRP3 inflammasome in inflammatory diseases. *Nat Rev Drug Discov* **17**, 588–606 (2018).
5. Ramachandran, R., Manan, A., Kim, J. & Choi, S. NLRP3 inflammasome: a key player in the pathogenesis of life-style disorders. *Exp Mol Med* **56**, 1488–1500 (2024).
6. Latz, E. & Duewell, P. NLRP3 inflammasome activation in inflammaging. *Seminars in Immunology* **40**, 61–73 (2018).
7. Booshehri, L. M. & Hoffman, H. M. CAPS and NLRP3. *J Clin Immunol* **39**, 277–286 (2019).
8. Lin, B. & Goldbach-Mansky, R. Pathogenic insights from genetic causes of autoinflammatory inflammasomopathies and interferonopathies. *Journal of Allergy and Clinical Immunology* **149**, 819–832 (2022).
9. Spel, L. & Martinon, F. Inflammasomes contributing to inflammation in arthritis. *Immunol Rev* **294**, 48–62 (2020).
10. Paik, S., Kim, J. K., Silwal, P., Sasakawa, C. & Jo, E.-K. An update on the regulatory mechanisms of NLRP3 inflammasome activation. *Cell Mol Immunol* **18**, 1141–1160 (2021).
11. Zheng, D., Liwinski, T. & Elinav, E. Inflammasome activation and regulation: toward a better understanding of complex mechanisms. *Cell Discov* **6**, 36 (2020).
12. Fu, J. & Wu, H. Structural Mechanisms of NLRP3 Inflammasome Assembly and Activation. *Annu. Rev. Immunol.* **41**, 301–316 (2023).
13. Yu, X. *et al.* Structural basis for the oligomerization-facilitated NLRP3 activation. *Nat Commun* **15**, 1164 (2024).

14. Stutz, A. *et al.* NLRP3 inflammasome assembly is regulated by phosphorylation of the pyrin domain. *Journal of Experimental Medicine* **214**, 1725–1736 (2017).
15. Bauernfeind, F. G. *et al.* Cutting Edge: NF-κB Activating Pattern Recognition and Cytokine Receptors License NLRP3 Inflammasome Activation by Regulating NLRP3 Expression. *The Journal of Immunology* **183**, 787–791 (2009).
16. Tannahill, G. M. *et al.* Succinate is an inflammatory signal that induces IL-1β through HIF-1α. *Nature* **496**, 238–242 (2013).
17. Midwood, K. *et al.* Tenascin-C is an endogenous activator of Toll-like receptor 4 that is essential for maintaining inflammation in arthritic joint disease. *Nat Med* **15**, 774–780 (2009).
18. Bezbradica, J. S., Coll, R. C. & Schroder, K. Sterile signals generate weaker and delayed macrophage NLRP3 inflammasome responses relative to microbial signals. *Cell Mol Immunol* **14**, 118–126 (2017).
19. Fernandes-Alnemri, T. *et al.* Cutting Edge: TLR Signaling Licenses IRAK1 for Rapid Activation of the NLRP3 Inflammasome. *The Journal of Immunology* **191**, 3995–3999 (2013).
20. Juliana, C. *et al.* Non-transcriptional Priming and Deubiquitination Regulate NLRP3 Inflammasome Activation. *Journal of Biological Chemistry* **287**, 36617–36622 (2012).
21. Fischer, F. A. *et al.* TBK1 and IKKε act like an OFF switch to limit NLRP3 inflammasome pathway activation. *Proc Natl Acad Sci USA* **118**, e2009309118 (2021).
22. Swanson, K. V., Deng, M. & Ting, J. P.-Y. The NLRP3 inflammasome: molecular activation and regulation to therapeutics. *Nat Rev Immunol* **19**, 477–489 (2019).

23. Chen, J. & Chen, Z. J. PtdIns4P on dispersed trans-Golgi network mediates NLRP3 inflammasome activation. *Nature* **564**, 71–76 (2018).
24. He, Y., Zeng, M. Y., Yang, D., Motro, B. & Núñez, G. NEK7 is an essential mediator of NLRP3 activation downstream of potassium efflux. *Nature* **530**, 354–357 (2016).
25. Sharif, H. *et al.* Structural mechanism for NEK7-licensed activation of NLRP3 inflammasome. *Nature* **570**, 338–343 (2019).
26. Andreeva, L. *et al.* NLRP3 cages revealed by full-length mouse NLRP3 structure control pathway activation. *Cell* **184**, 6299-6312.e22 (2021).
27. Masumoto, J. *et al.* ASC, a novel 22-kDa protein, aggregates during apoptosis of human promyelocytic leukemia HL-60 cells. *J Biol Chem* **274**, 33835–33838 (1999).
28. Afonina, I. S., Müller, C., Martin, S. J. & Beyaert, R. Proteolytic Processing of Interleukin-1 Family Cytokines: Variations on a Common Theme. *Immunity* **42**, 991–1004 (2015).
29. Shi, J. *et al.* Cleavage of GSDMD by inflammatory caspases determines pyroptotic cell death. *Nature* **526**, 660–665 (2015).
30. de Vasconcelos, N. M., Van Opdenbosch, N., Van Gorp, H., Parthoens, E. & Lamkanfi, M. Single-cell analysis of pyroptosis dynamics reveals conserved GSDMD-mediated subcellular events that precede plasma membrane rupture. *Cell Death Differ* **26**, 146–161 (2019).
31. Monteleone, M. *et al.* Interleukin-1β Maturation Triggers Its Relocation to the Plasma Membrane for Gasdermin-D-Dependent and -Independent Secretion. *Cell Reports* **24**, 1425–1433 (2018).

32. Kayagaki, N. *et al.* NINJ1 mediates plasma membrane rupture during lytic cell death. *Nature* **591**, 131–136 (2021).
33. Demarco, B. *et al.* Caspase-8–dependent gasdermin D cleavage promotes antimicrobial defense but confers susceptibility to TNF-induced lethality. *Sci. Adv.* **6**, (2020).
34. Hoffman, H. M., Mueller, J. L., Broide, D. H., Wanderer, A. A. & Kolodner, R. D. Mutation of a new gene encoding a putative pyrin-like protein causes familial cold autoinflammatory syndrome and Muckle–Wells syndrome. *Nat Genet* **29**, 301–305 (2001).
35. Sönmez, H. E. & Özen, S. A clinical update on inflammasomopathies. *International Immunology* **29**, 393–400 (2017).
36. Aksentijevich, I. & Kastner, D. L. Genetics of monogenic autoinflammatory diseases: past successes, future challenges. *Nat Rev Rheumatol* **7**, 469–478 (2011).
37. Agostini, L. *et al.* NALP3 Forms an IL-1β-Processing Inflammasome with Increased Activity in Muckle-Wells Autoinflammatory Disorder. *Immunity* **20**, 319–325 (2004).
38. Lachmann, H. J. *et al.* Use of Canakinumab in the Cryopyrin-Associated Periodic Syndrome. *N Engl J Med* **360**, 2416–2425 (2009).
39. The International Fmf Consortium. Ancient Missense Mutations in a New Member of the RoRet Gene Family Are Likely to Cause Familial Mediterranean Fever. *Cell* **90**, 797–807 (1997).
40. The French Fmf Consortium *et al.* A candidate gene for familial Mediterranean fever. *Nat Genet* **17**, 25–31 (1997).

41. Xu, H. *et al.* Innate immune sensing of bacterial modifications of Rho GTPases by the Pyrin inflammasome. *Nature* **513**, 237–241 (2014).
42. Heilig, R. & Broz, P. Function and mechanism of the pyrin inflammasome. *Eur J Immunol* **48**, 230–238 (2018).
43. Park, Y. H., Wood, G., Kastner, D. L. & Chae, J. J. Pyrin inflammasome activation and RhoA signaling in the autoinflammatory diseases FMF and HIDS. *Nat Immunol* **17**, 914–921 (2016).
44. Park, Y. H. *et al.* Ancient familial Mediterranean fever mutations in human pyrin and resistance to Yersinia pestis. *Nat Immunol* **21**, 857–867 (2020).
45. Abu Shtaya, A. *et al.* High frequency of MEFV disease-causing variants in children with very-early-onset inflammatory bowel disease. *Pediatr Res* **97**, 268–272 (2025).
46. Ayaz, N. A. *et al.* MEFV mutations in systemic onset juvenile idiopathic arthritis. *Rheumatology* **48**, 23–25 (2008).
47. Cañete, J. D. *et al.* An unexpectedly high frequency of *MEFV* mutations in patients with anti–citrullinated protein antibody–negative palindromic rheumatism. *Arthritis & Rheumatism* **56**, 2784–2788 (2007).
48. Rabinovich, E. *et al.* Severe disease in patients with rheumatoid arthritis carrying a mutation in the Mediterranean fever gene. *Ann Rheum Dis* **64**, 1009–1014 (2005).
49. Guarda, G. *et al.* Differential expression of NLRP3 among hematopoietic cells. *J Immunol* **186**, 2529–2534 (2011).
50. Nobs, S. P. & Kopf, M. Tissue-resident macrophages: guardians of organ homeostasis. *Trends in Immunology* **42**, 495–507 (2021).

51. Mass, E. *et al.* Specification of tissue-resident macrophages during organogenesis. *Science* **353**, aaf4238 (2016).
52. Guilliams, M. & Svedberg, F. R. Does tissue imprinting restrict macrophage plasticity? *Nat Immunol* **22**, 118–127 (2021).
53. Ipseiz, N. *et al.* Tissue-resident macrophages actively suppress IL-1beta release via a reactive prostanoid/IL-10 pathway. *EMBO J* **39**, (2020).
54. Culemann, S. *et al.* Locally renewing resident synovial macrophages provide a protective barrier for the joint. *Nature* **572**, 670–675 (2019).
55. Huang, Q.-Q. *et al.* Critical role of synovial tissue–resident macrophage niche in joint homeostasis and suppression of chronic inflammation. *Sci. Adv.* **7**, eabd0515 (2021).
56. Alivernini, S. *et al.* Distinct synovial tissue macrophage subsets regulate inflammation and remission in rheumatoid arthritis. *Nat Med* **26**, 1295–1306 (2020).
57. Adomati, T. *et al.* Dead Cells Induce Innate Anergy via Mertk after Acute Viral Infection. *Cell Reports* **30**, 3671-3681.e5 (2020).
58. Rothlin, C. V., Ghosh, S., Zuniga, E. I., Oldstone, M. B. A. & Lemke, G. TAM Receptors Are Pleiotropic Inhibitors of the Innate Immune Response. *Cell* **131**, 1124–1136 (2007).
59. Gurung, P. *et al.* Chronic TLR Stimulation Controls NLRP3 Inflammasome Activation through IL-10 Mediated Regulation of NLRP3 Expression and Caspase-8 Activation. *Sci Rep* **5**, 14488 (2015).
60. Waterborg, C. E. J., Koenders, M. I., van Lent, P. L. E. M., van der Kraan, P. M. & van de Loo, F. A. J. Tyro3/Axl/Mertk-deficient mice develop bone marrow edema

which is an early pathological marker in rheumatoid arthritis. *PLoS ONE* **13**, e0205902 (2018).

61. Du, Y. *et al.* MerTK inhibits the activation of the NLRP3 inflammasome after subarachnoid hemorrhage by inducing autophagy. *Brain Research* **1766**, 147525 (2021).
62. Buckley, C. D., Ospelt, C., Gay, S. & Midwood, K. S. Location, location, location: how the tissue microenvironment affects inflammation in RA. *Nat Rev Rheumatol* **17**, 195–212 (2021).
63. Misharin, A. V. *et al.* Nonclassical Ly6C− Monocytes Drive the Development of Inflammatory Arthritis in Mice. *Cell Reports* **9**, 591–604 (2014).
64. Kuo, D. *et al.* HBEGF+ macrophages in rheumatoid arthritis induce fibroblast invasiveness. *Sci. Transl. Med.* **11**, eaau8587 (2019).
65. Koch, A. E. *et al.* Enhanced production of monocyte chemoattractant protein-1 in rheumatoid arthritis. *J. Clin. Invest.* **90**, 772–779 (1992).
66. Croxford, A. L. *et al.* The Cytokine GM-CSF Drives the Inflammatory Signature of CCR2+ Monocytes and Licenses Autoimmunity. *Immunity* **43**, 502–514 (2015).
67. Chen, Y. F. *et al.* Spontaneous Development of Autoimmune Uveitis Is CCR2 Dependent. *The American Journal of Pathology* **184**, 1695–1705 (2014).
68. Smolen, J. S. *et al.* Rheumatoid arthritis. *Nat Rev Dis Primers* **4**, 18001 (2018).
69. Tobón, G. J., Youinou, P. & Saraux, A. The environment, geo-epidemiology, and autoimmune disease: Rheumatoid arthritis. *Journal of Autoimmunity* **35**, 10–14 (2010).
70. Feldmann, M. & Maini, R. N. TNF defined as a therapeutic target for rheumatoid arthritis and other autoimmune diseases. *Nat Med* **9**, 1245–1250 (2003).

71. Chu, C. Q. *et al.* Detection of Cytokines at the Cartilage/Pannus Junction in Patients with Rheumatoid Arthritis: Implications for the Role of Cytokines in Cartilage Destruction and Repair. *Rheumatology* **31**, 653–661 (1992).
72. Weyand, C. M. & Goronzy, J. J. The immunology of rheumatoid arthritis. *Nat Immunol* **22**, 10–18 (2021).
73. Brennan, F. Inhibitory Effect of TNFα Antibodies on Synovial Cell Interleukin-1 Production in Rheumatoid Arthritis. *The Lancet* **334**, 244–247 (1989).
74. Campbell, I. K. *et al.* Protection from collagen-induced arthritis in granulocyte-macrophage colony-stimulating factor-deficient mice. *J Immunol* **161**, 3639–3644 (1998).
75. Firestein, G. S. & Manning, A. M. Signal transduction and transcription factors in rheumatic disease. *Arthritis & Rheumatism* **42**, 609–621 (1999).
76. Humby, F. *et al.* Synovial cellular and molecular signatures stratify clinical response to csDMARD therapy and predict radiographic progression in early rheumatoid arthritis patients. *Ann Rheum Dis* **78**, 761–772 (2019).
77. Friedrich, M. *et al.* IL-1-driven stromal–neutrophil interactions define a subset of patients with inflammatory bowel disease that does not respond to therapies. *Nat Med* **27**, 1970–1981 (2021).
78. Mathews, R. J. *et al.* Evidence of NLRP3-inflammasome activation in rheumatoid arthritis (RA); genetic variants within the NLRP3-inflammasome complex in relation to susceptibility to RA and response to anti-TNF treatment. *Ann Rheum Dis* **73**, 1202–1210 (2014).
79. Choulaki, C. *et al.* Enhanced activity of NLRP3 inflammasome in peripheral blood cells of patients with active rheumatoid arthritis. *Arthritis Res Ther* **17**, 257 (2015).

80. Dong, X. *et al.* ACPAs promote IL-1β production in rheumatoid arthritis by activating the NLRP3 inflammasome. *Cell Mol Immunol* **17**, 261–271 (2020).
81. Sode, J. *et al.* Anti-TNF treatment response in rheumatoid arthritis patients is associated with genetic variation in the NLRP3-inflammasome. *PLoS One* **9**, e100361 (2014).
82. Yin, H., Liu, N., Sigdel, K. R. & Duan, L. Role of NLRP3 Inflammasome in Rheumatoid Arthritis. *Front. Immunol.* **13**, 931690 (2022).
83. Altomonte, L., Zoli, A., Mirone, L., Scolieri, P. & Magaró, M. Serum levels of interleukin-1b, tumour necrosis factor-a and interleukin-2 in rheumatoid arthritis. Correlation with disease activity. *Clin Rheumatol* **11**, 202–205 (1992).
84. Rooney, M., Symons, J. A. & Duff, G. W. Interleukin 1 beta in synovial fluid is related to local disease activity in rheumatoid arthritis. *Rheumatol Int* **10**, 217–219 (1990).
85. Gracie, J. A. *et al.* A proinflammatory role for IL-18 in rheumatoid arthritis. *J Clin Invest* **104**, 1393–1401 (1999).
86. Zhai, Z. *et al.* Attenuation of Rheumatoid Arthritis Through the Inhibition of Tumor Necrosis Factor–Induced Caspase 3/Gasdermin E–Mediated Pyroptosis. *Arthritis & Rheumatology* art.41963 (2022) doi:10.1002/art.41963.
87. Guo, C. *et al.* NLRP3 inflammasome activation contributes to the pathogenesis of rheumatoid arthritis. *Clin Exp Immunol* **194**, 231–243 (2018).
88. Abramson, S. B. Blocking the effects of IL-1 in rheumatoid arthritis protects bone and cartilage. *Rheumatology* **41**, 972–980 (2002).
89. Plater-Zyberk, C. *et al.* Therapeutic effect of neutralizing endogenous IL-18 activity in the collagen-induced model of arthritis. *J. Clin. Invest.* **108**, 1825–1832 (2001).

90. Zhang, Y., Zheng, Y. & Li, H. NLRP3 Inflammasome Plays an Important Role in the Pathogenesis of Collagen-Induced Arthritis. *Mediators Inflamm* **2016**, 9656270 (2016).
91. Vande Walle, L. *et al.* Negative regulation of the NLRP3 inflammasome by A20 protects against arthritis. *Nature* **512**, 69–73 (2014).
92. Mertens, M. & Singh, J. A. Anakinra for rheumatoid arthritis: a systematic review. *J Rheumatol* **36**, 1118–1125 (2009).
93. Accelerating Medicines Partnership Rheumatoid Arthritis and Systemic Lupus Erythematosus (AMP RA/SLE) Consortium *et al.* Defining inflammatory cell states in rheumatoid arthritis joint synovial tissues by integrating single-cell transcriptomics and mass cytometry. *Nat Immunol* **20**, 928–942 (2019).

4. Materials

4.1 Primary antibodies and flow cytometry

Reagent	Source	Dilution	Catalogue Number
Caspase-1	Adipogen	1:1000	AG-20B-0042-C100
GAPDH	CST	1:5000	2118S
IL-1b	R&D Systems	1:1000	AF-401-NA
NLRP3 (Cryo-2)	Adipogen	1:1000	AG-20B-0014-C100
NLRP3 (NALPY-3b)	Enzo Life Sciences	1:1000	ALX-804-819
Tubulin	Sigma	1:2000	T5168
MerTK	R&D Systems	1:400	AF591
pMerTK	Invitrogen	1:400	PA5-143631
pAkt	CST	1:1000	4060S
ASC	Santa Cruz Biotechnologies	1:1000	Sc-22514-R
MerTK	BioLegend	1:200	151523
CD11b	BioLegend	1:200	101242
F4/80	BioLegend	1:200	123108
CX3CR1	BioLegend	1:200	149037
pro-IL-1b	Invitrogen	1:200	25-7114-80
Ly6G	BioLegend	1:200	127628
Ly6C	BioLegend	1:200	128008
UltraComp eBeads	Invitrogen	1:1000	01-2222-42
Fc Block	BioLegend	1:200	101320

4.2 Secondary antibodies

Reagent	Source	Dilution	Catalogue Number
Goat anti-mouse HRP	Jackson Immuno/Stratech Scientific	1:5000	115-035-146
Goat anti-rabbit HRP	Jackson Immuno/Stratech Scientific	1:5000	111-035-144
Bovine anti-goat HRP	Jackson Immuno/Stratech Scientific	1:5000	805-035-180

4.3 Functional grade antibodies

Reagent	Source	Catalogue Number
anti-mouse GM-CSF (inVivoMAb)	BioXCell	BE0259
anti-mouse IL-10R (inVivoMAb)	BioXCell	BE0050
Rat IgG2a isotype control (inVivoMAb)	BioXCell	BE0089

4.4 Biological samples

Reagent	Source	Catalogue Number
Human Blood	NHS Blood Bank Oxford	N/A

4.5 Chemicals, peptides, and recombinant proteins

Reagent	Source	Catalogue Number
20% SDS solution	Bio-Rad	1610418
4-20% Miniprotean TGX precast 12-well/15-well gel	Bio-Rad	4568095/4568096
4x Laemmli Sample Buffer	Bio-Rad	1610747
Actinomycin D	Sigma	A1410-2mg
Cytocholasin D	R&D Systems	1233/1
Collagenase D	Roche	11088858001
DNAse I	EMD Millipore	260913-10MU
ABT737	Stratech	A8193-APE
S63845 (MCL1i)	Stratech	S8383-SEL-1mg
Bovine serum albumin	Sigma	A7906-100g
DMSO	Sigma	D2650-100ml
E. Coli LPS K12 ultrapure	Invivogen	Tlrl-peklps
ECL Clarity	BioRad	1705061
ECL Clarity Max	Biorad	1705062
Ethanol	VWR	437433T
HEPES	Thermofisher Scientific	15630056
Lipofectamine RNAiMax	Invitrogen	13-778-075
Lipofectamine-2000	Invitrogen	11668019
Lipofectamine-3000	Invitrogen	L3000008
MCC950	Merck	538120
MfeI enzyme	New England Biolabs	R3589S
MSU	Invivogen	Tlrl-msu
Nigericin	Sigma Aldrich	N7143-5mg

Non-fat milk powder	VWR	84615.05
Protein ladder	Bio-Rad	1610394
Recombinant human M-CSF	Immunotools/Biolegend	11343118 / 574806
Recombinant mouse TNF	Biolegend	575204
Recombinant mouse GM-CSF	Biolegend	576306
5X First Strand Buffer	Takara	S4992
DTT	Takara	S4994
SMART MMLV RT	Takara	S4990
Oligo dT	Invitrogen	58862
UltraPure Distilled Water	Invitrogen	109770-035
dATP	New England BioLabs	N0440S
dGTP	New England BioLabs	N0443S
dCTP	New England BioLabs	N0441S
dTTP	New England BioLabs	N0442S
Cytofix	BD Biosciences	554655
Cytofix/Cytoperm	BD Biosciences	51-2090KZ
Perm/Wash	BD Biosciences	51-2091KZ

4.6 Cell culture reagents

Reagent	**Source**	**Catalogue Number**
DMEM	Thermofisher Scientific	41965039
RPMI	Thermofisher Scientific	21870076
IMDM	Thermofisher Scientific	21980032
100x Penicillin/Streptomycin/Glutamine	Thermofisher Scientific	10378016
Foetal Bovine Serum (low-endotoxin)	Thermofisher Scientific	26140079
Ficoll Paque	VWR	GE17-1440-02
Trypsin-EDTA	Corning	25-051-CI
PBS	Thermofisher Scientific	10010023
Opti-MEM	Thermofisher Scientific	31985070

4.7 Commercial assays and kits

Reagent	**Source**	**Catalogue Number**
Cytox96 nonradioactive cytotoxicity assay	Promega	G1780
Propodidium Iodide	Sigma-Aldrich	P4864-10ML
Mouse IL-1β ELISA	Invitrogen	88-7013-77
Mouse TNF ELISA	Invitrogen	88-7324-77

Human IL-1β ELISA	Invitrogen	88-7261-77
Human TNF ELISA	Invitrogen	88-7346-88
Mouse IL-18 ELISA	Invitrogen	BMS618-3TEN
CD14+ monocyte selection kit	Invitrogen	8802-6834-74
EasySep Mouse Neutrophil Enrichment Kit	StemCell	19762A

4.8 Mouse strains

Mouse/Cell line	**Source**	**Catalogue Number**
C57BL/6J mice	Charles River	RRID:IMSR_JAX:00 0664
WT control and TNFR1-KO BMDMs	Gift from Prof. Richard Williams, University of Oxford	N/A
WT control $CX_3CR1^{CreER/+}MerTK^{fl/fl}$	Gift from Prof. Mariola Kurowska-Stolarska, University of Glasgow	N/A

5. Methods

5.1 Computational methods

Mouse synovial macrophage data from Culemann et al. (GEO SuperSeries GSE134691)[1] were obtained, with processed barcodes, gene expression matrices, and gene annotations provided by Prof. Gerhard Krönke (University of Erlangen). The mouse synovium serum-transfer dataset from Wei et al. (GEO SuperSeries GSE145286)[2] and the human total synovial cell dataset from Alivernini et al. (EMBL-EBI accession E-MTAB-8322)[3], including barcodes, matrices, and gene lists, were downloaded. These datasets were imported into R Studio using Seurat's Read10X() function to create sparse matrices of gene expression, and individual Seurat objects were created for each sample with the CreateSeuratObject() to store raw counts and metadata while applying initial filters for low-quality cells or genes. Quality control removed cells with high mitochondrial gene content, low feature counts (suggesting poor quality), or excessive features (indicating potential doublets), with human dataset thresholds following Alivernini *et al.*'s study. Data integration was achieved by normalizing raw counts with NormalizeData(), identifying variable genes with FindVariableFeatures(), performing dimensionality reduction via RunPCA(), and applying RunHarmony() to correct batch effects, producing integrated embeddings for downstream clustering with FindNeighbors() and FindClusters(), visualization with RunUMAP(), and marker identification with FindMarkers(), enabling comprehensive analysis of synovial macrophage populations.

5.2 Mice

Wildtype (WT) C57Bl/6 mice were purchased from Charles River and housed in specific-pathogen free facility at the University of Oxford on a 12 h day-night cycle.

TNFR1$^{-/-}$ and WT matched control bone marrow was gifted from Prof. Richard Williams (University of Oxford, UK). $CX_3CR1^{CreER/+}MerTK^{fl/fl}$ and WT matched control bone marrow was gifted from Prof. Mariola Kurowska-Stolarska (University of Glasgow, UK). All mouse experiments and tissue isolations follow the ethical standards and regulations set by the Home Office and the University of Oxford.

5.3 Bone marrow collection

Bone marrow was obtained by extracting both hind limbs from mice. Excess soft tissue was carefully dissected away, and the bones were disinfected using 70% ethanol. The ends of the femurs and tibias were trimmed, and the marrow was expelled using syringes fitted with 30 G needles, filled with 10 mL of complete Dulbecco's Modified Eagle Medium (cDMEM), which was enriched with 10% heat-inactivated foetal bovine serum (FBS), 20 mM HEPES, 100 units/mL penicillin, 100 µg/mL streptomycin, and 58.4 µg/mL glutamine. The extracted bone marrow was gathered in 5 mL of cDMEM and centrifuged. The supernatant was discarded, and the resulting cell pellet was either immediately used for differentiation studies or cryopreserved as bone marrow in 2 mL of freezing medium (90% FBS with 10% dimethyl sulfoxide, DMSO) per mouse.

5.4 Generation of bone marrow derived macrophages (BMDMs)

To produce bone marrow-derived macrophages (BMDMs), approximately $15x10^6$ bone marrow cells were cultured in 10 cm circular petri dishes containing 10 mL of complete Dulbecco's Modified Eagle Medium (cDMEM), formulated with 10% heat-inactivated foetal bovine serum (FBS), 100 units/mL penicillin, 100 µg/mL streptomycin, 5.84 µg/mL glutamine, and 1% HEPES, supplemented with 50 ng/mL

recombinant human M-CSF (rhM-CSF). The cells were incubated at 37°C with 5% CO_2. On day 5, 5 mL of additional cDMEM containing 50 ng/mL rhM-CSF was added to the cultures. On day 7, adherent cells were detached using cold PBS, replated, and stimulated on day 8.

For granulocyte-macrophage BMDM (GM-BMDM) cultures, $15x10^6$ bone marrow cells were cultured in 10 mL of cDMEM supplemented with 20 ng/mL recombinant murine GM-CSF (rmGM-CSF) at 37°C with 5% CO2. Additional 5 mL of cDMEM with 20 ng/mL rmGM-CSF was added on days 2 and 5. On day 7, non-adherent cells were discarded (unless otherwise stated), and adherent cells were harvested using cold PBS and stimulated on day 8.

5.5 Human CD14+ monocyte isolation

Blood cones from healthy donors were obtained from NHS Oxford blood bank. Peripheral blood mononuclear cells were isolated using a centrifugation based Ficoll gradient. CD14+ monocytes were positively selected using the CD14+ magnetic bead selection kit from Invitrogen.

5.6 Generation of human monocyte-derived macrophages (HMDMs)

To generate HMDMs, $15x10^6$ CD14+ monocytes were cultured in 10 cm circular petri dishes in 10 mL complete RPMI (10% heat inactivated FBS, 100 units/mL penicillin, 100 ug/mL streptomycin, 5.84 ug/mL glutamine, and 1 % HEPES) with 100 ng/mL rhM-CSF at 37^{o}C in 5% CO_2. On day 5, cultures were refreshed with 5 mL of complete medium with 100 ng/mL rhM-CSF. On day 7, adherent cells were lifted with cold PBS, reseeded, and prepared for stimulation on day 8.

5.7 Cell stimulations

5.7.1 NLRP3 inflammasome activation

BMDMs were plated at a density of $1x10^6$ cells/mL in cDMEM. HMDMs were plated at $0.7x10^6$ cells/mL in cRPMI. Cells were stimulated with 100ng/mL ultrapure *Escherichia coli* K12 LPS or 100ng/mL TNF-α for 30 min (acute), 4 h (peak), or 24 h (chronic) unless otherwise indicated, and 7.5 μM nigericin or as indicated. The transcription inhibitor Actinomycin D was administered at 5 μg/ml, 30min prior to priming. The NLRP3 inhibitor MCC950 was applied at a concentration of 10 μM, 30 min prior to signal 1.

After stimulation, cells were centrifuged at 1500 rpm for 3 min at room temperature, and the supernatants were harvested. The cells were then lysed using SDS lysis buffer (2% SDS, 66 mM TRIS, pH 7.4). A portion of the supernatant was allocated for cell viability assessment, while the remaining supernatant and cell lysates were stored frozen for subsequent analysis.

5.7.2 Pyrin inflammasome activation

Pyrin inflammasome activation was triggered in BMDMs with 1 – 1.5 μg/ml *Clostridium difficile* Toxin B (TcdB) for 2.5 h.

5.7.3 Vaccine adjuvants

Differentiated HMDMs were plated at a density of $0.7x10^6$ cells/mL in complete RPMI with 100 ng/mL rh-MCSF. Adjuvants SQ, SMQ, LQ, LMQ were manufactured by the Vaccine Formulation Institute (VFI) as described previously[5]. The cells were treated with VFI adjuvants for 6 h (1:20 dilution). Positive control NLRP3 activation

was triggered by priming with 100 ng/mL ultrapure *Escherichia coli* K12 LPS for 4 h followed by stimulation with 10 μM nigericin 2 h.

5.8 Efferocytosis stimulations

5.8.1 Neutrophil isolation

Neutrophils were isolated from bone marrow progenitors. Bone marrow progenitors were collected as described above (5.3 Bone Marrow Collection). Neutrophils were isolated using the StemCell Technologies Neutrophil Enrichment kit using negative selection. Neutrophils were stained with CD11b and Ly6G to confirm their identity.

5.8.2 Apoptotic neutrophil generation

Apoptotic neutrophils were generated by treating freshly isolated neutrophils with 250 nM of ABT737 and MCL1i in serum-free medium for 2.5 h. Apoptosis was confirmed with Live/Dead staining and visual inspection.

5.8.3 Feeding of apoptotic cells to BMDMs

Apoptotic neutrophils were harvested, apoptotic drugs were washed away, and pellets were resuspended in serum-free medium and fed to recipient BMDMs at a ratio of 1.5:1 for 2.5 h +/- pre-treatment with 10 ug/mL Annexin V. Media was then aspirated to remove apoptotic cells and replaced with complete BMDM media. BMDMs were left for 16h before inflammasome stimulation.

5.9 Cell viability assays

5.9.1 Lactate dehydrogenase (LDH)

Cell death was assessed by measuring lactate dehydrogenase (LDH) release with the Cytox96 non-radioactive cytotoxicity assay (Promega). Fresh cell-free supernatants from stimulated cells were combined with LDH reagent in equal volumes and incubated until the colorimetric signal from the lysis control reached full development. The reactions were halted by adding an equivalent volume of stop solution (Promega), and absorbance readings were taken at 490 nm and background at 650 nm using a FLUOstar Omega microplate reader. The percentage of LDH release was determined by comparing the signal to that of untreated control samples fully lysed with 0.1% Triton-X100, representing 100% cell lysis.

5.9.2 Propidium iodide (PI)

Propidium iodide (PI) uptake was used to assess cell membrane permeabilization. Cell stimulations were conducted in 90 µl of Opti-MEM, and at the time of inflammasome activation signal 2, 10 µl of Opti-MEM containing PI was added, resulting in a final PI concentration of 1 µg/ml. Fluorescence measurements were taken every 30 to 60 min using a FLUOstar Omega microplate reader, with excitation at 544 nm and emission at 620/10 nm. The percentage of PI uptake was determined by comparing the fluorescence signal to that of untreated control samples fully lysed with 0.1% Triton-X100, which represented 100% cell lysis.

5.10 Immunoblotting

Cells were lysed in denaturing SDS lysis buffer (2% SDS, 66 mM TRIS, pH 7.4). Samples were mixed with 4x Laemmli buffer and 20 mM DTT, then boiled at 95°C for

5 min. Proteins were separated on 4-20% SDS-PAGE gradient gels and transferred to nitrocellulose membranes using a semi-dry transfer system (Trans-Blot Turbo, Bio-Rad). Membranes were blocked in 5% non-fat milk (NFM) in TBS-T (50 mM TRIS/HCl, 150 mM NaCl, pH 7.6, 0.1% Tween-20) for 1 h at room temperature. Primary antibodies (see Materials) were applied in 2.5% NFM in TBS-T with 0.02% sodium azide overnight at 4°C. The following day, membranes were washed with TBS-T for 1 h, then incubated with HRP-conjugated secondary antibodies (1:5000 dilution) in 2.5% NFM in TBS-T for 1 h at room temperature. After washing with TBS-T for 1 h, membranes were treated with chemiluminescence reagents (ECL or ECL-plus (Bio-Rad)) and developed on X-ray films. Membranes were reused by incubating with different primary antibodies as described. When needed, HRP was quenched using 30% hydrogen-peroxide or antibodies were stripped using stripping buffer (Thermofisher) for 30 min at room temperature, followed by 30 min TBS-T washing and re-blocking with 5% NFM in TBS-T for 1 h before reprobing with new primary antibodies.

5.11 Enzyme-linked immunosorbent assay (ELISA)

Cytokines in cell-free supernatants were measured using enzyme-linked immunosorbent assays (ELISA). Mouse IL-1β, mouse TNF-α, mouse IL-18, human TNF-α, and human IL-1β were quantified with ELISA kits as per the manufacturer's guidelines (Invitrogen). High-binding 96-well plates (Corning) were coated with coating buffer overnight at 4°C. The plates were washed three times with wash buffer (PBS containing 0.05% Tween-20) and blocked for 1 h at room temperature using ELISA blocking buffer. Samples and standards were added to the plates and incubated for 2 h. After washing, biotin-conjugated secondary antibodies were applied for 1 h, followed

by another wash. Plates were then incubated with HRP-conjugated streptavidin for 30 min. Following a final wash, tetramethylbenzidine (TMB) solution was added to produce a colorimetric signal, which was halted by adding an equal volume of 1 M sulfuric acid. Absorbance was read at 450 nm and 570 nm on a FLUOstar Omega microplate reader.

5.12 Flow cytometry

5.12.1 Extracellular staining

Cells were harvested with cold PBS and spun down at 400 xg for 8 min at 4°C. All remaining steps were performed on ice. All procedures involving fluorochromes were conducted in the dark to prevent photobleaching. To exclude dead cells, samples were incubated with a LIVE/DEAD® in PBS for 10 min in the dark, followed by two washes with PBS (centrifugation at 400 g for 5 min, supernatant discarded, and pellet resuspended). Next cells were treated with Fc block (1:200) in PBS with normal mouse serum (NMS) (1:200 dilution) for 15 min. Without washing, cells were spun down and the supernatant discarded, then incubated with extracellular staining antibodies (1:200 unless stated otherwise) and NMS (1:200) for 30 min on ice in FACS buffer (PBS supplemented with 2% FBS). Intracellular staining (if required) followed (5.12.2 Intracellular staining). Cells were then washed twice with PBS and fixed in 4 % paraformaldehyde for 5 min at room temperature before centrifugation and resuspension in 200µl PBS.

Controls included an unstained sample to assess autofluorescence, single-color bead controls for compensation to correct spectral overlap, and fluorescence minus one (FMO) controls to establish gating boundaries.

5.12.2 Intracellular staining

For intracellular staining, cells were fixed and permeabilized using a fixation/permeabilization buffer (BD Cytofix/Cytoperm) for 30 min in the dark. Cells were washed twice with permeabilization wash buffer, and intracellular staining antibodies (1:200) were added in permeabilization buffer. Samples were incubated for 30 min in the dark, followed by two washes with permeabilization wash buffer and resuspension in FACS buffer.

5.12.3 Sample acquisition and analysis

Samples were acquired on a LSRII cytometer and data were analysed using FlowJo software. Gating strategies involved identifying single cells using forward scatter area (FSC-A) versus height (FSC-H) or side scatter area (SSC-A) versus height (SSC-H), selecting live cells based on viability dye exclusion, and defining populations of interest based on marker expression. Population frequencies, fluorescence intensities, or other parameters were quantified and exported as needed.

5.13 Transcriptional analysis of cell cultures with quantitative PCR or bulk RNA sequencing

5.13.1 RNA extraction

Total RNA was extracted from cells using the RNeasy Mini Kit (Qiagen) according to the manufacturer's instructions. Cells were lysed in lysis buffer supplemented with β-mercaptoethanol to inactivate RNases. Lysates were mixed with an equal volume of 70% ethanol and applied spin columns. Columns were washed with provided wash buffers to remove contaminants, and RNA was eluted in 30µL of RNase-free water. RNA concentration and purity were assessed using a NanoDrop

spectrophotometer (Thermo Fisher Scientific), with A260/A280 ratios between 1.8 and 2.0 considered acceptable. RNA was stored at -80°C until use or shipment for external bulk RNA sequencing by NovoGene.

5.13.2 Complementary DNA (cDNA) synthesis

Complementary DNA (cDNA) was synthesized from 1000 ng of total RNA using a reverse transcription kit (Bio-Rad) following the manufacturer's protocol. RNA samples were brought up to a volume of 10.5 µl with ultrapure RNAase free water, mixed with 1 µl oligo-dT, incubated at 70°C for 3 min in a thermocycler, and immediately cooled on ice. RNA was then mixed with 4 µl 5X reaction buffer, 2µl dNTPs, and 2µl 100nM DTT, followed by 0.5µl reverse transcriptase (RT).

The mixture was incubated at 42°C for 30 min for cDNA synthesis, and 70°C for 15 min to inactivate the RT enzyme. The resulting cDNA was diluted with 200µL nuclease-free water and stored at -20°C until use.

5.13.3 Quantitative real-time PCR (qPCR)

Quantitative real-time PCR (qPCR) was performed using SYBR Green-based reagents (PowerUp SYBR Green Master Mix, Applied Biosystems) on a real-time PCR system (Viia7, ThermoFisher). Reactions were prepared in a 384-well plate with a 10 µL volume per well containing 5 µL of 2x SYBR Green Master Mix, 2 µL forward + reverse primer mix 3 uL and, 2 µL of diluted cDNA in nuclease-free water. The cycling conditions consisted of an initial denaturation at 95°C for 2 min, followed by 30 cycles of 95°C for 15 s and 60°C for 1 min, with fluorescence acquisition at the end of each extension step. A melt curve was generated post-amplification (95°C for 15 s, 60°C for 1 min, and a gradual increase to 95°C) to verify amplicon specificity.

Each sample was run in triplicate, and no-template controls (NTCs) and no-reverse-transcriptase controls (NRTs) were included to detect contamination and genomic DNA amplification, respectively. Relative gene expression was calculated using the 2^(-ΔΔCt) method, with target gene expression normalized to a HPRT. Data were analysed in Microsoft Excel and GraphPad Prism.

5.14 Antigen induced arthritis (AIA)

C57BL/6 WT mice were housed in specific-pathogen free facilities at the University of Oxford. Mice were immunized with a 100ul emulsion of 1.66mg/mL complete Freund's adjuvant (CFA) and 1mg/mL methylated bovine serum albumin (mBSA) and left for 21 days. The mBSA/CFA emulsion was prepared using the POWER-kit (BTB emulsions). One day before intra-articular challenge, mice were given either an anti-GM-CSF monoclonal antibody (MP1-22E9) or an isotype control antibody (150 ug in 100 ul PBS). The following day, mBSA was administered via intra-articular injection. Oedema measurements were conducted using a calliper and pain was quantified using the BioSeb weight-bearing system and software.

5.15 Isolation of murine synovium

On day 2 or day 4 after mBSA intra-articular challenge, mice were euthanised and synovial cells were isolated for flow cytometry staining. The affected hind limb was collected, and skin and muscle tissues surrounding the knee joint were carefully removed. The synovium was excised by making precise incisions around the joint capsule, avoiding contamination with cartilage or bone. Isolated synovial tissue was placed in cold cRPMI.

For tissue digestion, synovial samples were minced into small fragments using sterile scissors and transferred to a digestion buffer consisting of RPMI supplemented with collagenase D (Roche) and DNase I (EMD Millipore). The tissue was incubated at 37°C Celsius with gentle agitation for 30 min to facilitate enzymatic dissociation. The resulting cell suspension was filtered through a 70 µm nylon cell strainer to remove undigested debris and washed by centrifugation at 400 xg for 5 min at 4°C. The supernatant was discarded, and the cell pellet was resuspended in PBS.

5.16 Statistical Analysis

Unless stated otherwise, *in vitro* and *in vivo* data were analysed using GraphPad Prism. We tested for normal distribution and homogeneity of variance of our *in vivo* data and used one-way ANOVA for comparison between two groups and two-way ANOVA with multiple column comparisons for greater than two group comparisons. We did not assume a normal distribution with our *in vitro* data and used the non-parametric equivalents provided in GraphPad Prism. In all experiments, * $p<0.05$, ** $p<0.01$, *** $p<0.001$, **** $p<0.0001$.

6. Chapter 1 | Inflammasome expression is restricted to recruited inflammatory myeloid cells in mouse and human inflammatory arthritis

6.1 Introduction

6.1.1 Single-cell RNA sequencing (scRNAseq) in RA

Unravelling the mechanisms of complex tissue diseases including rheumatoid arthritis (RA) demands single-cell resolution across space and time. Single-cell RNA sequencing (scRNAseq) has transformed immunology by capturing the transcriptional profiles of individual cells, revealing heterogeneity obscured in bulk analyses. This approach has illuminated dynamic pathways, implicated diverse cell types, and tracked pathology through stages such as health, disease initiation, peak inflammation, resolution, persistence, and flares. In RA, scRNAseq identified two distinct fibroblast populations: sub-lining fibroblasts that amplify synovial inflammation and lining-layer fibroblasts that drive bone erosion and cartilage destruction[1]. Similarly, it has uncovered myeloid population diversity in the joint under healthy and diseased conditions.

The 2019 Accelerating Medicines Partnership (AMP) RA dataset integrated scRNAseq and mass cytometry to compare synovial cell populations in RA versus osteoarthritis (OA)[2]. It revealed an enrichment of IL-1B+ pro-inflammatory monocytes in RA synovium, suggesting a disease-specific role distinct from OA[2]. *Ex vivo* studies further showed that RA macrophages produce IL-1β and HB-EGF to enhance fibroblast invasiveness, reinforcing their pathogenic potential[3].

Historically, synovial macrophages were viewed as primary inflammatory drivers in RA. However, a landmark study using the serum-transfer-induced arthritis

(STIA) model redefined their role, identifying lining-layer tissue-resident macrophages as a homeostatic barrier[4]. Marked by CX_3CR1 expression, these cells form tight junctions to shield the intra-articular space from inflammatory infiltration in health[4]. In STIA, this barrier collapses during disease onset, indicating sensitivity to arthritic serum and disrupted joint homeostasis. The study also showed these macrophages are rarely replenished by circulating monocytes, instead relying on local sub-lining macrophage renewal, challenging the notion of synovial macrophages as solely pro-inflammatory.

Building on this, Alivernini *et al.* (2020) used minimally invasive biopsies and scRNAseq to profile synovial tissue macrophages (STMs) across RA states: active, treatment-naïve, remission, and healthy controls (histologically normal donors post-meniscal surgery)[5]. STMs were classified by MerTK (efferocytosis receptor) and CD206 (mannose receptor) expression. MerTK+ CD206+ STMs dominated in healthy synovium and remission RA, with tissue-resident TREM2-intermediate (sub-lining) and TREM2-high (lining) subsets displaying anti-inflammatory, pro-resolving profiles. Conversely, MerTK- CD206- STMs, enriched in active and flaring RA, exhibited pro-inflammatory signatures, including elevated *TNF*, *IL-1B*, *IL-6*, and chemokines (*CCL3*, *CCL4*, *CXCL8*). Longitudinal analysis revealed that a MerTK+/MerTK- ratio ≤2.5 predicted flares upon treatment withdrawal, while a higher ratio correlated with sustained remission, linking myeloid abundance to clinical outcomes[5].

The AMP2 dataset advanced this further with cell-type abundance phenotypes (CTAPs), proposing RA as a spectrum of cellular compositions rather than a uniform disease[6]. Some CTAPs reflect myeloid-driven pathology, others adaptive immunity or stromal activation, and complex profiles like the EFM (endothelial, fibroblast, myeloid) CTAP involve multiple cell types. I hypothesize that inflammasome activation may

drive pathology in specific CTAPs, potentially explaining the inconsistent efficacy of IL-1 blockade. Collectively, scRNAseq has highlighted contributions beyond adaptive immunity including fibroblasts, tissue-resident macrophages (which maintain joint health and resolution), and monocyte-derived macrophages (enriched in disease with pro-inflammatory cytokines and chemokines).

6.1.2 Spatial transcriptomics in RA

Pairing single-cell transcriptomics with spatial data enhances understanding of where, when, and in which cell types specific pathways activate within tissues. In 2023, Rudensky *et al.* used spatial transcriptomics to map an IL-1β response signature predominantly to the lining compartment in RA synovium, implicating IL-1β in lining fibroblast activation[7]. The reason for such a selective location of IL-1β response signature was unclear, as all synovial fibroblasts express similar levels of IL-1 receptor (IL-1R)[2]. A possible answer emerged when further analysis revealed co-localisation of lining layer fibroblasts with inflammatory macrophages in RA[7]. Given IL-1β's role in inducing matrix metalloproteinases (MMPs), this suggests IL-1 inhibition could mitigate joint destruction driven by lining fibroblasts[1].

6.2 Aims

We sought to characterize inflammasome expression in human and murine arthritis using publicly available and in-house time-resolved scRNAseq datasets, addressing:

1) Where, when, and in which cell types NLRP3 and other inflammasomes are expressed in health and disease.

2) Transcriptional differences in inflammasome profiles between human RA and murine K/BxN STIA.

6.3 Results

6.3.1 NLRP3 inflammasome expression is restricted to macrophages in the human and mouse synovium

To investigate the expression of NLRP3 and other inflammasomes in the synovium under steady-state and inflammatory conditions, I analysed scRNAseq datasets from human RA and murine STIA. These included publicly available datasets and an in-house generated dataset (Figure 2)[4,5,8]. The human dataset, from Alivernini *et al.*, comprised 40,057 cells from 20 patients across healthy, treatment-naïve RA, remission RA, and treatment-resistant RA states, collected from cohorts in Oxford and Glasgow (Figure 2a).

For mice, I used Wei *et al.*'s whole-synovium dataset (Figure 2b), Culemann *et al.*'s time-resolved STIA dataset of flow-sorted synovial macrophages (Figure 2c), and an in-house time-resolved STIA dataset from collaborator Adam Croft at the University of Birmingham (Figure 2d, unpublished)[4,8].

Batch effects from different patients or biological replicates were corrected using Harmony integration, with UMAP visualizations confirming substantial reduction of these effects (Figure 3a-h). In the human synovium, I identified ten transcriptionally distinct clusters, including two *CD14+ CD68+* macrophage subsets, split, very broadly at this stage, into resident *MARCO+ and recruited CCR2+* (Figure 4a, b). *NLRP3* emerged as the most highly expressed inflammasome sensor, restricted to macrophage clusters alongside *IL-1B*, while other cell types showed no

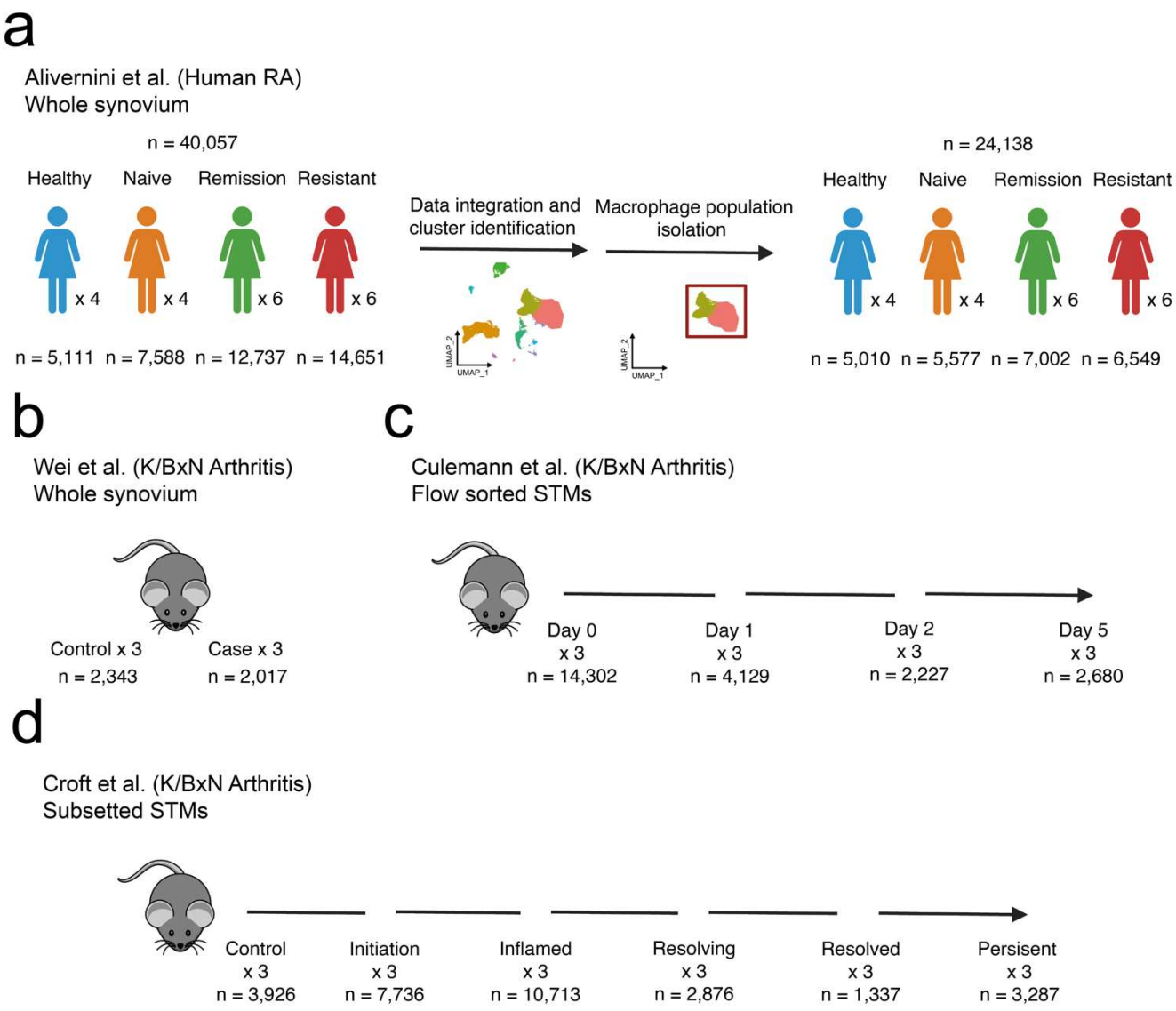

Figure 2 | Overview of scRNAseq datasets analysed in this chapter. a) Human RA disease-stratified dataset from Alivernini *et al.*, including healthy, treatment naïve, remission, and treatment-resistant RA samples. b) Murine whole-synovium dataset from Wei *et al.*, capturing synovial cell populations in K/BxN STIA. c) Murine time-resolved dataset of flow-sorted synovial tissue macrophages from Culemann *et al.*, spanning day 0 to day 5 of K/BxN STIA. d) In-house murine time-resolved dataset of pre-annotated synovial macrophage subsets from Croft *et al.*, covering control, peak, resolution, and persistent phases of K/BxN STIA.

expression (Figure 4c). Downstream components *PYCARD* (encoding the adaptor protein ASC), *CASPASE-1*, and *IL-18* were predominantly, though not exclusively, expressed in macrophages (Figure 4c). Lowly expressed sensors *MEFV*, *AIM2*, and *NLRC4* were also macrophage-specific (data not shown). *IL-1R1* was expressed by

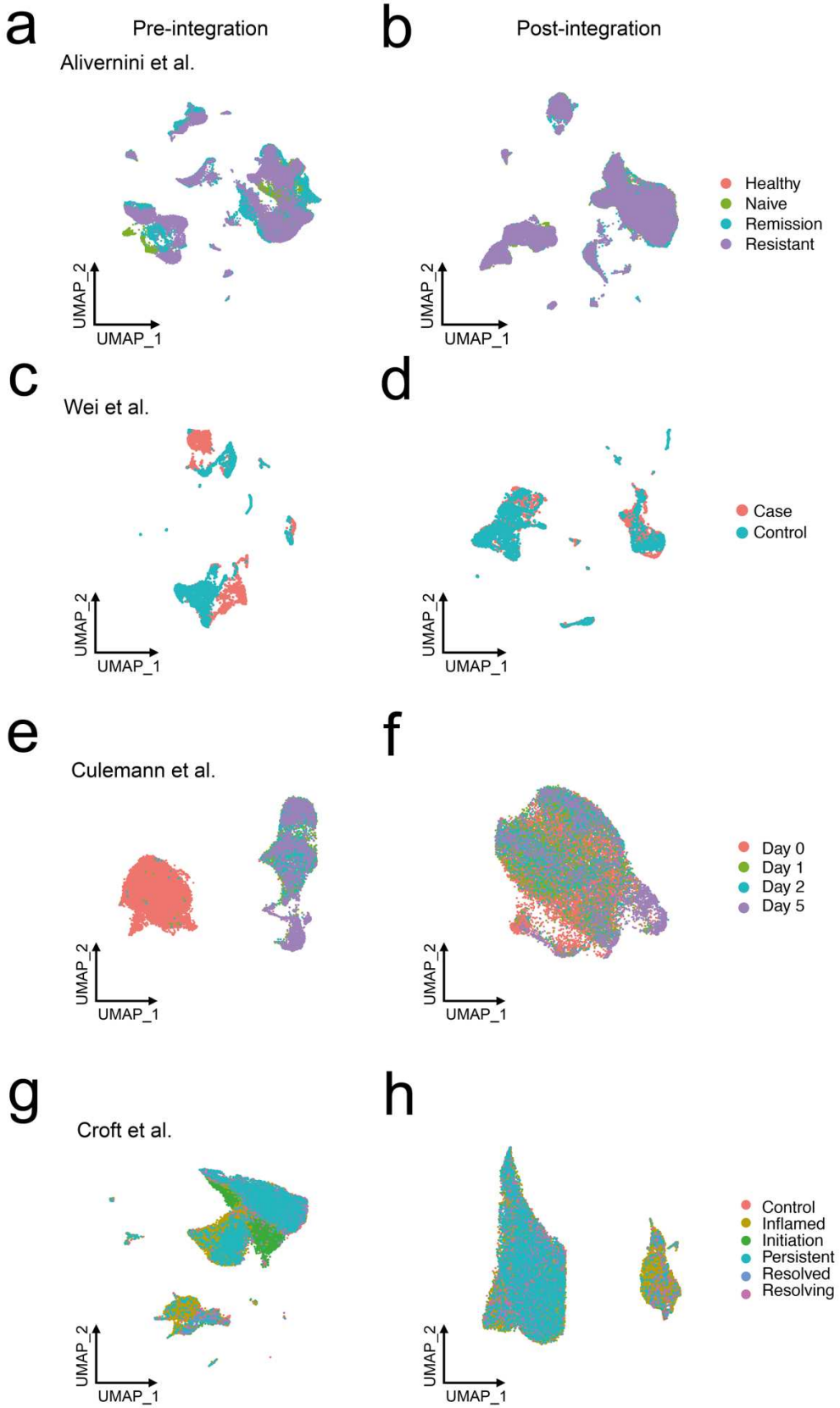

Figure 3 | Batch effect correction in scRNAseq datasets using Harmony integration. Datasets from individual patients or biological replicates were merged and integrated with Harmony to minimize batch effects, visualized via UMAP plots. a, b) Pre- and post-integration of the human RA whole-synovium dataset (Alivernini *et al.*). c, d) Pre- and post-integration of the murine K/BxN arthritis whole-synovium dataset (Wei *et al.*). e, f) Pre- and post-integration of the flow-sorted synovial tissue macrophage (STM) dataset (Culemann *et al.*). g, h) Pre- and post-integration of the synovial macrophage subset dataset (Croft *et al.*).

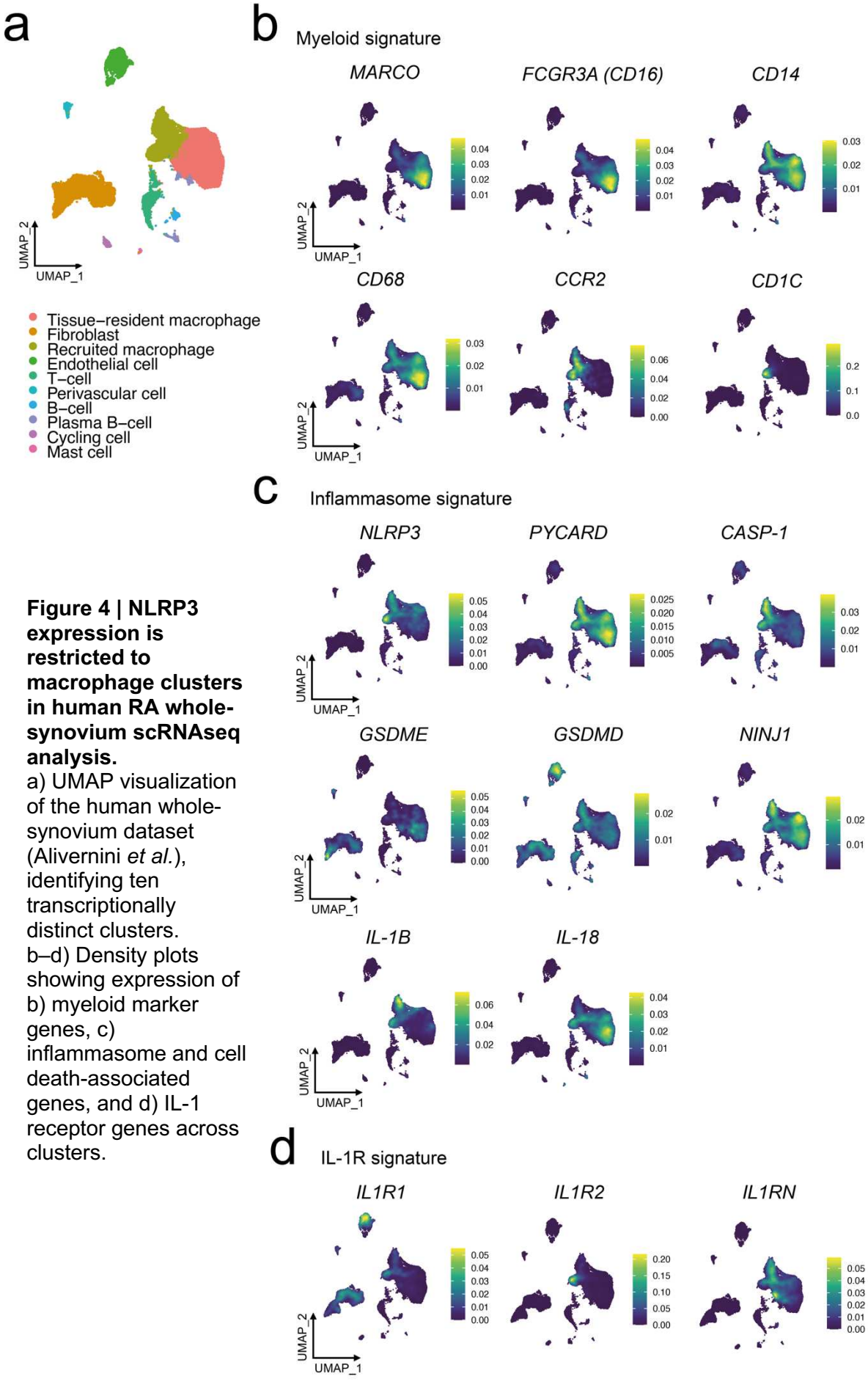

Figure 4 | NLRP3 expression is restricted to macrophage clusters in human RA whole-synovium scRNAseq analysis.
a) UMAP visualization of the human whole-synovium dataset (Alivernini *et al.*), identifying ten transcriptionally distinct clusters. b–d) Density plots showing expression of b) myeloid marker genes, c) inflammasome and cell death-associated genes, and d) IL-1 receptor genes across clusters.

most endothelial cells and fibroblasts, and the *CD1C*+ macrophage subset, whereas *IL-1R2* and *IL-1RN* were macrophage-restricted (Figure 4d).

In the murine whole-synovium dataset (Wei *et al.*), macrophages were identified by *Cd14* and *Cd68*, with monocyte-derived recruited subsets marked, like in humans, by *Ccr2* (Figure 5a,b). *Nlrp3* was the dominant inflammasome sensor, with its expression, and that of *IL-1b,* confined to macrophages, like in humans, and neutrophils, cell types captured here but absent from the human dataset (Figure 5b, c). *Pycard*, *Caspase-1*, *Ninj1* and *Il-18* expression were primarily macrophage-associated, though more diffuse (Figure 5c), while *Mefv* was macrophage-specific (data not shown). Unlike humans, *Il-1r1* was exclusively fibroblast-expressed, *Il-1r2* appeared in fibroblasts, some macrophages, and neutrophils, and *Il-1b* was restricted to macrophages and neutrophils (Figure 5d).

Across species, *NLRP3/Nlrp3* expression was highest among other inflammasome sensors, and was confined to myeloid lineage cells, establishing it as the primary synovial inflammasome sensor. Therefore, subsequent disease-stratified and time-resolved analyses focused on synovial myeloid populations. For human RA, I re-integrated 24,138 macrophage-derived cells from Alivernini *et al.* (Figure 2a). In mice, I used Culemann *et al.*'s flow-sorted synovial tissue macrophage (STM) dataset (Figure 2c), as the whole synovium dataset lacked sufficient cell numbers for detailed analysis.

6.3.2 NLRP3 and IL-1B expression peak in recruited macrophages and are suppressed in tissue-resident subsets in human RA and murine STIA

Re-integration of human macrophage clusters from Alivernini et al. revealed ten transcriptionally distinct macrophage subsets (Figure 6a), consistent with prior

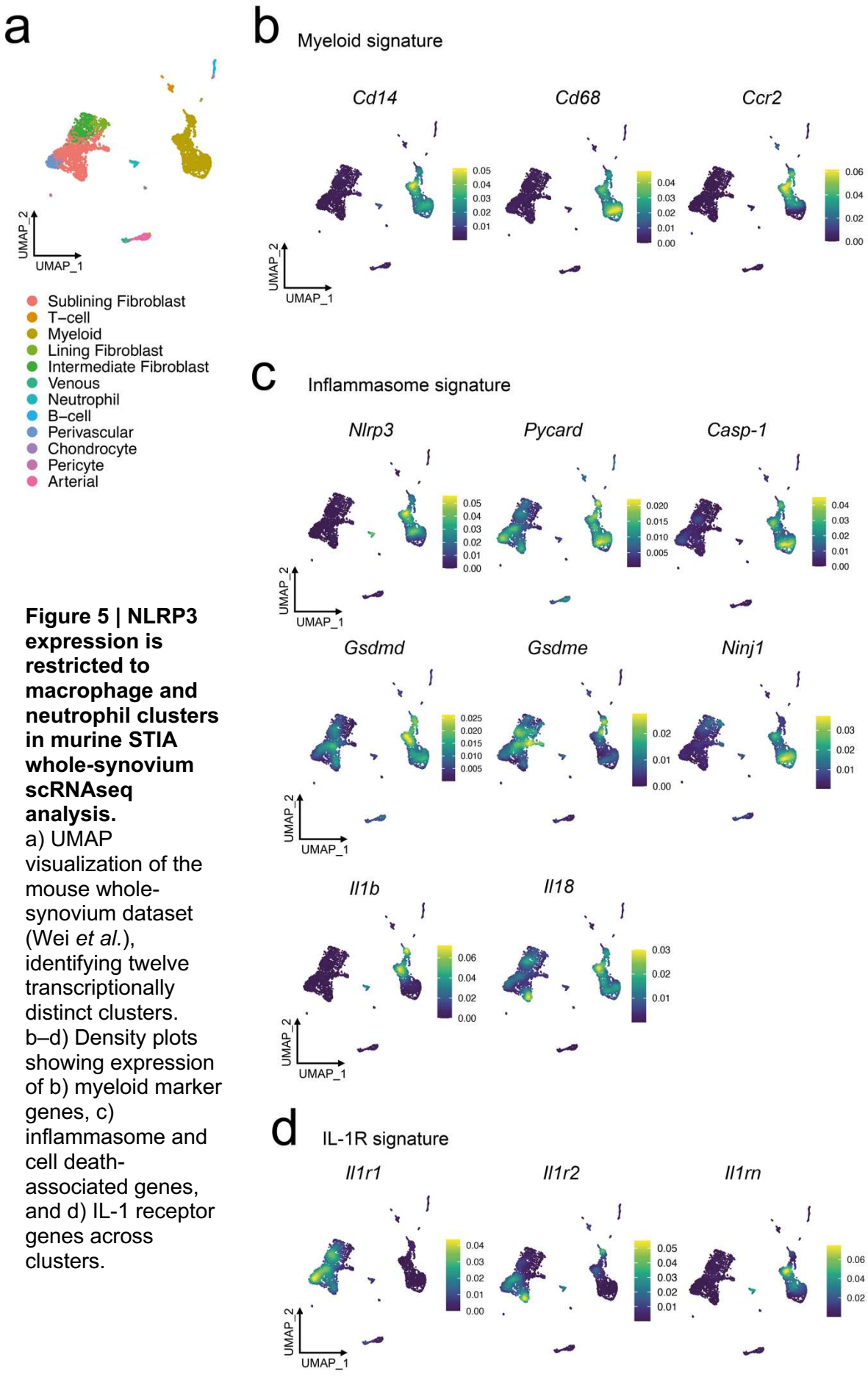

Figure 5 | NLRP3 expression is restricted to macrophage and neutrophil clusters in murine STIA whole-synovium scRNAseq analysis.
a) UMAP visualization of the mouse whole-synovium dataset (Wei *et al.*), identifying twelve transcriptionally distinct clusters. b–d) Density plots showing expression of b) myeloid marker genes, c) inflammasome and cell death-associated genes, and d) IL-1 receptor genes across clusters.

reports[5]. Within this transcriptional heterogeneity, I found two mutually exclusive gene signatures emerge: a tissue-resident signature, associated with expression of *MERTK* and *FOLR2*, and a recruited signature associated with *CCR2* expression and intermediate to high levels of *NLRP3* and *IL-1B* (Figure 6a). I found *NLRP3* expression was highest in inflammatory *(CCR2+ CSF2RA+)* recruited macrophages. (Figure 6a). NLRP3 inflammasome expression was low in tissue-resident synovial macrophages and not observed in lining layer macrophages, identified by their high expression of *MERTK*, *TREM2, FOLR2*, and *TIMD4* (Figure 6a).

In the murine STIA model (Culemann *et al.*), *Csf2ra* was broadly expressed across STMs, but other markers still clearly separated recruited *Ccr2*+ macrophages from tissue resident *Mertk*+, *Trem2*+, Folr2+ and Timd4+ clusters (Figure 6b). Like in humans, *Nlrp3* and *Il-1b* were enriched in recruited Ccr2+ macrophages, whereas tissue-resident subsets (*Mertk*+, *Trem2*+, *Timd4*+) had low *Nlrp3* expression (Figure 6b). Differential gene expression analysis confirmed transcriptional distinction between clusters, with some gene signature conservation between human tissue-resident subsets (e.g., TREM2-low, FOLR2+ LYVE1+, and TREM2-high lining) and murine subsets (e.g., LYVE1+, MHC-high, TREM2-high lining) (Figure 6c, d). Lining-layer macrophages in both species shared enriched *APOE/Apoe*, *TIMD4/Timd4*, and *VSIG4/Vsig4* expression (Figure 6c, d), suggesting a conserved tissue-resident signature despite heterogeneity.

Recruited macrophages consistently showed elevated *NLRP3/Nlrp3* and *IL-1B/Il-1b* expression. In humans, *IL-1B* appeared in three subsets (FOLR2+ ICAM1+, CD48-high S100A12+, CD1C+) (Figure 6c, 7a), while in mice, one subset (Ccr2+ Il-1b+) was particularly enriched (Figure 6d, 7b). This pattern prompted temporal

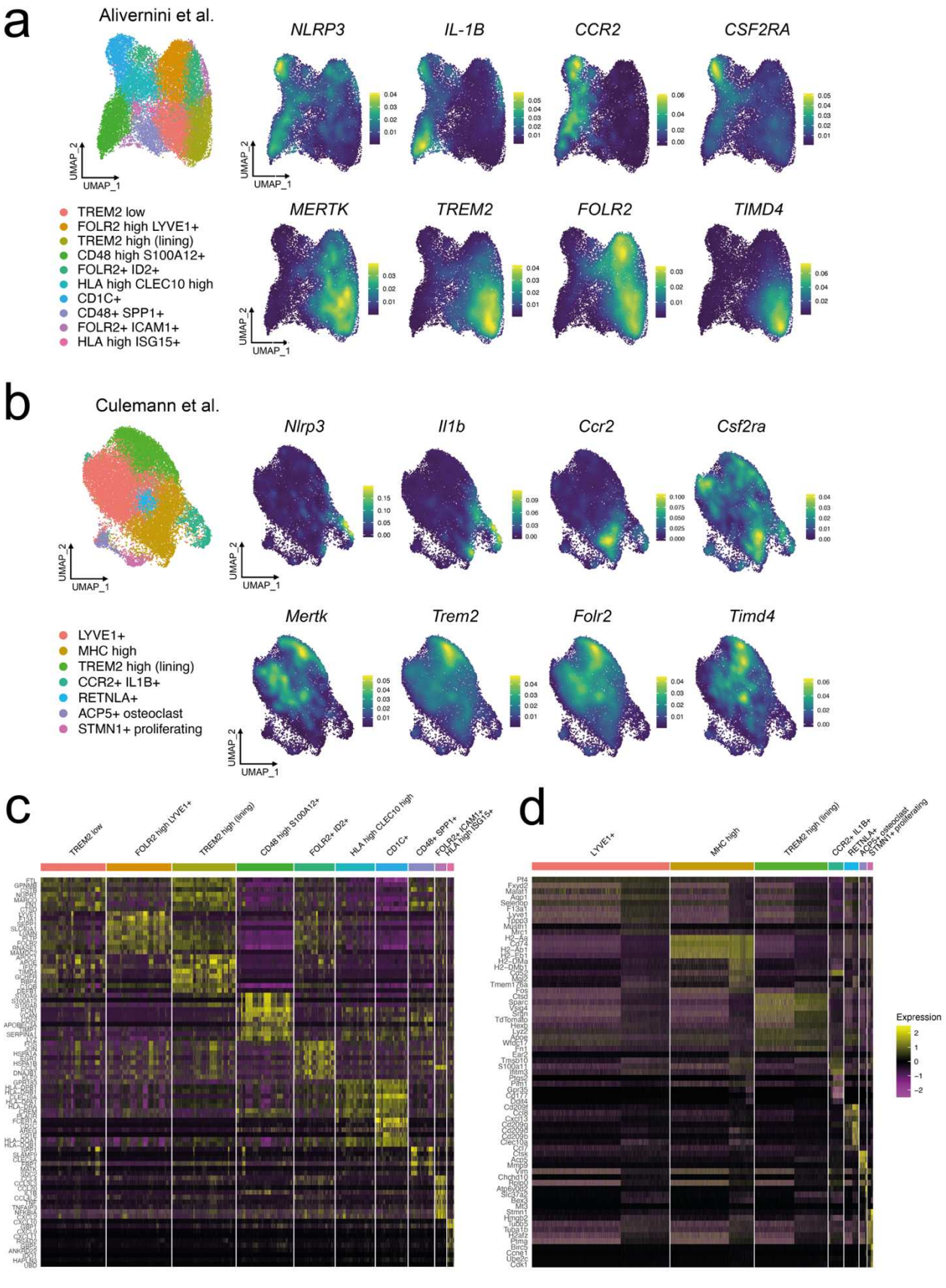

Figure 6 | NLRP3 expression is restricted to recruited macrophage clusters in scRNAseq analysis of Human RA and murine STIA.
a) UMAP visualization of ten transcriptionally distinct synovial tissue macrophage clusters from human RA (Alivernini *et al.*). b) UMAP visualization of seven transcriptionally distinct synovial tissue macrophage clusters from murine K/BxN STIA (Culemann *et al.*). c, d) Heatmaps of the top five differentially expressed genes (DEGs) per cluster in the human (c) and murine (d) datasets, respectively.

analysis of macrophage recruitment and NLRP3 expression during disease progression.

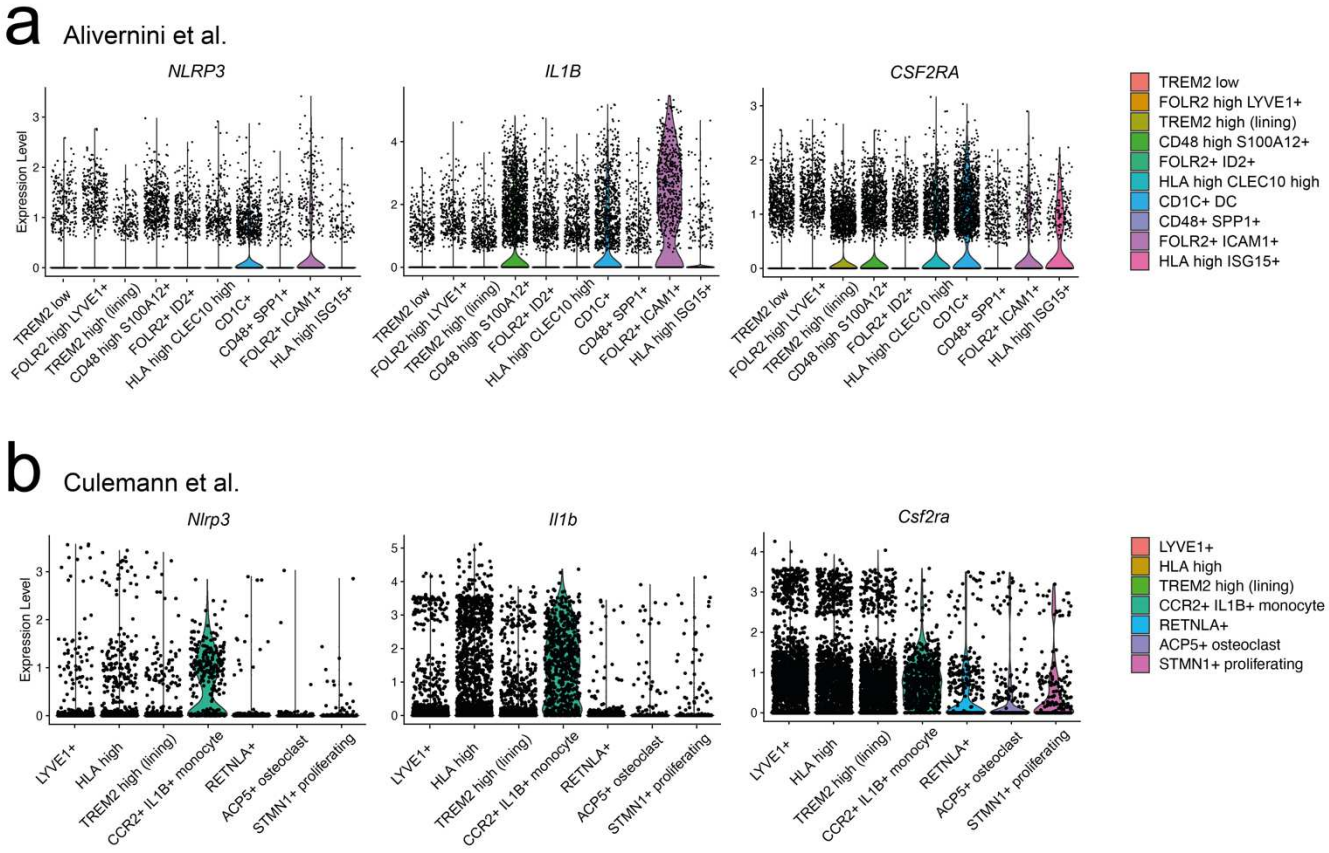

Figure 7 | NLRP3 and IL-1B expression in recruited macrophage subsets in human RA and murine STIA. a) Violin plots showing expression of NLRP3, IL1B, and CSF2RA across synovial macrophage subsets in human RA (Alivernini et al.), highlighting three recruited subsets. b) Violin plots showing expression of Nlrp3, Il1b, and Csf2ra across synovial macrophage subsets in murine K/BxN STIA (Culemann et al.), identifying one predominant cluster.

6.3.3 Recruited monocyte-derived macrophages are hallmarks of human RA and murine STIA

Time-resolved analysis of the Alivernini (human) and Culemann (murine) datasets assessed macrophage dynamics across disease states. In the healthy human synovium, recruited macrophages comprised ~12% of the population, rising to ~32% in treatment-naïve RA, ~29% in treatment-resistant RA, and ~24% in remission

RA (Figure 8a, b). I estimated the percentage of recruited macrophages by adding the relative abundance of individual recruited subclusters (HLA high ISG15+, FOLR2 ICAM1+, CD48+ SPP1+, and CD48+ S100A12+). This influx reduced the relative abundance of tissue-resident macrophages, a known RA hallmark and flare risk factor, though patient variability was notable (Figure 8c).

In murine STIA, ~95% of macrophages were tissue-resident in health, dropping to ~70% at peak disease due to the influx of Ccr2+ Il-1b+ monocyte-derived macrophages, which now made 30% of the synovium (Figure 8d, e). Both human RA and murine STIA thus feature a characteristic influx of recruited, tissue-infiltrating macrophages[2,5,9].

6.3.4 NLRP3 and IL-1B are highest during peak disease and are maintained, albeit at a lower level, during persistence in human RA and murine STIA

Both human RA and murine STIA resulted in a loss of tissue-resident macrophages relative to recruited macrophages during active disease (Figure 8).

In human RA, tissue-resident macrophages (clusters TREM2 low, TREM2 high (lining), FOLR2+ LYVE1+, and FOLR2+ ID2+) lacked *NLRP3* and *IL-1B* expression across all disease stages, though they expressed modest *IL-18*, *PYCARD*, and *GSDME* (Figure 9a). The FOLR2+ ICAM1+ subset, hypothesized as newly infiltrating due to adhesion molecule expression, showed low NLRP3 and IL-1B in health, peaking in naïve and remission RA, and remaining elevated (but reduced) in treatment-resistant RA (Figure 9a). This subset also expressed high *TNF* and *IL-6* (Figure 9a).

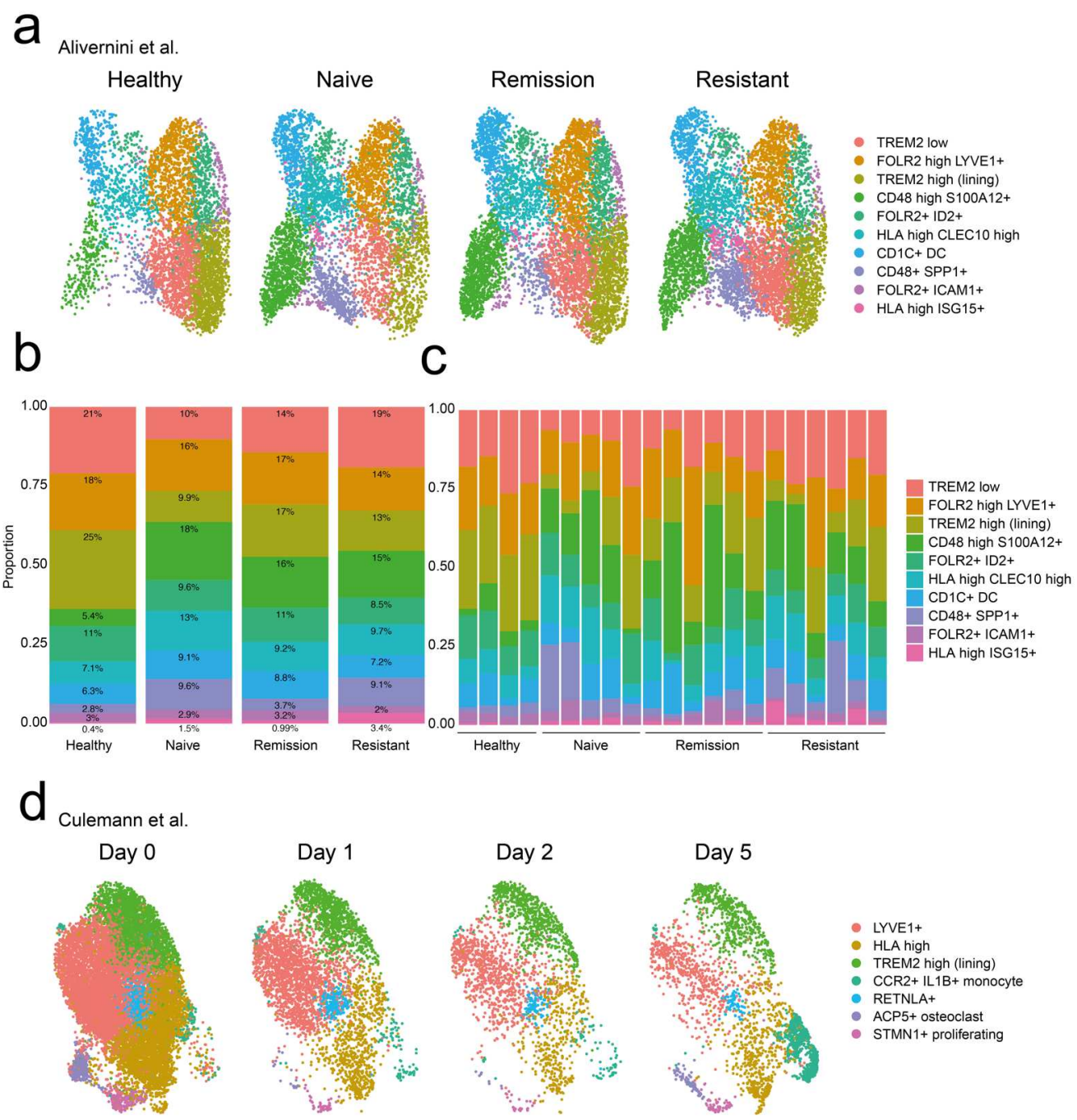

Figure 8 | Recruited, tissue-infiltrating macrophages characterize human RA and murine STIA.
a) UMAP of human synovial tissue macrophages (Alivernini *et al.*) split by disease subtype (healthy, treatment-naïve, remission, treatment-resistant RA). b) Relative cluster abundance plot stratified by disease subtype in human RA. c) Relative cluster abundance plot by individual patient ID, annotated with respective disease subtype. d) UMAP of murine synovial tissue macrophages (Culemann *et al.*) split by day post-K/BxN serum transfer (day 0 as healthy control). e) Relative cluster abundance plot by day post-K/BxN serum transfer.

The other two subsets of recruited cells, the CCR2+ CSF2RA+ CD1C+ and CD48+ S100A12+ expressed intermediate NLRP3 levels (Figure 9a).

In murine STIA, tissue-resident subsets (Trem2^{high} lining, Lyve1+, Retnla+ sub-lining) also never upregulated *Nlrp3* or *Il-1b* (Figure 9b). Post-K/BxN serum transfer, *Nlrp3*-enriched Ccr2+ Csf2ra+ macrophages infiltrated, with the expression of inflammasome signature, *Nlrp3*, *Pycard*, *Il-1b*, *Il-18*, *Gsdmd*, and *Mefv* peaking at day 5 (Figure 9b). The in-house STIA time course dataset (Croft) confirmed low *Nlrp3* in health, with expression peaking at maximum inflammation, resolving thereafter, and maintained expression, albeit at lower levels in persistent arthritis (Figure 9c).

We next examined time-resolved expression of known negative NLRP3 inflammasome regulators in health and disease from our human and mouse datasets. In human RA, remission was characterized by *SOCS3* and *IL10* expression in the *NLRP3*^{high} FOLR2+ ICAM1+ subset, rather than downregulation of *NLRP3* transcriptionally (Figure 10a). This cluster also had high expression of *TNFAIP3* (encoding A20, a known NLRP3 regulator) and a negative regulator of NF-KB signalling, *NFKBIA* (Figure 10a). Treatment naïve and patients with persistent RA did not express IL-10 (Figure 10a).

In murine STIA, the *Nlrp3*-enriched Ccr2+ Il-1b+ cluster expressed *Tnfaip3* and *Nfkbia* at peak inflammation, also gaining *Socs3* and *Il-10* (Figure 10b). There was no remission in this dataset. The in-house time-resolved model showed *Tnfaip3* and *Nfkbia* upregulation in Nlrp3-high subsets at peak, and downregulation at resolution, with low *Socs1* (not *Socs3*) expression and no *Il-10* (Figure 10c).

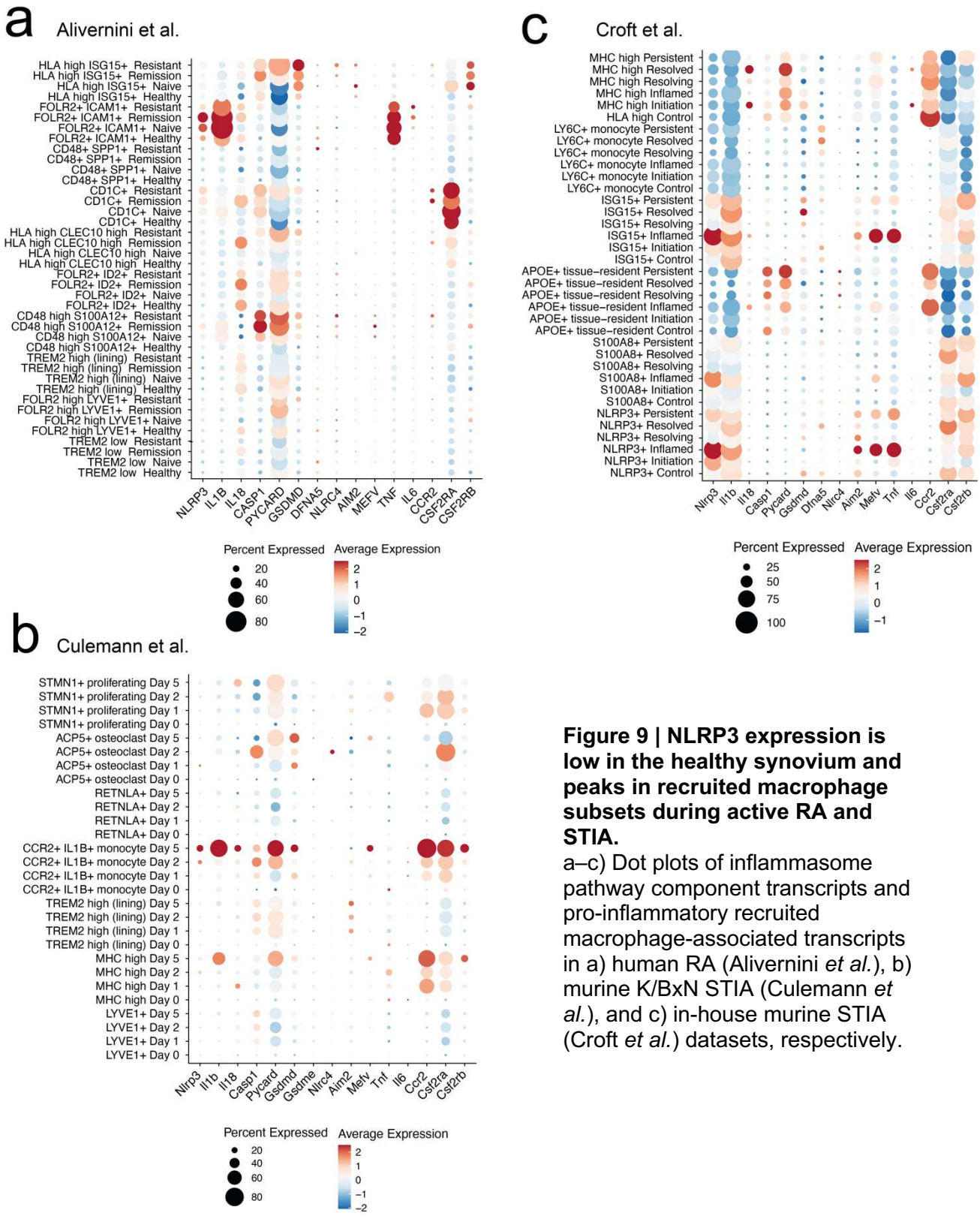

Figure 9 | NLRP3 expression is low in the healthy synovium and peaks in recruited macrophage subsets during active RA and STIA.
a–c) Dot plots of inflammasome pathway component transcripts and pro-inflammatory recruited macrophage-associated transcripts in a) human RA (Alivernini *et al.*), b) murine K/BxN STIA (Culemann *et al.*), and c) in-house murine STIA (Croft *et al.*) datasets, respectively.

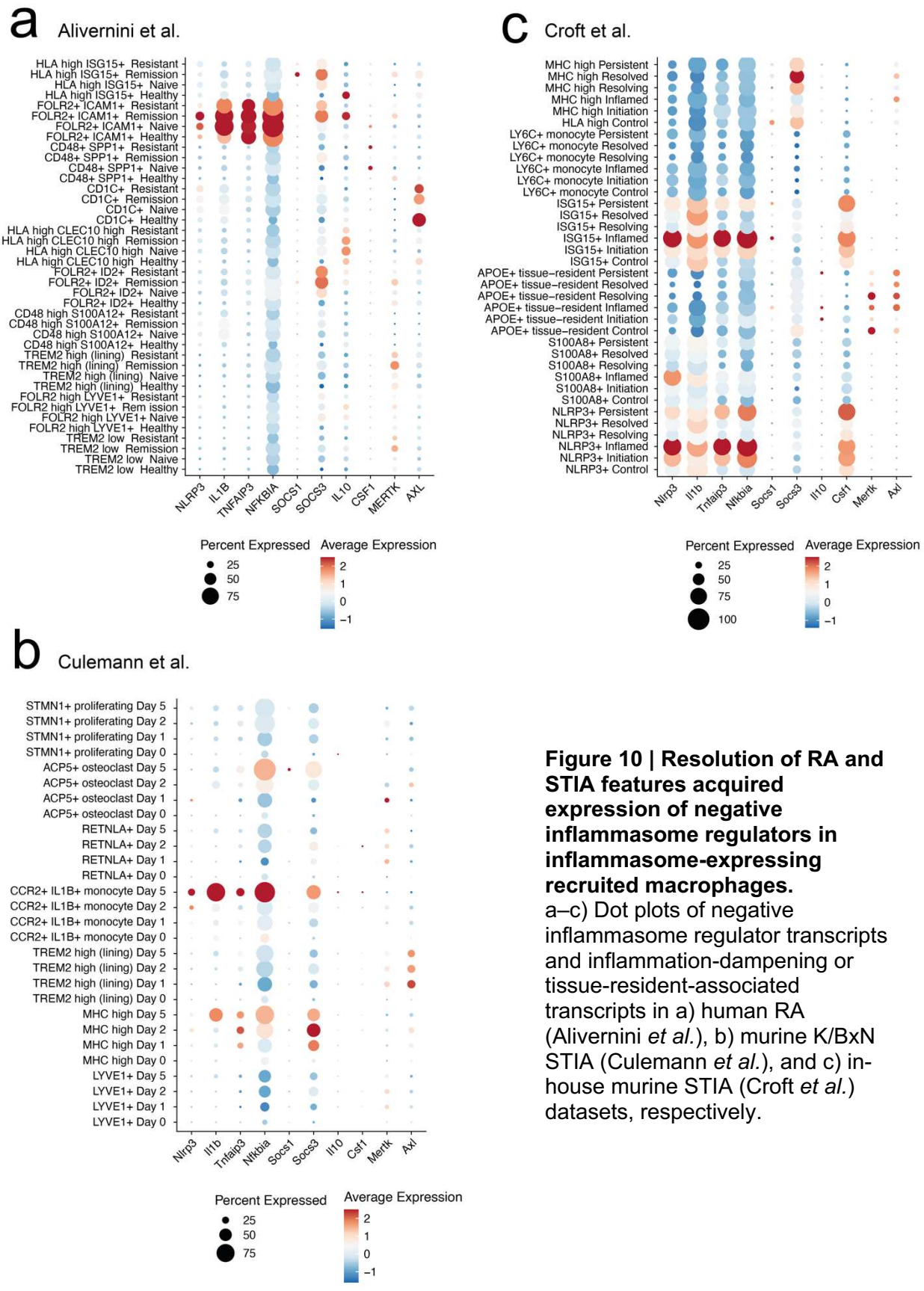

Figure 10 | Resolution of RA and STIA features acquired expression of negative inflammasome regulators in inflammasome-expressing recruited macrophages.
a–c) Dot plots of negative inflammasome regulator transcripts and inflammation-dampening or tissue-resident-associated transcripts in a) human RA (Alivernini *et al.*), b) murine K/BxN STIA (Culemann *et al.*), and c) in-house murine STIA (Croft *et al.*) datasets, respectively.

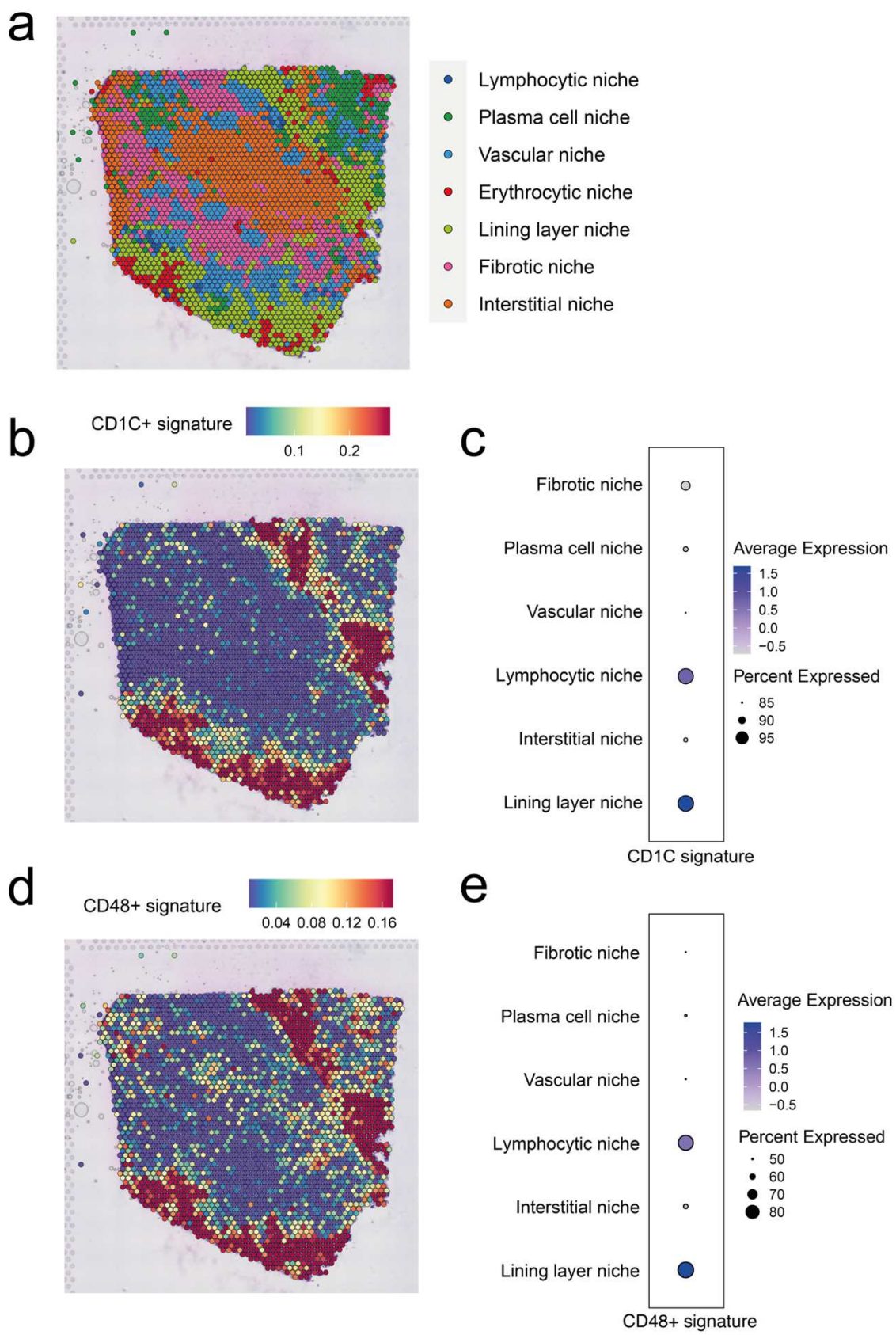

Figure 11 | NLRP3-enriched recruited macrophage subsets localise to the lining layer in RA.
a) Spatial transcriptomic niches defined in patient-derived RA biopsies using Visium.
b–e) Spatial mapping of NLRP3+ IL-1B+ macrophage subset signatures (CD1C+ and CD48+ clusters, defined by the top 30 differentially expressed genes [DEGs] from Alivernini *et al.*) onto myeloid signatures within the spatial transcriptomic niches.

6.3.5 Spatial transcriptomics localise NLRP3+ IL-1B+ macrophages to the lining layer in human RA

To address the spatial limitations of scRNAseq, I analysed Visium spatial transcriptomics data from treatment-naïve human RA biopsies (Figure 11a). The CD1C+ and CD48+ subsets (intermediate *NLRP3* and *IL-1B*) localized to the lining layer, a region previously linked to the highest IL-1 response signatures in fibroblasts, and to a lesser extent, the lymphocytic niche (Figure 11b-d)[7,10]. The rarer FOLR2+ ICAM1+ subset, i.e. the remaining *NLRP3*+ subset, also appeared lining-layer-associated, though its sparsity limited mapping (data not shown).

6.4 Discussion

This chapter addressed a key gap in understanding tissue inflammasome and macrophage biology, using arthritis as a model. Prior to this work, no studies had systematically explored inflammasome expression across the natural history of arthritis (spanning health, disease onset, resolution, and persistence) or compared its profile across human RA and murine models. Our analysis revealed that NLRP3 inflammasome expression is absent from tissue-resident macrophages (MERTK+ TREM2+ in humans; Mertk+ Trem2+ in mice) in both healthy and diseased states. During inflammation, monocyte-derived macrophages expressing *NLRP3/Nlrp3* infiltrate the synovium, reducing the relative abundance of resident macrophages. These pro-inflammatory, tissue-infiltrating cells localize to the lining layer, where stromal cells exhibit an enriched IL-1 response signature. NLRP3 expression rises during disease initiation, peaks at maximal pathology, and declines with resolution, accompanied by upregulation of negative regulators like *SOCS3* and *IL-10*. In STIA, resolution is characterised by a reduction in *Nlrp3* and *Il1b,* rather than expression of

negative regulators. This may be due to human disease being spontaneous, where remission is induced therapeutically, whereas murine models are induced inflammatory arthritis that spontaneously resolves.

My findings align with prior observations that IL-1β-expressing macrophages are enriched in RA synovium compared to healthy controls, correlating positively with the RA disease activity score (DAS28)[11]. *In vitro* studies further support a pro-inflammatory role for recruited IL-1β+ monocyte-derived macrophages in driving fibroblast invasiveness[3]. This biology extends beyond RA: in experimental autoimmune encephalomyelitis (EAE), a murine model of multiple sclerosis, Ccr2+ monocytes similarly drive pathology via GM-CSF-induced Il-1β expression, with disease severity mitigated by their depletion or deletion of GM-CSF[12,13,14]. Thus, murine STIA closely mirrors human RA, with both showing peak inflammasome expression in recruited macrophages during active disease, while tissue-resident macrophages remain immunologically quiescent throughout.

6.5 Limitations

While scRNAseq has revolutionized immunological research, its limitations warrant consideration. First, mRNA transcript levels do not directly reflect protein abundance, post-translational modifications, or function. Thus, transcriptional heterogeneity observed here represents an estimate of cellular states at a given time, not a definitive measure of inflammasome activity. Second, read depth affects sensitivity for detecting rare transcripts. Low read depth risks missing such transcripts, potentially leading to false negatives when concluding a gene is unexpressed. The datasets analysed here, sourced from high-impact studies, had sufficient read depth, and I mitigated model-specific biases by integrating multiple murine STIA datasets.

In the human RA dataset, definitions of “healthy,” “remission,” and “resistant” states posed challenges. Healthy controls were derived from donors with meniscal tears or ligament damage, deemed “normal” by MRI and macroscopic analysis. However, nearby tissue damage may subtly alter synovial steady-state biology. Treatment-resistant RA was defined by inadequate methotrexate response, while remission required at least six months of clinical and radiographic response to methotrexate plus a TNF inhibitor. Differing treatments between remission and resistant groups complicate molecular comparisons. Moreover, the AMP2 dataset suggests clinical stratification by treatment response may be less informative than cell-type abundance phenotypes (CTAPs). For instance, CTAP-F (stromal-dominant, low immune signature) correlated with poor treatment response, while CTAP-M (myeloid-dominant) linked to ACPA negativity. Future studies should align inflammasome expression with CTAPs to identify patients likely to benefit from IL-1 or inflammasome-targeted therapies (Chapter 5), as seen in inflammatory bowel disease where an IL-1β-activated fibroblast signature predicts anti-TNF resistance[15].

In mice, the STIA model’s well-defined progression simplifies disease stratification compared to the heterogeneous, years-long development of human RA, where autoantibodies precede symptoms by 3–5 years. This temporal disparity hinders direct cross-species comparisons, particularly for persistence, which in STIA arises rapidly via serum reinoculation. Finally, spatial transcriptomics (such as 10x Visium, used here) lacks single-cell resolution due to its 55μm feature size. While this captures cellular “neighbourhoods,” it cannot distinguish whether NLRP3-enriched macrophages reside precisely in the lining layer or adjacent sub-lining regions near fibroblasts. Recent evidence of vasculature near the lining as a potential entry point

for recruited cells underscores the need for high-resolution imaging (such as multi-fluorescence microscopy) to confirm their location and infiltration routes[16].

6.6 Conclusions

This chapter demonstrates that human RA and murine inflammatory arthritis models share a defining feature: an influx of monocyte-derived macrophages into the synovium, enriched for *NLRP3* and *IL-1B* expression. These recruited macrophages infiltrate during disease, with inflammasome expression peaking at maximum pathology and persisting at lower levels in chronic states. In remission, their abundance declines, though not to healthy levels, and they acquire expression of negative regulators like *SOCS3* and *IL-10*. Tissue-resident macrophages, by contrast, consistently suppress *NLRP3* expression across all disease stages. Spatial transcriptomics revealed that IL-1B+ recruited macrophages predominantly localize to the lining layer, aligning with the heightened IL-1 response signature in lining fibroblasts.

6.7 References

1. Croft, A. P. *et al.* Distinct fibroblast subsets drive inflammation and damage in arthritis. *Nature* **570**, 246–251 (2019).
2. Accelerating Medicines Partnership Rheumatoid Arthritis and Systemic Lupus Erythematosus (AMP RA/SLE) Consortium *et al.* Defining inflammatory cell states in rheumatoid arthritis joint synovial tissues by integrating single-cell transcriptomics and mass cytometry. *Nat Immunol* **20**, 928–942 (2019).

3. Kuo, D. *et al.* HBEGF+ macrophages in rheumatoid arthritis induce fibroblast invasiveness. *Sci. Transl. Med.* **11**, eaau8587 (2019).
4. Culemann, S. *et al.* Locally renewing resident synovial macrophages provide a protective barrier for the joint. *Nature* **572**, 670–675 (2019).
5. Alivernini, S. *et al.* Distinct synovial tissue macrophage subsets regulate inflammation and remission in rheumatoid arthritis. *Nat Med* **26**, 1295–1306 (2020).
6. Zhang, F. *et al.* Deconstruction of rheumatoid arthritis synovium defines inflammatory subtypes. *Nature* **623**, 616–624 (2023).
7. Smith, M. H. *et al.* Drivers of heterogeneity in synovial fibroblasts in rheumatoid arthritis. *Nat Immunol* **24**, 1200–1210 (2023).
8. Accelerating Medicines Partnership Rheumatoid Arthritis & Systemic Lupus Erythematosus (AMP RA/SLE) Consortium *et al.* Notch signalling drives synovial fibroblast identity and arthritis pathology. *Nature* **582**, 259–264 (2020).
9. Misharin, A. V. *et al.* Nonclassical Ly6C− Monocytes Drive the Development of Inflammatory Arthritis in Mice. *Cell Reports* **9**, 591–604 (2014).
10. Reis Nisa, P. *et al.* Spatial programming of fibroblasts promotes resolution of tissue inflammation through immune cell exclusion. Preprint at https://doi.org/10.1101/2024.09.20.614064 (2024).
11. Hanlon, M. M. *et al.* Loss of synovial tissue macrophage homeostasis precedes rheumatoid arthritis clinical onset. *Sci. Adv.* **10**, eadj1252 (2024).
12. Chen, Y. F. *et al.* Spontaneous Development of Autoimmune Uveitis Is CCR2 Dependent. *The American Journal of Pathology* **184**, 1695–1705 (2014).
13. Croxford, A. L. *et al.* The Cytokine GM-CSF Drives the Inflammatory Signature of CCR2+ Monocytes and Licenses Autoimmunity. *Immunity* **43**, 502–514 (2015).

14. Amorim, A. *et al.* IFNγ and GM-CSF control complementary differentiation programs in the monocyte-to-phagocyte transition during neuroinflammation. *Nat Immunol* **23**, 217–228 (2022).
15. Friedrich, M. *et al.* IL-1-driven stromal–neutrophil interactions define a subset of patients with inflammatory bowel disease that does not respond to therapies. *Nat Med* **27**, 1970–1981 (2021).
16. Hasegawa, T. *et al.* Macrophages and nociceptor neurons form a sentinel unit around fenestrated capillaries to defend the synovium from circulating immune challenge. *Nat Immunol* **25**, 2270–2283 (2024).

7. Chapter 2 | GM-CSF increases and potentiates NLRP3 inflammasome responses to microbial and sterile signals *in vitro*

7.1 Introduction

Chapter 1 utilized scRNAseq to delineate the expression of NLRP3 and associated inflammasome components in the synovium of human RA and murine STIA. My findings established that NLRP3 is predominantly expressed in recruited, pro-inflammatory macrophage subsets, marked by CSF2RA (GM-CSF receptor alpha), peaking during active disease and localizing to the lining layer, while tissue-resident macrophages remain quiescent. These transcriptional insights, while powerful, reflect steady-state mRNA profiles rather than functional protein activity or dynamic responses to synovial cues. To interrogate the mechanistic role of GM-CSF in driving NLRP3 inflammasome activation, complementary approaches using *in vitro* and *in vivo* models are essential. This chapter investigates GM-CSF-driven NLRP3 inflammasome activation *in vitro*.

7.1.1 GM-CSF *in vitro*

GM-CSF is a pleiotropic cytokine and colony stimulating factor. Unlike M-CSF, which generates a homogenous mono-colony of adherent macrophages from bone marrow progenitors *in vitro*, GM-CSF cultured bone marrow populations contain adherent macrophages and monocytic-DCs in suspension[1]. Heterogeneity in GM-CSF cultures comes from individual cell lineage commitments at the progenitor level[1]. However, the concentration of GM-CSF in an *in vitro* culture can change the relative numbers of adherent macrophages and floating moDCs[2]. This heterogeneity of

response is only further amplified *in vivo*, where GM-CSF biology is even more complex and poorly understood.

In mixed GM-CSF cultures, others have shown macrophages and not DCs are responsible for NLRP3 inflammasome activation and IL-1β release *in vitro*[3]. Previous work by John Hamilton has demonstrated that the cytokine profiles and transcriptional activation of M-CSF and GM-CSF BMDMs differ strikingly, with GM-BMDMs generating more TNF-α, IL-6, IL-12p70, and IL-23 and M-BMDMs producing more IL-10 and CCL2[4,5].

7.1.2 GM-CSF *in vivo*

GM-CSF has also been implicated as a key driver of myeloid inflammation *in vivo*. I will briefly address the homeostatic and disease-associated roles of M-CSF and GM-CSF *in vivo* here. However, a more in-depth review of GM-CSF in human RA and murine inflammatory arthritis models will be covered in the subsequent chapter.

GM-CSF is undetectable in healthy human sera, and its expression is largely restricted to barrier sites and mucosal tissues with microbial exposure[6]. GM-CSF is not essential for steady-state haematopoiesis in mice[7]. GM-CSF-deficient mice exhibit no abnormalities in their macrophage compartment, with a notable exception being the complete absence of alveolar macrophages[8,9]. To date, alveolar macrophages appear to be the only tissue-resident macrophage population that requires GM-CSF as a survival and differentiation factor. GM-CSF-deficient mice develop pulmonary alveolar proteinosis (PAP), a lung condition marked by the accumulation of surfactant in the alveoli, which would normally be cleared by alveolar macrophages, leading to impaired gas exchange and respiratory dysfunction. This mirrors human PAP, where

GM-CSF deficiency (typically due to anti-GM-CSF autoantibodies) leads to similar pathology[10].

More generally, GM-CSF enhances the antimicrobial activity of macrophages and neutrophils by promoting phagocytosis, reactive oxygen species (ROS) production, and zinc sequestration, which starves pathogens of essential nutrients[11,12]. As a result, GM-CSF deficient mice show heightened susceptibility to pulmonary and soft-tissue infections, including bacterial (group B *Streptococcus*) and fungal pathogens[13].

GM-CSF is protective in acute models of infection but has been implicated as a pathogenic factor in multiple models of autoimmunity. For example, GM-CSF deficient mice are resistant to EAE, a model of multiple sclerosis[14–16]. They show reduced immune cell infiltration into the central nervous system (CNS) and lack clinical symptoms like demyelinating lesions. GM-CSF is critical for mobilizing monocytes (especially CCR2+ Ly6C+ subsets) from the bone marrow to the CNS, and driving inflammasome expression and ROS induction [15,17].

In another sterile model of inflammation, crescentic glomerulonephritis (GN), GM-CSF-deficient mice are protected from severe crescentic injury, with reduced glomerular macrophage infiltration, lowered IL-1β expression, and preserved renal function. In a murine model of Kawasaki's disease, GM-CSF deficiency protects from the development of cardiac disease and lowers *Il-1b* in the hearts of challenged mice[18].

Collectively, several models suggest GM-CSF plays a role in initiating and driving pathogenic inflammation. However, simply referring to GM-CSF as a pro-inflammatory cytokine would be a misnomer.

Many cancers constitutively express GM-CSF, driving myeloid-derived suppressor cell (MDSC) phenotypes and dampening anti-tumour responses[19,20]. GM-

CSF-depleted gliomas result in smaller tumours, reduced microglia/macrophage infiltration, and improved survival in mice[21].

Therefore GM-CSF may act in a time, dose, and context dependent manner with protective functions in infection but potentially pathogenic roles in autoimmunity and cancer.

7.2 Aims

This chapter transitions from transcriptional profiling to functional validation, leveraging *in vitro* BMDM cultures to test whether GM-CSF enhances NLRP3 inflammasome activation, as hypothesised from our human and mouse inflammatory arthritis datasets. Specific aims include:

1) Characterize differences in NLRP3 inflammasome responses to pathogen-derived (LPS) and sterile (TNF) signals in M-CSF- and GM-CSF-derived BMDMs, assessing how well GM-CSF BMDMs represent tissue-recruited macrophages in RA,.
2) Elucidate transcriptional and translational differences in inflammasome-associated genes (e.g., *Nlrp3*, *Il1b*) and negative regulators (IL-10) between M-CSF- and GM-CSF-derived BMDMs, defining mechanisms underlying their distinct inflammasome activities.

7.3 Results

7.3.1 GM-CSF macrophages recapitulate cell surface markers of tissue-recruited macrophages

Given the conserved expression of the GM-CSF receptor (CSF2RA) on NLRP3-enriched, infiltrating macrophages in human RA, murine STIA, and other sterile inflammation models, I explored GM-CSF's impact on NLRP3 responses in murine BMDMs *in vitro*. BMDMs were differentiated with M-CSF or GM-CSF and assessed for NLRP3 activation in response to pathogen-derived (LPS) and sterile (TNF) signals. To exclude monocyte-derived dendritic cells, I used only the adherent fraction of GM-CSF cultures, confirming their macrophage phenotype by flow cytometry for cell surface markers (Figure 12a). Both M-CSF- and GM-CSF-derived BMDMs expressed comparable levels of the pan-myeloid marker CD11b (Figure 12b). However, GM-CSF-derived BMDMs mirrored recruited, monocyte-derived inflammatory macrophages, exhibiting lower levels of tissue-resident and homeostatic markers CX3CR1, MerTK, and F4/80 (not significant) compared to M-CSF-derived BMDMs, which resembled tissue-resident macrophage surface phenotypes (Figure 12c–e).

7.3.2 NLRP3 inflammasome responses to microbial and sterile signals are elevated in GM-CSF macrophages compared to M-CSF macrophages

To assess NLRP3 inflammasome responses, I primed M-CSF- and GM-CSF-derived BMDMs with LPS (a TLR4 ligand from Gram-negative bacteria) or TNF-α (a sterile TNFR1 ligand) for 30 min (acute inflammasome priming protocol), 4 h (peak

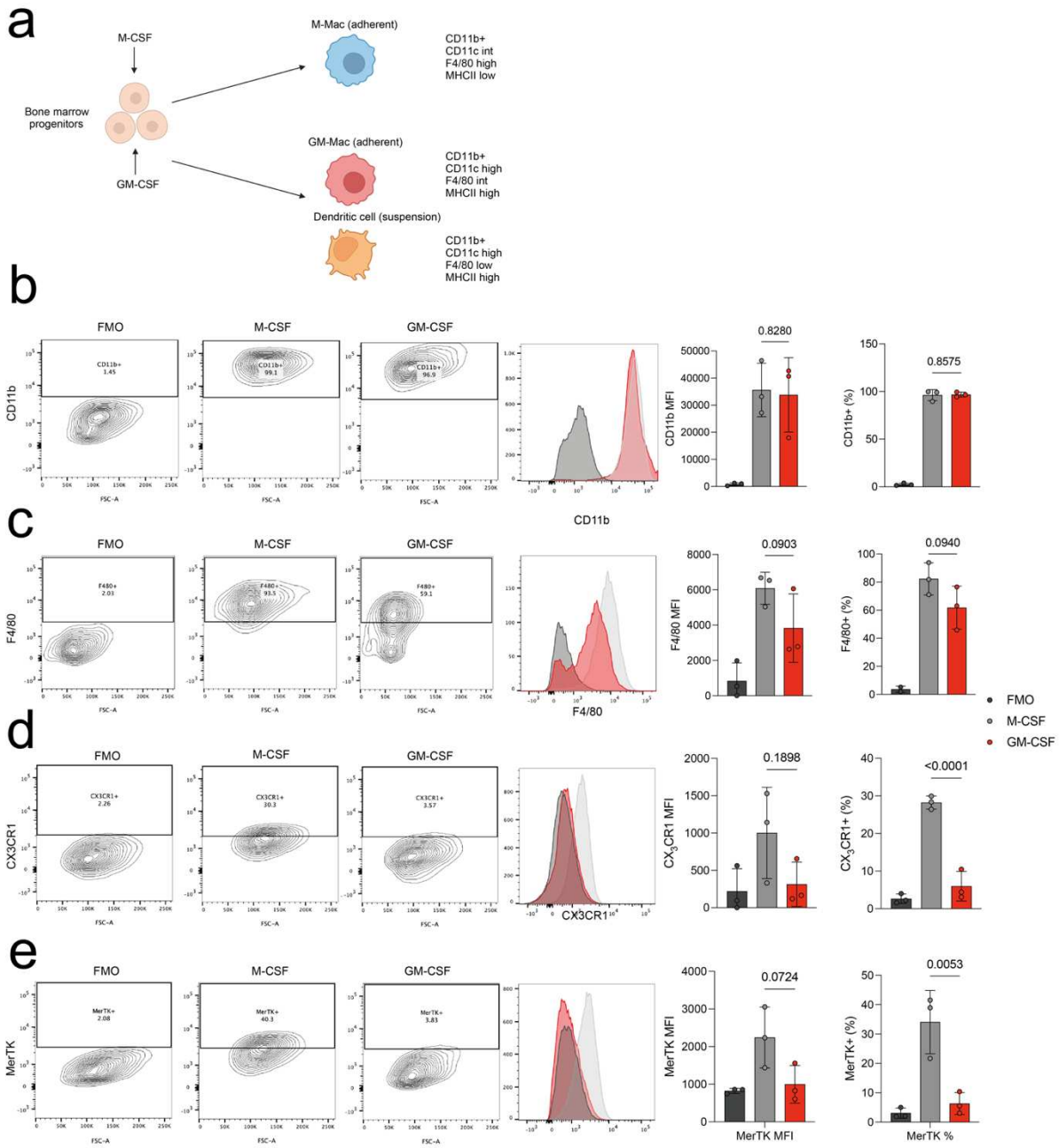

Figure 12 | M-CSF and GM-CSF macrophages recapitulate cell surface markers of synovial tissue-resident vs recruited macrophages, respectively.
a) Schematic of bone marrow-derived macrophage (BMDM) differentiation using M-CSF or GM-CSF.
b–e) Cell surface expression of b) CD11b, c) F4/80, d) CX3CR1, and e) MerTK measured by flow cytometry in M-CSF-derived BMDMs (light grey) and GM-CSF-derived BMDMs (red), with fluorescence minus one (FMO) controls in dark grey. Data are presented as representative gating and histograms from three independent biological replicates.

protocol), or 24 h (chronic protocol), followed by 1 h of nigericin, a bacterial pore-forming toxin, to trigger inflammasome signalling. LPS activates NF-κB and induces both NLRP3 transcription and posttranslational modifications necessary for

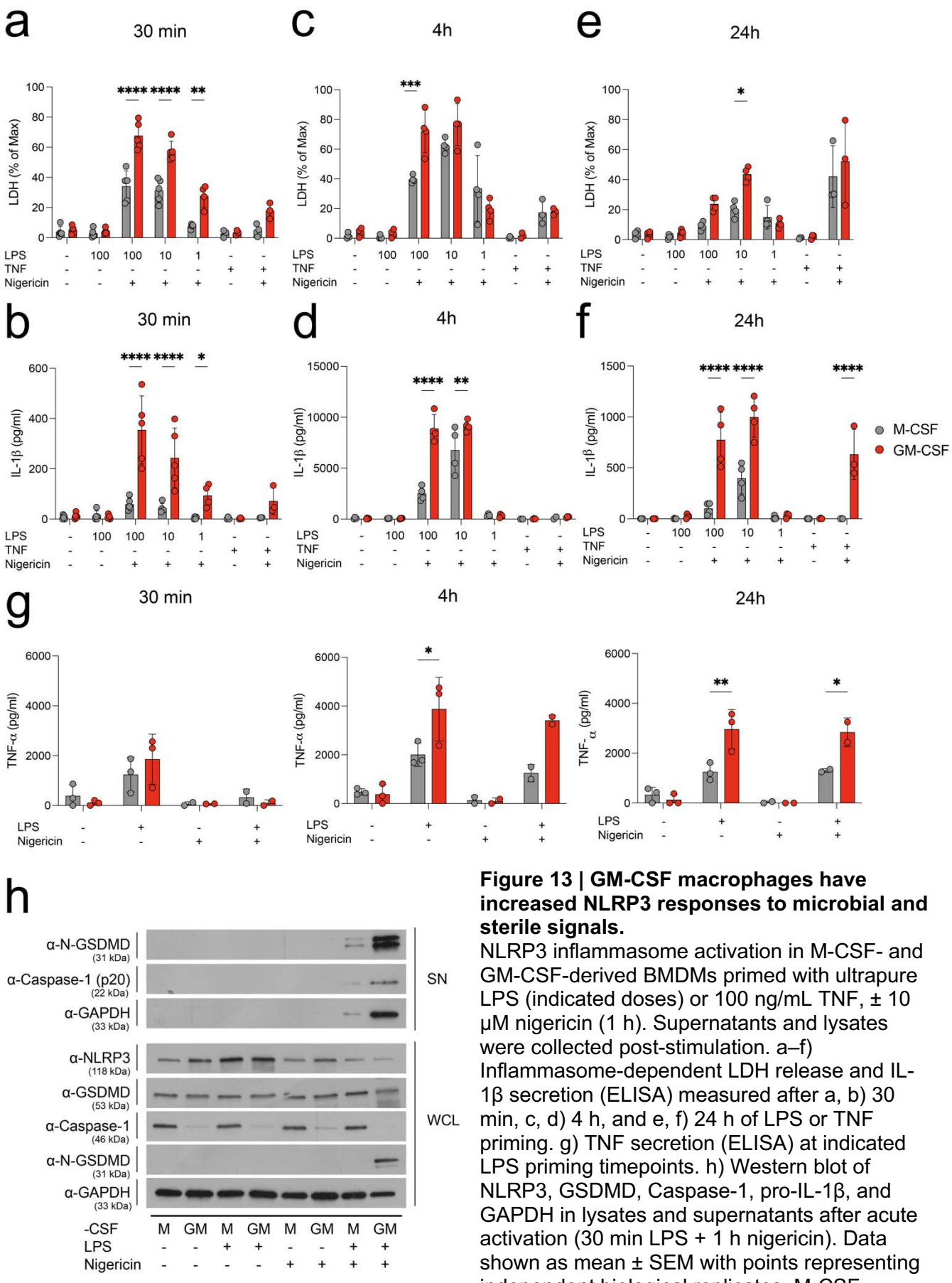

Figure 13 | GM-CSF macrophages have increased NLRP3 responses to microbial and sterile signals.
NLRP3 inflammasome activation in M-CSF- and GM-CSF-derived BMDMs primed with ultrapure LPS (indicated doses) or 100 ng/mL TNF, ± 10 μM nigericin (1 h). Supernatants and lysates were collected post-stimulation. a–f) Inflammasome-dependent LDH release and IL-1β secretion (ELISA) measured after a, b) 30 min, c, d) 4 h, and e, f) 24 h of LPS or TNF priming. g) TNF secretion (ELISA) at indicated LPS priming timepoints. h) Western blot of NLRP3, GSDMD, Caspase-1, pro-IL-1β, and GAPDH in lysates and supernatants after acute activation (30 min LPS + 1 h nigericin). Data shown as mean ± SEM with points representing independent biological replicates. M-CSF BMDMs (grey), GM-CSF BMDMs (red).

subsequent signalling, while TNF-α, a key RA therapeutic target, signals via NF-κB, MAPK, and RIPK1, offering a sterile inflammation model relevant to tissue contexts. Pyroptosis (LDH release) and IL-1β secretion (ELISA) were measured as inflammasome-dependent outcomes, with TNF secretion (ELISA) serving as an inflammasome-independent NF-κB proxy.

After 30 min of LPS priming, GM-CSF-derived BMDMs exhibited elevated pyroptosis and IL-1β release compared to M-CSF-derived BMDMs, which typically show delayed IL-1β induction (Figure 13a, b). By 4 h, M-CSF BMDMs matched GM-CSF BMDMs in cell death, but GM-CSF BMDMs sustained higher IL-1β secretion across all timepoints (Figure 13c, d). At 24 h, LPS-induced NLRP3 responses diminished in both populations, suggesting a conserved endotoxin-induced negative feedback loop, though GM-CSF BMDMs retained elevated pyroptosis at 10 ng/mL and 100 ng/mL LPS (not significant) (Figure 13e). Notably, GM-CSF BMDMs secreted significant IL-1β after 24 h of TNF priming, despite minimal cell death differences, a contrast to M-CSF BMDMs, where TNF priming poorly induces IL-1β at all time points tested (Figure 13b,d,f). Consistent with their pro-inflammatory profile, GM-CSF BMDMs also produced more TNF in response to LPS (Figure 13g).

Given the strong NLRP3 activation in GM-CSF-derived BMDMs as early as 30 min, i.e. before major transcriptional shifts, I examined intracellular NLRP3 and downstream effector levels with western blot. At baseline, GM-CSF BMDMs showed lower Caspase-1 levels, similar full-length GSDMD, and slightly higher NLRP3 compared to M-CSF BMDMs (Figure 13h). Post-30-min LPS priming with nigericin, GM-CSF BMDMs displayed markedly increased Caspase-1 and GSDMD cleavage, reflecting heightened pathway activity (Figure 13h). This enhanced activity was detectable within 30 min of nigericin addition via propidium iodide (PI) uptake,

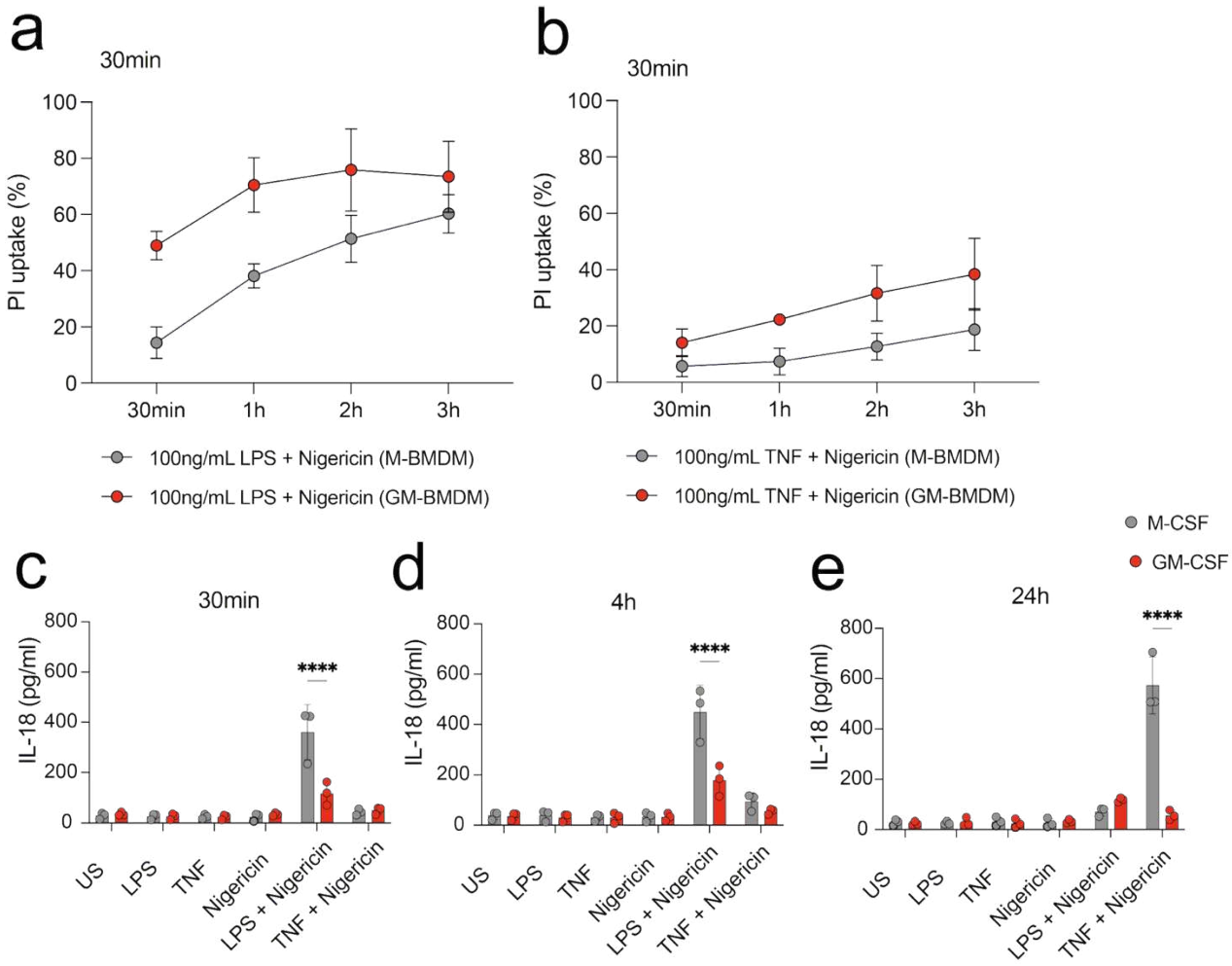

Figure 14 | GM-CSF-Derived BMDMs show enhanced NLRP3 downstream activity within 30 minutes of signal 2, but less IL-18 release.
Propidium iodide (PI) uptake in M-CSF- and GM-CSF-derived BMDMs primed for 30 min with a) 100 ng/mL LPS or b) 100 ng/mL TNF, measured at 30 min, 1 h, 2 h, and 3 h post-nigericin treatment. c-e) Inflammasome-dependent IL-18 secretion (ELISA) measured after c) 30 min, d) 4 h, and e) 24 h of LPS or TNF priming. Data shown as mean ± SEM, points representing three independent biological replicates. M-CSF BMDMs (grey), GM-CSF BMDMs (red).

indicating rapid sub-lytic NLRP3 activation (Figure 14a). Like LPS, TNF priming (30 min) also elicited elevated NLRP3 responses in GM-CSF BMDMs 1–2 h post-nigericin, though less robustly than LPS (Figure 14b), as expected for sterile priming signals. The increase in NLRP3 pathway activity as measured by LDH, IL-1β, caspase-1 p20 fragment release, and propidium iodide uptake was not reflected in levels of secreted IL-18. At all time points tested, M-CSF BMDMs released more IL-18 than GM-CSF BMDMs (Figure 14c-e). The reasons for the unexpectedly low IL-18 secretion despite heightened inflammasome pathway activity in GM CSF BMDMs will be explored later

using bulkRNAseq. In summary, GM-CSF BMDMs not only recapitulate the surface phenotype of tissue recruited inflammatory macrophages but also demonstrate faster, stronger and longer NLRP3 responses to both microbial and sterile priming signals, when compared to M-CSF BMDMs.

7.3.3 Heightened cell death and IL-1β release in GM-CSF macrophages are NLRP3-dependent

Inflammasome-dependent cell death and IL-1β release in M-CSF- and GM-CSF-derived BMDMs relied on canonical NLRP3 activation, as both were fully blocked by the NLRP3 inhibitor MCC950 (10 μM, 30 min pre-nigericin) at all priming timepoints tested, 30 min and 24 h (Figure 15a, b). Notably, IL-1β processing after 24 h of TNF priming was also NLRP3-dependent and inhibited by MCC950 (Figure 15b). Given GM-CSF BMDMs' elevated TNF secretion, which could amplify NF-κB priming in an autocrine manner, I compared NLRP3 responses in wild-type (WT) and *Tnfr1-/-* GM-CSF BMDMs across 30 min, 4 h, and 24 h. Inflammasome activity remained comparable between genotypes, indicating independence from autocrine TNF signalling (Figure 15c, d).

Prior work at the Kennedy Institute showed IRF5 drives pro-inflammatory cytokine production (IL-12b and IL-23) in mixed GM-CSF cultures containing BMDMs and BMDCs[22]. In our adherent GM-CSF pure macrophage cultures, however, peak NLRP3 responses and TNF secretion were unaffected by IRF5 deficiency (*Irf5-/-*), suggesting IRF5 is dispensable for these outcomes (Figure 16a–c). Thus, faster, stronger, and longer IL-1β secretion by GM-CSF is still fully NLRP3 dependent and is not driven by increased autocrine TNF signalling.

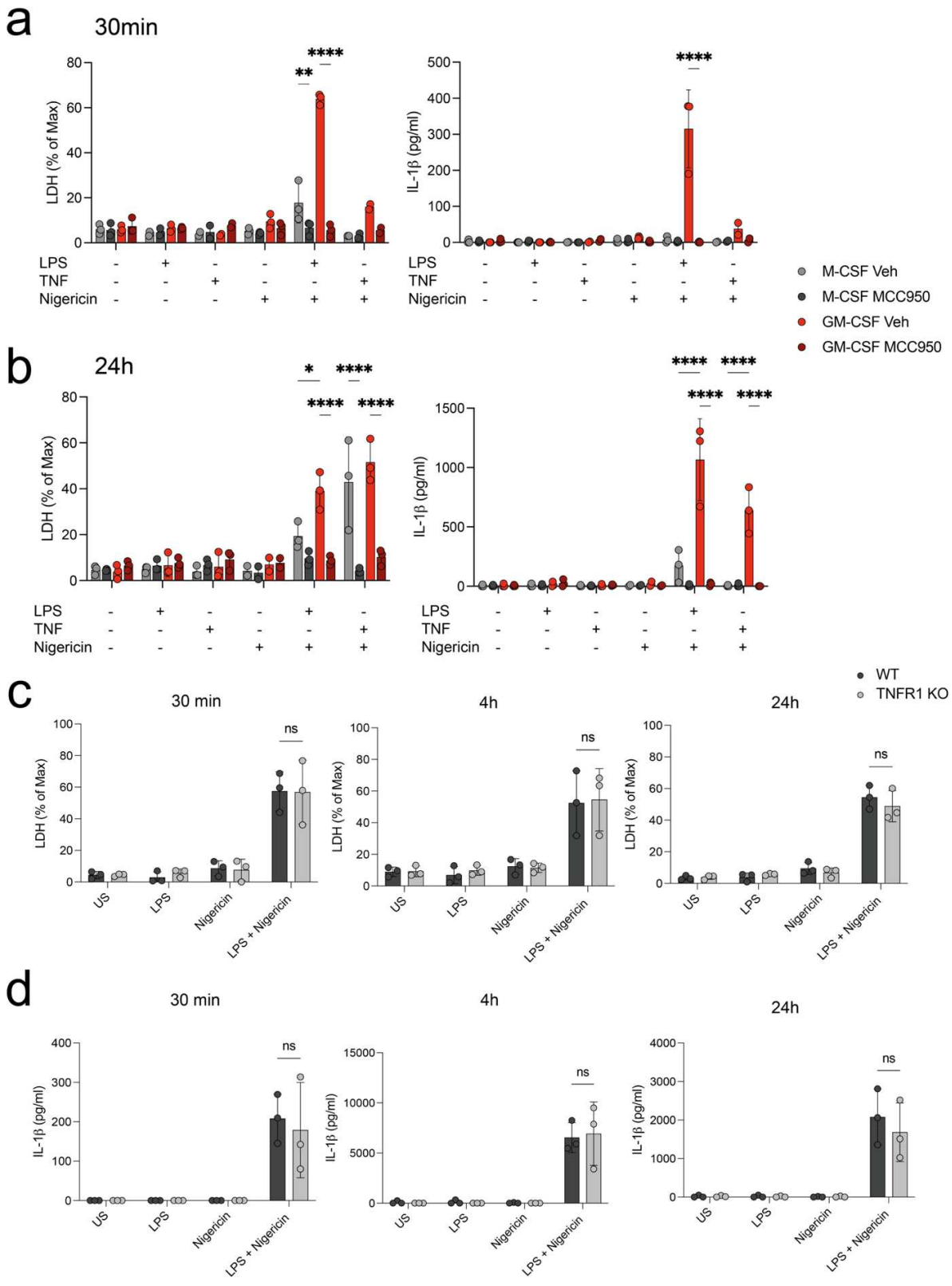

Figure 15 | Enhanced NLRP3 responses in GM-CSF-derived BMDMs depend on canonical NLRP3 activation, not autocrine TNF signalling.
a-b) M-CSF and GM-CSF BMDMs were primed for a) 30 min or b) 24 h with 100ng/L ultrapure LPS or 100 ng/mL TNF. BMDMs were pre-treated with 10 uM MCC950 30 min prior to 1 h 10uM nigericin. Inflammasome-dependent cell death was measured by LDH release. IL-1β release was measured by ELISA. c,d) WT and TNFR1 KO GM-CSF derived BMDMs were stimulated with 30 min, 4 h, 24 h with 100 ng/L ultrapure LPS ± 10uM nigericin. Inflammasome-dependent cell death was measured by LDH release. IL-1β release was measured by ELISA.Data shown as mean ± SEM, points representing three independent biological replicates. M-CSF BMDMs (grey), GM-CSF BMDMs (red).

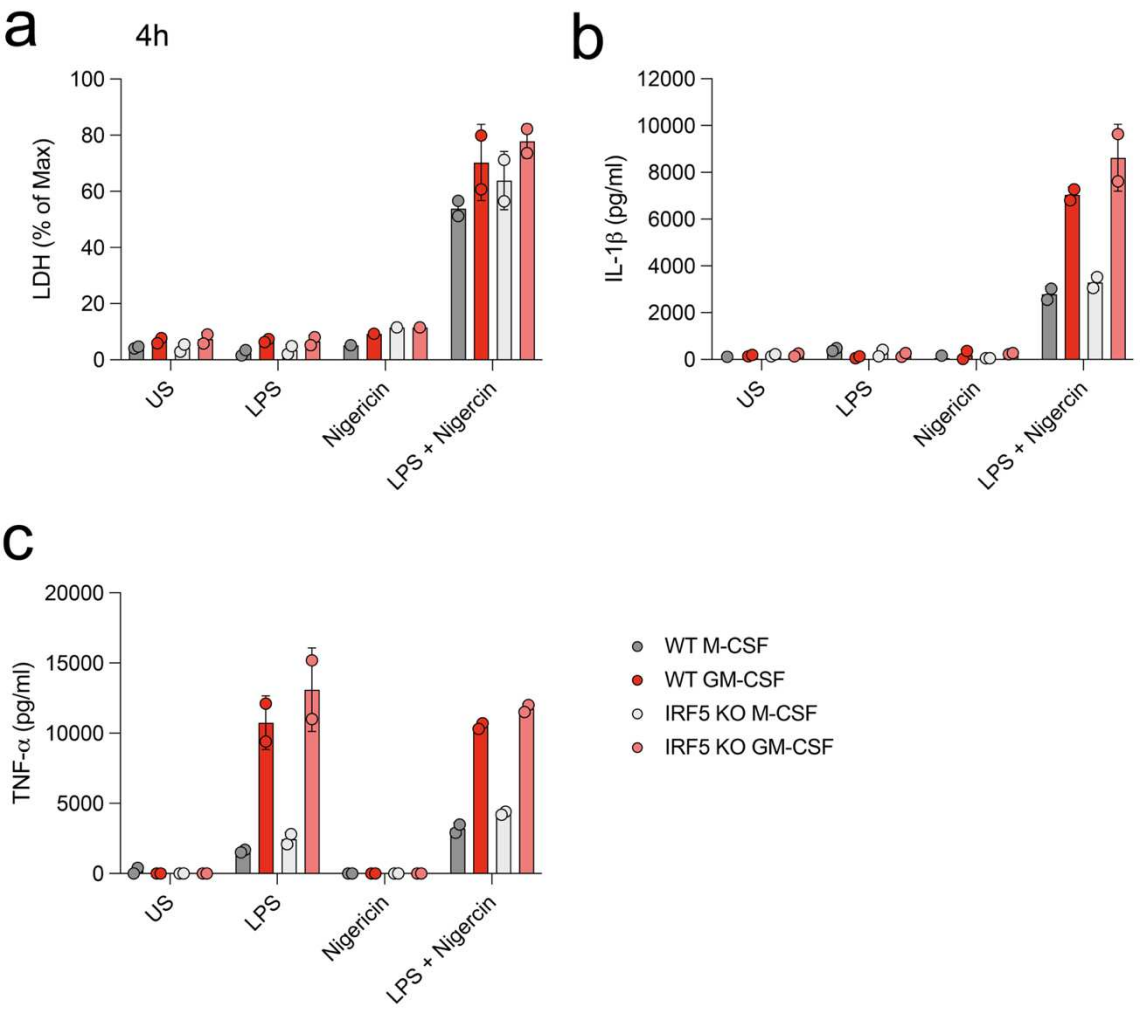

Figure 16 | IRF5 is dispensable for peak NLRP3 responses in GM-CSF-derived BMDMs. WT and *Irf5-/-* bone marrow progenitors differentiated into BMDMs with M-CSF or GM-CSF, primed with 100 ng/mL ultrapure LPS for 4 h ± 10 μM nigericin (1 h). Supernatants and lysates collected post-stimulation. a) Inflammasome-dependent LDH release. b) IL-1β and c) TNF secretion measured by ELISA. Data shown as mean ± SEM, points representing two independent biological replicates. M-CSF BMDMs (grey), GM-CSF BMDMs (red), M-CSF IRF5 KO BMDMs (white), GM-CSF IRF5 KO BMDMs (pink).

7.3.4 Increased inflammasome responses in GM-CSF differentiated macrophages track with delayed IL-10 and rapid pro-IL-1β production compared to M-CSF macrophages

To elucidate the mechanisms driving elevated and sustained NLRP3 responses in GM-CSF-derived BMDMs, I examined IL-10, an established negative regulator of NLRP3 produced by tissue-resident macrophages (for example, peritoneal macrophages) to suppress inflammasome activity[23]. M-CSF-derived BMDMs

exhibited steady-state *Il10* mRNA expression, leading to rapid IL-10 secretion within 30 min of LPS priming (Figure 17a). In contrast, GM-CSF-derived BMDMs showed low basal *Il10* mRNA and delayed IL-10 release compared to M-CSF BMDMs (Figure 17a). In contrast, GM-CSF BMDMs rapidly upregulated *Il1b* transcription, with higher pro-IL-1β protein levels at all timepoints, including 24 h post-LPS, when M-CSF BMDMs are known to already shut down pro-IL-1β via IL-10 negative feedback (Figure 17b). TNF priming induced pro-IL-1β in GM-CSF BMDMs at 24 h, and was unable to do so in M-CSF BMDMs, at all points tested, in line with the previous report (Figure 17c).

Given the rapid appearance of pro-IL1β and secretion of IL-1β in GM-CSF BMDMs, I tested the dependence of NLRP3 responses on *de novo* transcription using Actinomycin-D (30 min pre-LPS). NLRP3-driven cell death was transcription-independent, as expected, reflecting basal inflammasome component expression in both BMDM types (Figure 17d). However, pro-IL-1β induction required transcription and was more robust in GM-CSF BMDMs (Figure 17e), consistent with undetectable steady-state pro-IL-1β by Western blot (Figure 17c).

Thus, the heightened inflammasome responses in GM-CSF-derived BMDMs, compared to M-CSF-derived BMDMs, stem not from pre-existing pro-IL-1β protein stores but correlate with delayed IL-10 production and accelerated *Il1b* transcription. Additional transcriptional differences emerged in response to LPS and TNF (Figure 18). GM-CSF BMDMs exhibited higher basal *Nlrp3* expression and sustained elevated *Nlrp3* levels across all timepoints post-LPS priming compared to M-CSF BMDMs (Figure 18a). They also transcribed greater levels of *Tnf*, *Ccl17*, and *Mmp12*, consistent with prior reports in BMDMs and human monocytes (Figure 18b–d)[24].

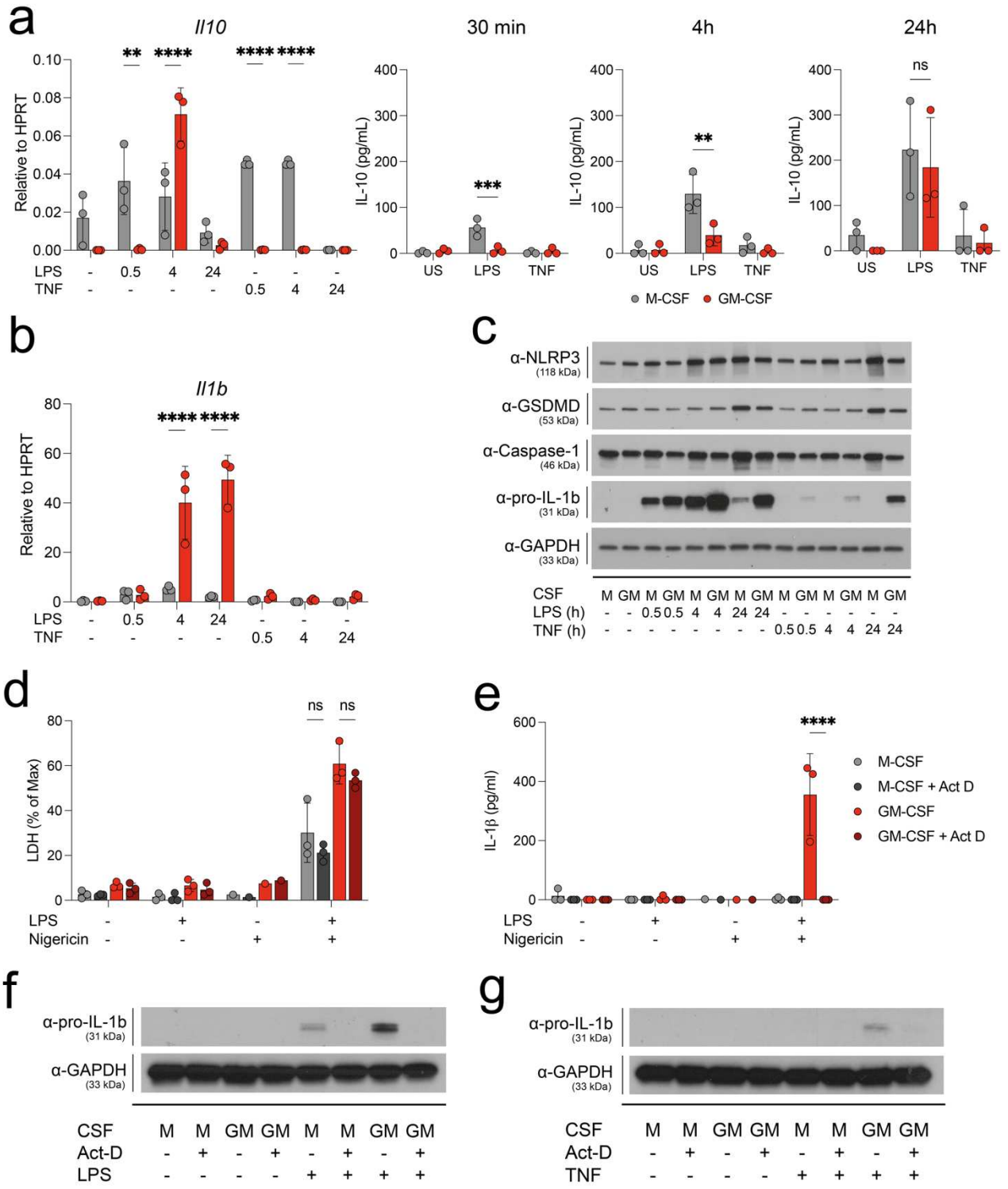

Figure 17 | GM-CSF-derived BMDMs show delayed IL-10 production and rapid *Il1b* transcription compared to M-CSF-derived BMDMs.
M-CSF- and GM-CSF-derived BMDMs primed with 100 ng/mL ultrapure LPS or 100 ng/mL TNF for 30 min, 4 h, or 24 h. Supernatants and lysates collected post-stimulation. a) *Il10* mRNA (qPCR, relative to *HPRT*) and IL-10 secretion (ELISA). b) *Il1b* mRNA (qPCR, relative to *HPRT*). c) NLRP3, pro-IL-1β, GSDMD-FL, pro-Caspase-1, and GAPDH protein levels in lysates (Western blot). d, e) BMDMs stimulated with 100 ng/mL LPS ± 10 μM nigericin (30 min), pre-treated with Actinomycin-D (30 min pre-LPS): d) LDH release, e) IL-1β secretion (ELISA). f) Intracellular pro-IL-1β (Western blot). g) BMDMs pre-treated with Actinomycin-D (30 min pre-TNF), intracellular pro-IL-1β (Western blot). Data shown as mean ± SEM, points representing independent biological replicates. M-CSF BMDMs (grey), GM-CSF BMDMs (red).

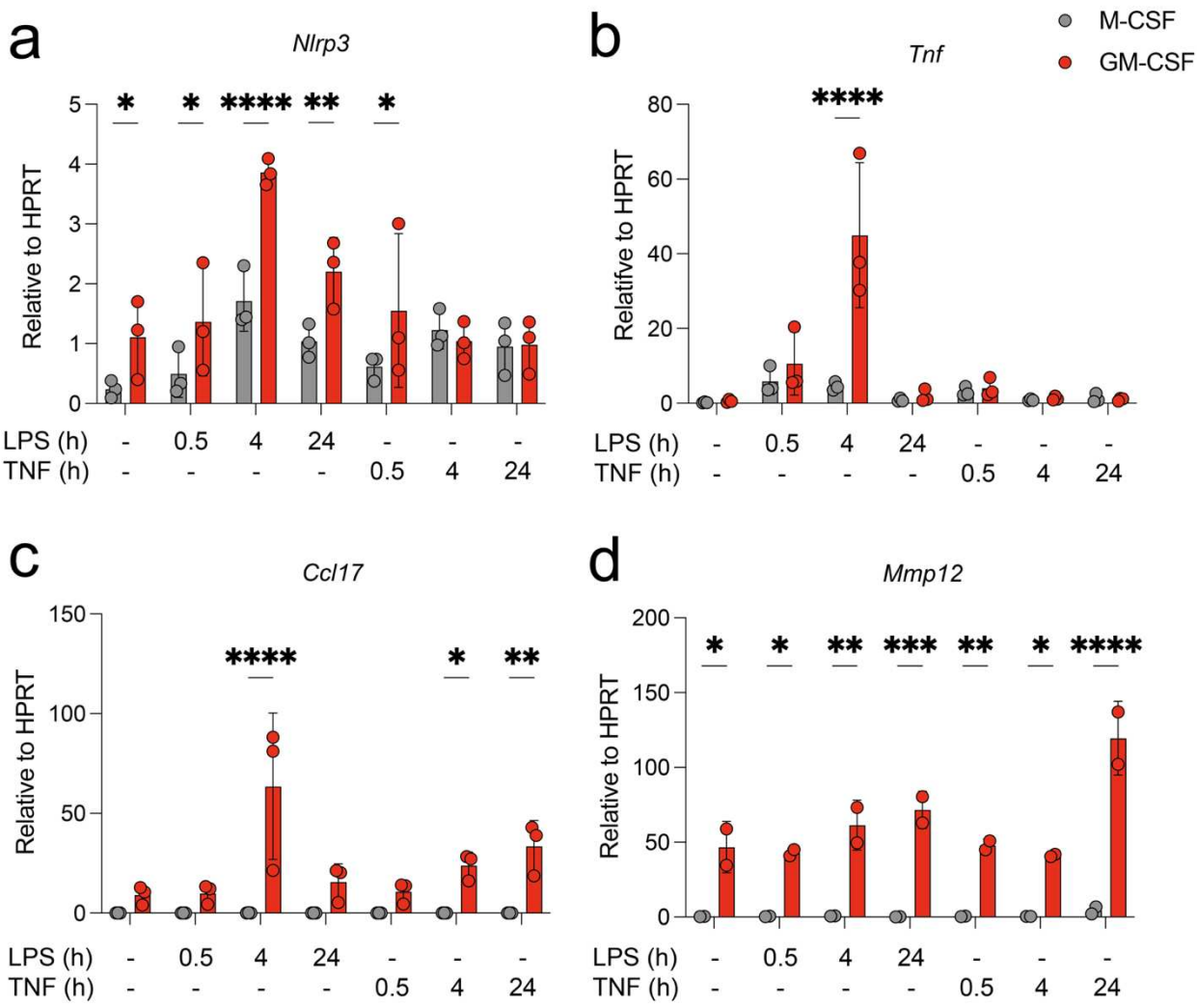

Figure 18 | GM-CSF-derived BMDMs exhibit enhanced transcription of *Nlrp3*, *Tnf*, *Ccl17*, and *Mmp12*.
M-CSF- and GM-CSF-derived BMDMs primed with 100 ng/mL ultrapure LPS or 100 ng/mL TNF for 30 min, 4 h, or 24 h, lysed in RLT buffer. a) *Nlrp3*, b) *Tnf*, c) *Ccl17*, d) *Mmp12* mRNA expression measured by qPCR, relative to *HPRT*. Data shown as mean ± SEM, points representing independent biological replicates. M-CSF BMDMs (grey), GM-CSF BMDMs (red).

To support our findings with Western blot and qPCR, I compared the transcriptional states of M-CSF and GM-CSF BMDMs using bulk RNAseq for higher sensitivity and found most genes are shared in steady state (Figure 19a). However, GM-CSF BMDMs expressed higher levels of monocytic markers including *Ccr2*, *Ccr5*, and *Ly6c2* (Figure 19b-d). In steady state, GM-CSF BMDMs expressed more *Ccl17*, *Mmp12*, *Hbegf*, *Il1a*, and *Il1b* (Figure 19e-i). Surprisingly GM-CSF BMDMs expressed more *Mertk* (despite less surface protein MerTK expression as measured by flow

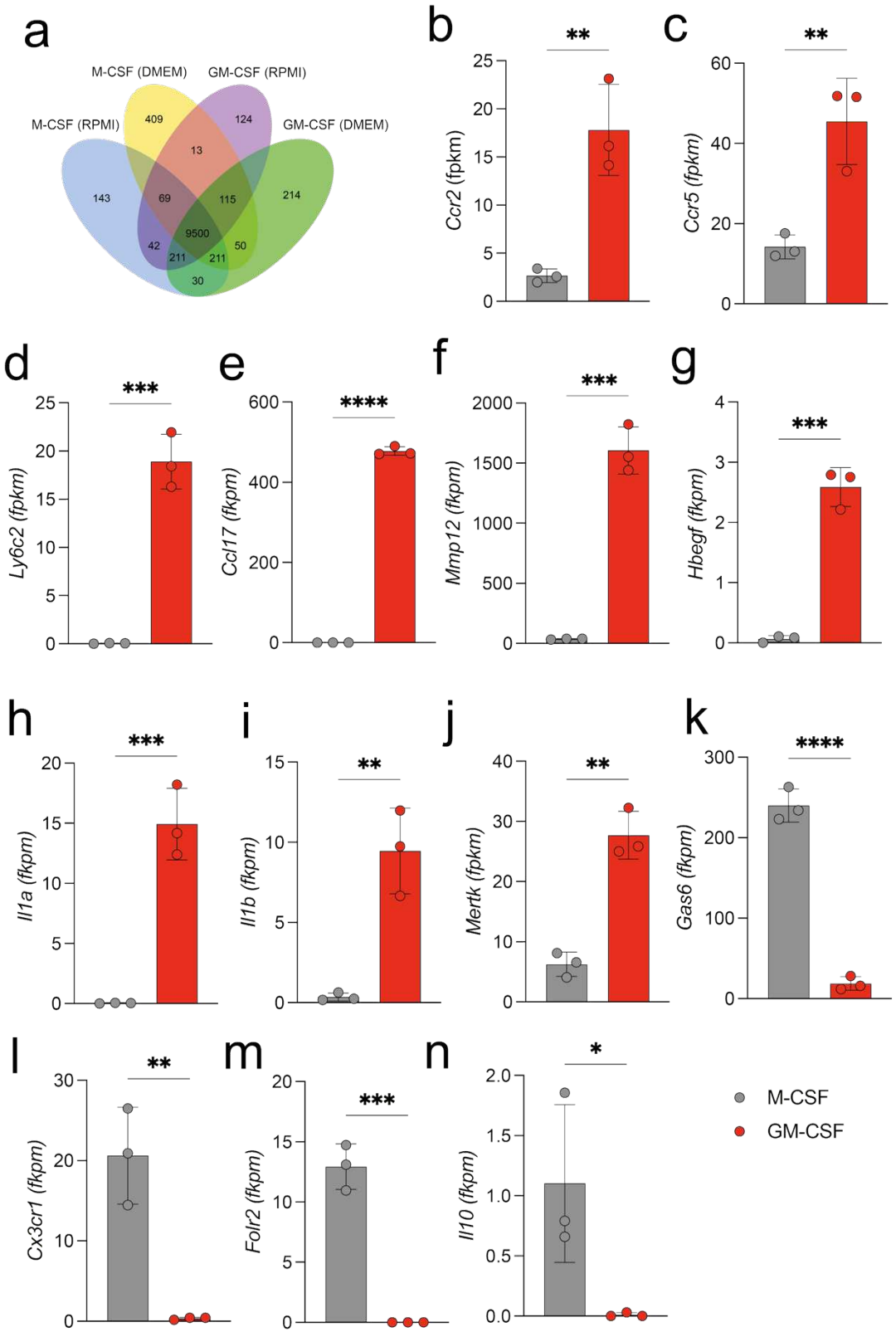

Figure 19 | M-CSF and GM-CSF BMDMs have distinct steady state transcriptional states. M-CSF- and GM-CSF-derived BMDMs lysed in RLT buffer and RNA was isolated and sent for bulk sequencing a) Venn diagram of shared and distinct transcript numbers across M-CSF and GM-CSF BMDMs grown in RPMI and DMEM. b-n) mRNA expression measured by bulk RNA sequencing of indicated DEGs. Data shown as mean ± SEM, points representing independent biological replicates. M-CSF BMDMs (grey), GM-CSF BMDMs (red).

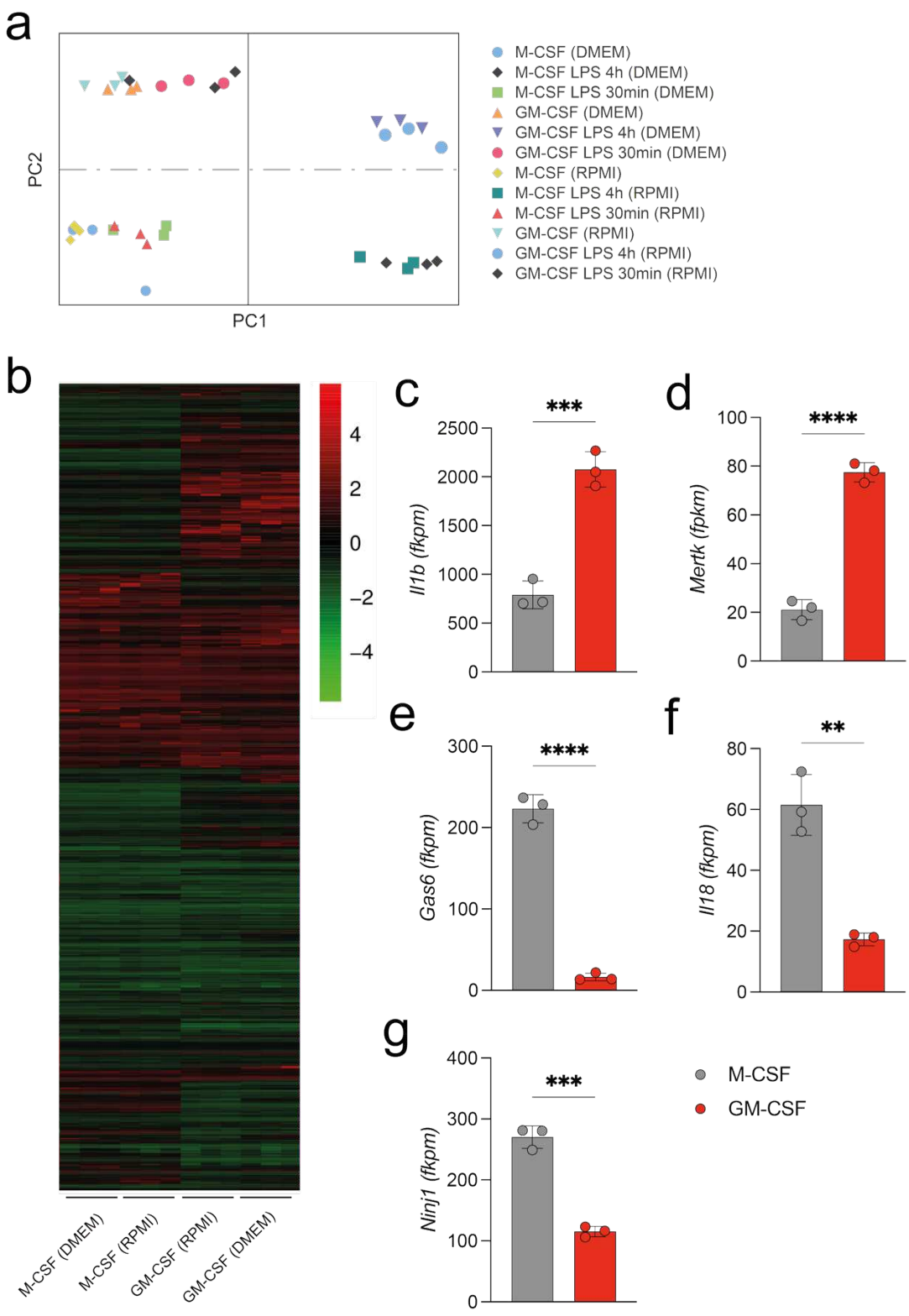

Figure 20 | M-CSF and GM-CSF BMDMs have distinct transcriptional responses to LPS. M-CSF- and GM-CSF-derived BMDMs lysed in RLT buffer and RNA was isolated and sent for bulk sequencing a) Principal component analysis (PCA) plot of bulk RNA expression in M-CSF and GM-CSF BMDMs grown in RPMI and DMEM and stimulated for 30 min or 4 h with LPS. b) Heatmap of M-CSF and GM-CSF BMDMs in RPMI or DMEM stimulated for 4 h with LPS. c-g) mRNA expression measured by bulk RNA sequencing of indicated DEGs. Data shown as mean ± SEM, points representing independent biological replicates. M-CSF BMDMs (grey), GM-CSF BMDMs (red).

cytometry), but less *Gas6*, *Cx3rc1*, *Folr2*, and *Il10* than steady state M-CSF BMDMs (Figure 19j-n). *Nlrp3* was not differentially expressed between M-CSF and GM-CSF BMDMs in steady state or after 4 h LPS, contradicting our findings with qPCR (data not shown).

After 4h LPS stimulation, both M-CSF and GM-CSF BMDMs underwent substantial transcriptional changes and upregulated a shared cassette seen by PCA and heatmap visualisation (Figure 20a,b). However, GM-CSF BMDMs continued to express more *Il1b* and fewer *Il18* transcripts than M-CSF BMDMs (Figure 20c-f). Similar to steady state, M-CSF BMDMs also expressed more *Gas6* and less *Mertk* (Figure 20d,e). M-CSF BMDMs also expressed higher levels of *Ninj1*, despite having less measurable plasma membrane rupture (LDH release) in our models of NLRP3 activation (Figure 20g).

Our scRNAseq data from Data Chapter 1 further revealed pyrin (*MEFV/Mefv*) expression in the arthritic joints in the same recruited macrophages that expressed *NLRP3/Nlrp3*, prompting us to compare pyrin inflammasome responses in M-CSF- and GM-CSF-derived BMDMs. Pyrin is typically activated when the normal function of RhoA is blocked. *Clostridium difficile* Toxin B (TcdB) is a tool used to induce pyrin activation via RhoA inhibition, though LPS priming is still required for pro-IL-1 β induction and subsequent IL-1β release[25]. Stimulating BMDMs with TcdB (1 or 1.5 μg/mL, 3 h), I found GM-CSF BMDMs exhibited higher IL-1β secretion when compared to M-CSF BMDMs, albeit they slightly resisted pyrin-induced cell death (Figure 21a,b). Thus, due to their higher *Il1b* steady state transcript levels and rapid pro-IL1β induction, GM-CSF BMDMs induce elevated IL-1β secretion downstream of multiple inflammasomes.

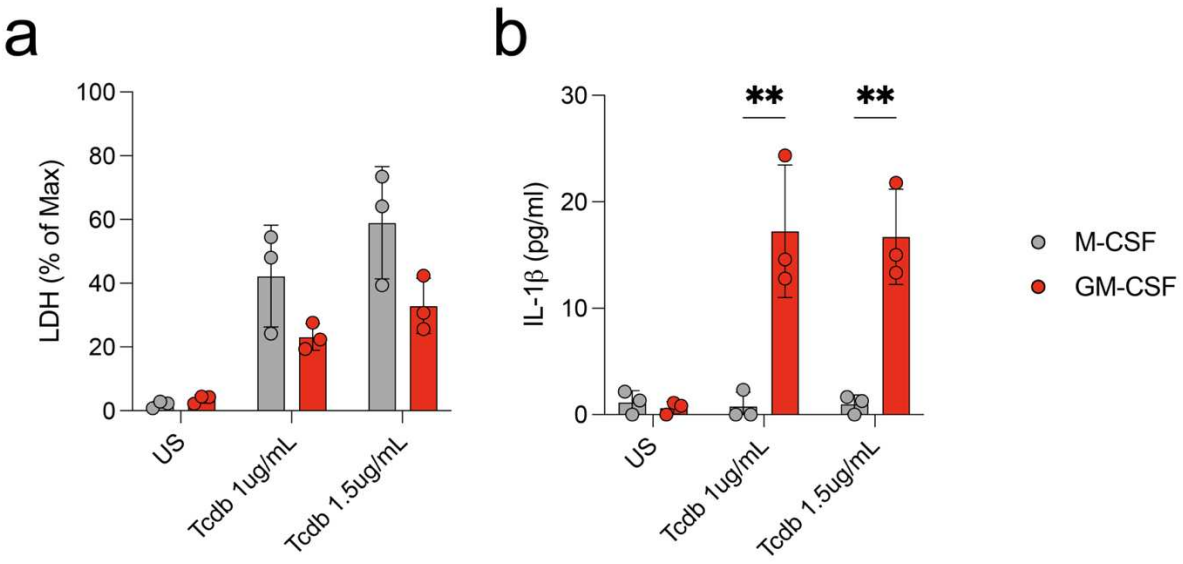

Figure 21 | GM-CSF macrophages resist cell death but have enhanced IL-1β release upon pyrin inflammasome activation.
M-CSF- and GM-CSF-derived BMDMs treated with 1 μg/mL or 1.5 μg/mL TcdB for 3 h. a) Pyrin inflammasome-dependent LDH release. b) IL-1β secretion measured by ELISA.

7.3.5 GM-CSF HMDMs resist cell death and have increased, albeit delayed IL-1β production

To understand if GM-CSF's ability to boost NLRP3 responses was conserved in humans, I differentiated CD14+ monocytes from healthy human blood for 7 days in M-CSF or GM-CSF to generate HMDMs. I then stimulated HMDMs with LPS for 4 h or 24 h. I found no difference in cell death, IL-1β, or TNF-α release at 4 h between M-CSF and GM-CSF HMDMs, agreeing with previously published data that GM-CSF HMDMs have a slower but prolonged response to LPS (Figure 22a-f)[26]. At 24 h, GM-CSF HMDMs secreted more TNF-α and IL-1β but resisted cell death (Figure 22a-f). Thus, in humans, like in mice, GM-CSF HMDMs show elevated, albeit delayed IL-1β secretion. Their unexpected resistance to cell death is being explored in a separate DPhil project in the lab.

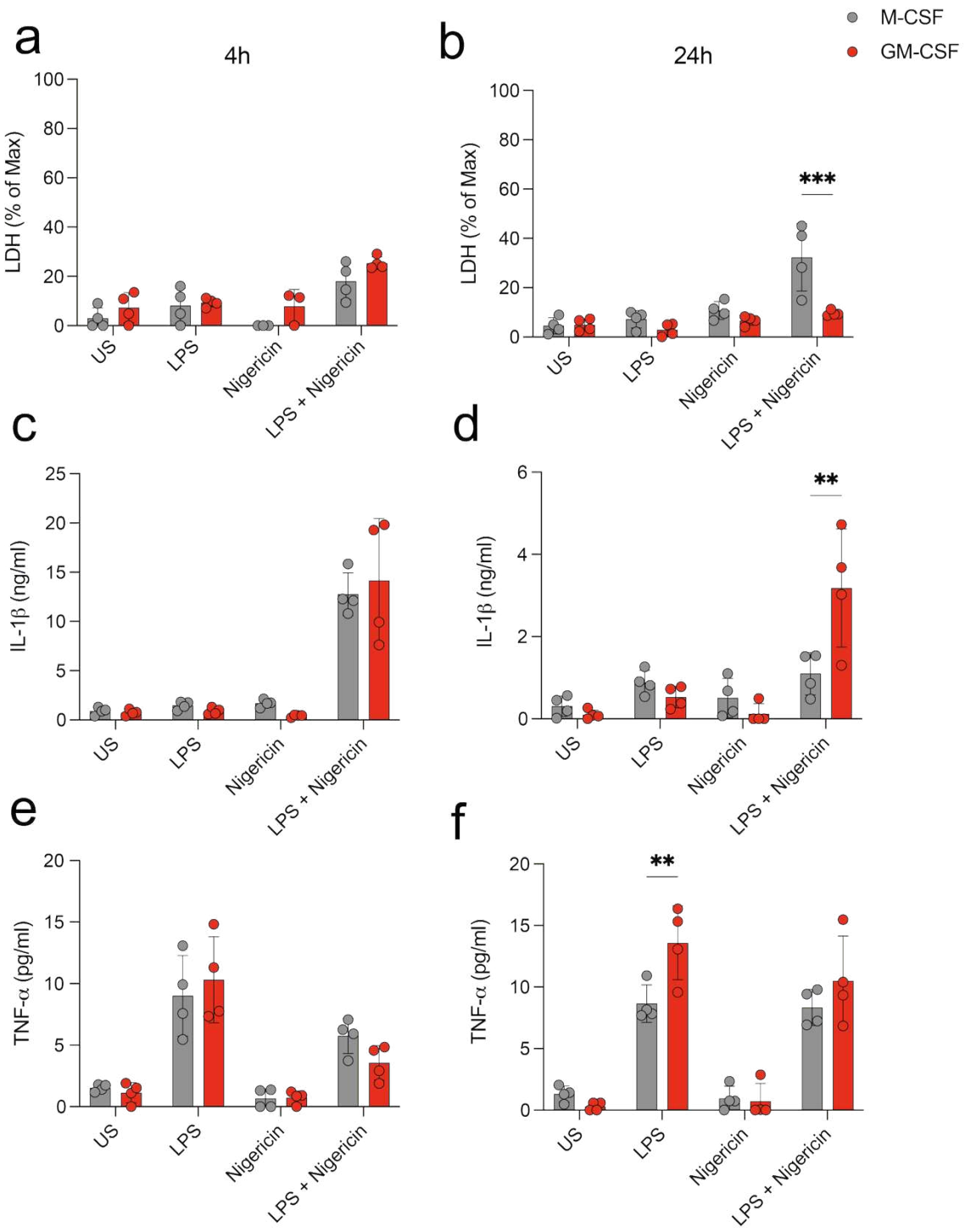

Figure 22 | GM-CSF HMDMs resist cell death after NLRP3 activation and have delayed induction of IL-1β. NLRP3 inflammasome activation in M-CSF- and GM-CSF-derived HMDMs primed with ultrapure 100ng/mL LPS (4h or 24h) ± 10 μM nigericin (1 h). Supernatants and lysates were collected post-stimulation. a–d) Inflammasome-dependent a,b) LDH release and c,d) IL-1β secretion (ELISA) measured after 4 h and 24 h of LPS priming. e,f) TNF secretion (ELISA) at 4h and 24h following LPS priming. h) Data shown as mean ± SEM with points representing four independent healthy human donors. M-CSF BMDMs (grey), GM-CSF BMDMs (red).

7.4 Discussion

Much of the current understanding of NLRP3 inflammasome biology stems from *in vitro* studies using M-CSF-differentiated BMDMs or HMDMs. In our hands, M-CSF-derived BMDMs exhibit a tissue-resident-like cell surface phenotype, marked by high F4/80, CX_3CR1, and MerTK expression, consistent with homeostatic macrophages. Conversely, GM-CSF-derived BMDMs display low CX3CR1 and MerTK and high CCR2, CCR5, and Ly6C, mirroring the transcriptional profile of recruited, inflammatory macrophages in the STIA model and human RA synovium, as observed in our scRNAseq data (Chapter 6).

While prior studies note GM-CSF enhances NLRP3 inflammasome activity and IL-1β release, none have systematically compared the kinetics of NLRP3 responses to pathogen-derived (LPS) and sterile (TNF) signals across M-CSF- and GM-CSF-derived BMDMs[3,4]. Here, GM-CSF BMDMs recapitulated the pro-inflammatory phenotype of recruited macrophages, exhibiting higher and more sustained inflammasome activity than quiescent M-CSF BMDMs. Within 30 min of LPS priming, GM-CSF BMDMs showed elevated NLRP3 pathway activity, evidenced by caspase-1 autoproteolysis, GSDMD cleavage, and IL-1β processing (Figure 13h). M-CSF BMDMs required longer priming (4 h) to reach comparable cell death levels (Figure 12c).

A novel finding is the observation that GM-CSF BMDMs secrete IL-1β after sterile TNF priming, a response that is typically absent in M-CSF BMDMs and other tissue-resident macrophages (Figure 13e). This suggests GM-CSF licenses IL-1β release in sterile inflammation, potentially explaining its role in RA synovial pathology. Mechanistically, this heightened activity may stem from delayed IL-10 production in GM-CSF BMDMs, a known NLRP3 suppressor abundant in M-CSF BMDMs from 30

min post-LPS (Figure 17a). Alternatively, GM-CSF-induced epigenetic changes, such as DNA methylation could facilitate this rapid pro-IL-1β upregulation, warranting further exploration[27].

In line with our STIA scRNAseq data, GM-CSF BMDMs and recruited macrophages share elevated basal *Nlrp3 and Il1b* transcription (Figure 18a), alongside higher *Tnf*, *Ccl17*, and *Mmp12* expression post-priming (Figure 18b–d), echoing findings in BMDMs and human monocytes[24]. However, enhanced NLRP3 responses *in vitro* were independent of autocrine TNF signalling, as *Tnfr1-/-* GM-CSF BMDMs matched WT responses (Figure 15c, d). Our scRNAseq also identified pyrin (*Mefv*) expression in arthritic joint macrophages. *In vitro*, GM-CSF BMDMs released more IL-1β even without LPS priming, unlike M-CSF BMDMs, suggesting their elevated responses to multiple inflammasome triggers (Figure 21).

Integrating scRNAseq and in vitro findings, GM-CSF emerges as a key driver of NLRP3 responses, accelerating *Il1b* transcription and pro-IL-1β production in response to both microbial and sterile cues. This positions GM-CSF BMDMs as a valuable model for studying inflammasome dynamics reflective of RA tissue biology.

7.5 Limitations

Conclusions from this chapter are restricted to murine BMDMs, though our findings have inspired a subsequent DPhil project comparing NLRP3 responses in M-CSF- and GM-CSF-differentiated HMDMs. Prior studies and our preliminary data presented here report kinetic differences in HMDMs, with M-HMDMs releasing more IL-1β after 2 h of LPS priming, only to be surpassed by GM-HMDMs at 6 h, 12 h, and 24 h, suggesting species-specific nuances our murine data may not fully capture[26].

In vitro studies BMDMs offer valuable insights into macrophage biology but face several limitations when modelling synovial inflammation in RA or STIA. First, BMDMs are derived from bone marrow precursors cultured with M-CSF or GM-CSF in a dish, which drives a generic macrophage phenotype distinct from the tissue-specific transcriptional and functional states of synovial macrophages. This artificial differentiation overlooks the microenvironmental cues, such as synovial stromal interactions or joint-specific inflammatory signals, that shape resident and recruited macrophage subsets *in vivo*, as observed in our scRNAseq data.

BMDMs lack the heterogeneity seen in synovial populations, where tissue-resident (e.g., TREM2-high lining) and recruited (e.g., CCR2+ NLRP3+) macrophages exhibit distinct inflammasome profiles and exist within the same tissue. *In vitro* cultures typically produce a homogeneous population, limiting their ability to recapitulate this diversity.

The absence of a physiological tissue context *in vitro* restricts BMDM responses to simplified stimuli (LPS or TNF), which may not mimic the complex, dynamic interplay of cytokines, chemokines, DAMPs, ECM, and nutrient availability in the arthritic synovium. This can exaggerate or mask inflammasome activation compared to *in vivo* conditions, where spatial localization (lining layer homing) and cell-cell interactions regulate expression.

Finally, BMDMs are murine-derived, introducing species-specific differences in inflammasome regulation that complicate translation to human RA. *In vitro* studies also cannot replicate the temporal progression of arthritis, from health to peak disease to resolution, captured in our time-resolved datasets, potentially missing dynamic shifts in NLRP3 expression or negative regulator induction.

An additional limitation of *in vitro* studies with BMDMs is the dose of GM-CSF used for differentiation, which may not reflect the *in vivo* concentrations relevant to RA. Typically, BMDMs are generated using standardized GM-CSF doses (20ng/mL in mice and 50ng/mL in humans for this study) to promote a pro-inflammatory phenotype. However, synovial GM-CSF levels in RA patients vary widely. This discrepancy could skew inflammasome activation profiles, such as NLRP3 and IL-1B expression, away from those observed in the arthritic joint, where physiological GM-CSF concentrations may act in a dose, time, and context-dependent manner. Without mirroring the *in vivo* 'RA-relevant' dose, BMDM models risk over- or underestimating the inflammatory potential of recruited macrophages, limiting their fidelity to the synovial environment.

7.6 Conclusions

GM-CSF differentiation of bone marrow progenitors yields a mixed population of floating and adherent cells *in vitro*, with the adherent fraction comprising macrophages that mirror the cell surface profile (low CX3CR1 and low MerTK) of recruited, inflammatory macrophages in the arthritic synovium of human RA and murine STIA. These GM-CSF-derived BMDMs exhibit elevated basal *Nlrp3* expression and, upon priming with LPS or TNF, rapidly produce pro-IL-1β, aligning with heightened NLRP3 and IL-1β signatures in our scRNAseq data (Data Chapter 1). With 30 min of NLRP3 inflammasome priming, GM-CSF BMDMs have greater levels of capase-1 cleavage (despite less steady state pro-caspase-1 levels) and IL-1β release but secrete less IL-18 than M-CSF BMDMs, due to less *Il18*. Future work should quantify NLRP3 inflammasome activation through ASC speck formation or ASC oligomerisation to understand the enhanced activity in GM-CSF BMDMs. Overall GM-CSF differentiation results in stronger, and more sustained NLRP3 responses

across all timepoints tested compared to M-CSF-derived BMDMs, driven by accelerated *Il1b* transcription and delayed IL-10 production rather than pre-existing IL-1β stores. Functionally testing IL-10R blockade or IL-10 deficient BMDMs differentiated in M-CSF or GM-CSF would reveal how instrumental IL-10 is in negatively regulating NLRP3 activity in both types of macrophages. Importantly, These the canonical NLRP3 activation observed was independent of autocrine TNF signalling or IRF5, and extend to pyrin-mediated IL-1β release with TcdB stimulation. Transcriptionally, GM-CSF BMDMs upregulate *Nlrp3*, *Tnf*, *Ccl17*, and *Mmp12*, reflecting profiles of synovial recruited macrophages. This suggests both M-CSF and GM-CSF should be used to understand tissue biology of inflammasome competent macrophages in tissue. Future work should dissect the importance of IL-1α, IL-1β, and IL-18 signalling in the presence of absence of alarmins release from pyroptosis.

These findings establish GM-CSF as a potential enhancing and prolonging factor of NLRP3 inflammasome activity in inflammatory arthritis, with GM-CSF-derived BMDMs serving as a robust *in vitro* model to recapitulate RA-relevant macrophage behaviour. This platform enables mechanistic dissection of NLRP3 and supports future exploration of GM-CSF or IL-1β blockade as therapeutic strategies in RA.

7.7 References

1. Helft, J. *et al.* GM-CSF Mouse Bone Marrow Cultures Comprise a Heterogeneous Population of CD11c+MHCII+ Macrophages and Dendritic Cells. *Immunity* **42**, 1197–1211 (2015).
2. Sun, L. *et al.* GM-CSF Quantity Has a Selective Effect on Granulocytic vs. Monocytic Myeloid Development and Function. *Front. Immunol.* **9**, 1922 (2018).

3. Erlich, Z. *et al.* Macrophages, rather than DCs, are responsible for inflammasome activity in the GM-CSF BMDC model. *Nat Immunol* **20**, 397–406 (2019).
4. Fleetwood, A. J., Lawrence, T., Hamilton, J. A. & Cook, A. D. Granulocyte-Macrophage Colony-Stimulating Factor (CSF) and Macrophage CSF-Dependent Macrophage Phenotypes Display Differences in Cytokine Profiles and Transcription Factor Activities: Implications for CSF Blockade in Inflammation. *J Immunol* **178**, 5245–5252 (2007).
5. Fleetwood, A. J., Dinh, H., Cook, A. D., Hertzog, P. J. & Hamilton, J. A. GM-CSF- and M-CSF-dependent macrophage phenotypes display differential dependence on Type I interferon signaling. *Journal of Leukocyte Biology* **86**, 411–421 (2009).
6. Hamilton, J. A. GM-CSF in inflammation and autoimmunity. *Trends in Immunology* **23**, 403–408 (2002).
7. Hibbs, M. L. *et al.* Mice Lacking Three Myeloid Colony-Stimulating Factors (G-CSF, GM-CSF, and M-CSF) Still Produce Macrophages and Granulocytes and Mount an Inflammatory Response in a Sterile Model of Peritonitis. *The Journal of Immunology* **178**, 6435–6443 (2007).
8. Gschwend, J. *et al.* Alveolar macrophages rely on GM-CSF from alveolar epithelial type 2 cells before and after birth. *Journal of Experimental Medicine* **218**, e20210745 (2021).
9. Schneider, C. *et al.* Alveolar Macrophages Are Essential for Protection from Respiratory Failure and Associated Morbidity following Influenza Virus Infection. *PLoS Pathog* **10**, e1004053 (2014).
10. Salvator, H. *et al.* Neutralizing GM-CSF autoantibodies in pulmonary alveolar proteinosis, cryptococcal meningitis and severe nocardiosis. *Respir Res* **23**, 280 (2022).

11. Subramanian Vignesh, K., Landero Figueroa, J. A., Porollo, A., Caruso, J. A. & Deepe, G. S. Granulocyte Macrophage-Colony Stimulating Factor Induced Zn Sequestration Enhances Macrophage Superoxide and Limits Intracellular Pathogen Survival. *Immunity* **39**, 697–710 (2013).

12. Kasahara, S. *et al.* Role of Granulocyte-Macrophage Colony-Stimulating Factor Signaling in Regulating Neutrophil Antifungal Activity and the Oxidative Burst During Respiratory Fungal Challenge. *J Infect Dis.* **213**, 1289–1298 (2016).

13. LeVine, A. M., Reed, J. A., Kurak, K. E., Cianciolo, E. & Whitsett, J. A. GM-CSF–deficient mice are susceptible to pulmonary group B streptococcal infection. *J. Clin. Invest.* **103**, 563–569 (1999).

14. McQualter, J. L. *et al.* Granulocyte Macrophage Colony-Stimulating Factor. *The Journal of Experimental Medicine* **194**, 873–882 (2001).

15. Croxford, A. L. *et al.* The Cytokine GM-CSF Drives the Inflammatory Signature of CCR2+ Monocytes and Licenses Autoimmunity. *Immunity* **43**, 502–514 (2015).

16. Komuczki, J. *et al.* Fate-Mapping of GM-CSF Expression Identifies a Discrete Subset of Inflammation-Driving T Helper Cells Regulated by Cytokines IL-23 and IL-1β. *Immunity* **50**, 1289-1304.e6 (2019).

17. Amorim, A. *et al.* IFNγ and GM-CSF control complementary differentiation programs in the monocyte-to-phagocyte transition during neuroinflammation. *Nat Immunol* **23**, 217–228 (2022).

18. Stock, A. T., Hansen, J. A., Sleeman, M. A., McKenzie, B. S. & Wicks, I. P. GM-CSF primes cardiac inflammation in a mouse model of Kawasaki disease. *Journal of Experimental Medicine* **213**, 1983–1998 (2016).

19. Su, X. *et al.* Breast cancer–derived GM-CSF regulates arginase 1 in myeloid cells to promote an immunosuppressive microenvironment. *Journal of Clinical Investigation* **131**, e145296 (2021).

20. Schroeder, M. A., Ritchey, J. & DiPersio, J. F. Myeloid Suppressive Cells Mobilized by GM-CSF in Non-Tumor Bearing Mice Are Dependent On Interferon Gamma for Function. *Blood* **120**, 832–832 (2012).

21. Sielska, M. *et al.* Tumour-derived CSF2/granulocyte macrophage colony stimulating factor controls myeloid cell accumulation and progression of gliomas. *Br J Cancer* **123**, 438–448 (2020).

22. Weiss, M. *et al.* IRF5 controls both acute and chronic inflammation. *Proc Natl Acad Sci U S A* **112**, 11001–11006 (2015).

23. Ipseiz, N. *et al.* Tissue-resident macrophages actively suppress IL-1beta release via a reactive prostanoid/IL-10 pathway. *EMBO J* **39**, (2020).

24. Achuthan, A. *et al.* Granulocyte macrophage colony-stimulating factor induces CCL17 production via IRF4 to mediate inflammation. *J Clin Invest* **126**, 3453–3466 (2016).

25. Xu, H. *et al.* Innate immune sensing of bacterial modifications of Rho GTPases by the Pyrin inflammasome. *Nature* **513**, 237–241 (2014).

26. Budai, M. M., Tőzsér, J. & Benkő, S. Different dynamics of NLRP3 inflammasome-mediated IL-1β production in GM-CSF– and M-CSF–differentiated human macrophages. *J Leukoc Biol* **101**, 1335–1347 (2017).

27. Rodriguez, R. M. *et al.* Signal Integration and Transcriptional Regulation of the Inflammatory Response Mediated by the GM-/M-CSF Signaling Axis in Human Monocytes. *Cell Reports* **29**, 860-872.e5 (2019).

8. Chapter 3 | GM-CSF blockade in AIA reduces inflammation and pain while promoting homeostatic myeloid phenotypes

8.1 Introduction

8.1.1 Biologics in RA

RA is a chronic autoimmune disease characterized by synovial inflammation, cartilage destruction, and debilitating pain, driven by complex interactions among immune cells, cytokines, and inflammasome pathways. Early studies revealed elevated TNF-α, IL-1, IL-6, and GM-CSF in RA synovium, sparking the development of biologics like anti-TNF (etanercept, infliximab), IL-6R (tocilizumab, sarilumab), and IL-1R (anakinra) therapies[1]. Despite transforming RA management, these treatments often fail to address persistent pain, suggesting distinct inflammatory and nociceptive pathways. In gouty arthritis, IL-1R blockade (anakinra) effectively reduces pain, highlighting IL-1's role in arthritic hypernociception[2–4].

GM-CSF, a newer therapeutic target, promotes proinflammatory macrophage and neutrophil activation, yet its clinical trials show mixed results. Early trials (EARTH EXPLORER Phase I, mavrilimumab Phase IIa, contRAst Phase II) demonstrated pain and inflammation reductions, but Phase III trials, including contRAst with otilimab, did not show superior efficacy when compared to TNF blockade or JAK inhibition (possibly due to broader inclusion of established RA patients), leading GSK to pause otilimab's development in 2023.

Clinical evidence, such as GM-CSF-induced joint flares and pain in Felty's syndrome, a condition marked by RA, granulocytopenia, anaemia, and splenomegaly underscores its pathogenic potential[5]. In COVID-19, GM-CSF blockade early in

disease (CRP <150 mg/mL) reduced ventilation and mortality risks but was ineffective later (CRP >150 mg/mL), suggesting GM-CSF initiates inflammatory cascades, a principle relevant to RA's early pathogenesis[6–8].

8.1.2 GM-CSF *in vivo:* timing matters

Timing is critical in GM-CSF's proinflammatory role, as shown in other sterile inflammation models. In a Kawasaki disease model, GM-CSF blockade within five days of induction prevented cardiac inflammation, but delayed treatment (day 7) was less effective[9]. Similarly, in experimental autoimmune encephalomyelitis (EAE), a multiple sclerosis model, GM-CSF receptor deletion protected mice from disease by blocking NLRP3 and IL-1β expression in myeloid cells, with prophylactic blockade fully effective unlike partial benefits in established disease[10,11]. These findings align with NLRP3/ASC-deficient mice showing abrogated EAE, emphasizing GM-CSF's early pathogenic programming[12,13].

8.1.3 *In vivo* models exploring GM-CSF in arthritis

In murine arthritis, seminal work by John Hamilton and colleagues established GM-CSF as a pivotal orchestrator of synovial inflammation across collagen-induced arthritis (CIA), antigen-induced arthritis (AIA), K/BxN serum transfer-induced arthritis (STIA), streptococcal cell wall (SCW) arthritis, and monosodium urate (MSU) crystal-induced gout models.

Systemic administration of GM-CSF exacerbates CIA[14]. GM-CSF deficient mice are protected from CIA, with some mice completely protected and some mice only displaying mild inflammation on one digit[15]. GM-CSF blockade can also reduce

the severity of AIA[16]. Similarly, local subcutaneous injections of GM-CSF or IL-1β in the methylated bovine serum albumin (mBSA) AIA model enhanced synovitis and histopathological severity[17]. These data are consistent with the clinical reporting that exogenous GM-CSF can drive joint inflammation flares and pain[5]. CIA and AIA are also ameliorated by anti-IL-1 treatment[18,19]. GM-CSF deficiency also reduces severity of K/BxN STIA, where others have also shown IL-1 blockade is effective, suggesting an interplay with GM-CSF and IL-1[20–22].

A mouse arthritis model that mimics anti-TNF non-response is the acute unilateral arthritis caused by direct injection of streptococcal cell wall bacterial extracts (SCW). In SCW arthritis, GM-CSF blockade reduces joint inflammation and prevents from cartilage destruction[23]. GM-CSF blockade also significantly reduces local IL-1β in this model, as measured by patellae washouts[23].

Gouty arthritis, which is highly driven by NLRP3 activation and downstream IL-1β release, can be modelled *in vivo* using the MSU crystal–induced inflammation model[24]. However, to induce joint inflammation in this model, LPS priming is typically required. MSU-induced peritoneal inflammation does not require LPS priming, hence it is a valuable tool to investigate sterile, NLRP3-dependent tissue inflammation. GM-CSF neutralization *in vivo* decreased MSU crystal–induced IL-1β levels and neutrophil infiltration[25].

Seminal studies, notably by John Hamilton and colleagues, have established GM-CSF as a pivotal orchestrator of synovial inflammation across diverse murine arthritis models. These models highlight GM-CSF and IL-1β's interplay in driving inflammation and pain, yet clinical translation requires mechanistic clarity and patient stratification. In this chapter, we evaluate GM-CSF blockade in the AIA model, assessing its impact on synovial inflammation, pro-IL-1β, neutrophil recruitment, and

pain via dynamic weight-bearing, a novel readout, while exploring myeloid phenotype shifts, particularly MerTK upregulation.

8.2 Aims

GM-CSF had been implicated in the pathogenesis of multiple *in vivo* models of inflammatory arthritis, but dynamic weight bearing as a measurement for pain in the AIA model, the connection with licensing inflammasome signature expression, and the effect on myeloid phenotype shifts in the synovium had not yet been elucidated. The core aims of this chapter are:

1) Evaluate the efficacy of GM-CSF blockade in reducing synovial inflammation, pro-IL-1β expression, and joint swelling in the AIA model.
2) Investigate the impact of GM-CSF blockade on pain outcomes and its correlation with pro-IL-1β expression and neutrophil recruitment in the synovium.
3) Assess the modulation of synovial myeloid cell phenotypes, particularly the upregulation of homeostatic marker MerTK, following GM-CSF neutralization *in vivo*.

8.3 Results

8.3.1 Clinical scoring reveals reduced joint swelling after GM-CSF blockade *in vivo*

To investigate GM-CSF's role in NLRP3 inflammasome expression and activity *in vivo*, I evaluated the efficacy of anti-GM-CSF monoclonal antibody (mAb) blockade in a murine AIA model using mBSA (Figure 23a). C57BL/6 mice were immunized with

mBSA in complete Freund's adjuvant (CFA) to prime autoantibody induction. On days -1 and 0 of disease induction, mice received intraperitoneal injections of anti-GM-CSF mAb or isotype control. On day 21 post-immunization, arthritis was induced (day 0 of disease induction) by intra-articular mBSA injection into the right rear knee, recruiting inflammatory immune cells. We assessed joint swelling (caliper measurements), non-evoked pain (BioSeb dynamic weight-bearing chambers), and synovial myeloid profiles (flow cytometry). GM-CSF blockade did not affect body weight but significantly reduced right knee oedema at peak inflammation on day 2 (Figure 23b).

8.3.2 Flow cytometry analysis reveals reduced pro-IL-1β and synovial inflammation after GM-CSF blockade *in vivo*

GM-CSF blockade did not affect total CD11b+ myeloid cell numbers in the synovium (Figure 23c), however, it changed their phenotypic profile. GM-CSF blockade significantly increased the percentage and mean fluorescence intensity (MFI) of the homeostatic and tissue-resident marker MerTK on CD11b+ myeloid cells while reducing inflammatory Ly6G+ neutrophil recruitment (Figure 23d,e). Although Ly6C+ CD11b+ monocyte-like cells trended higher in the synovium of anti-GM-CSF-treated mice, these Ly6C+ monocytes expressed elevated MerTK compared to those from isotype-treated mice (Figure 23d). Notably, CD11b+ cells from anti-GM-CSF-treated mice exhibited significantly lower pro-IL-1β expression (Figure 23f). Collectively, data suggest that GM-CSF blockade does not affect the number of macrophages in the synovium but reduces their pro-inflammatory phenotype.

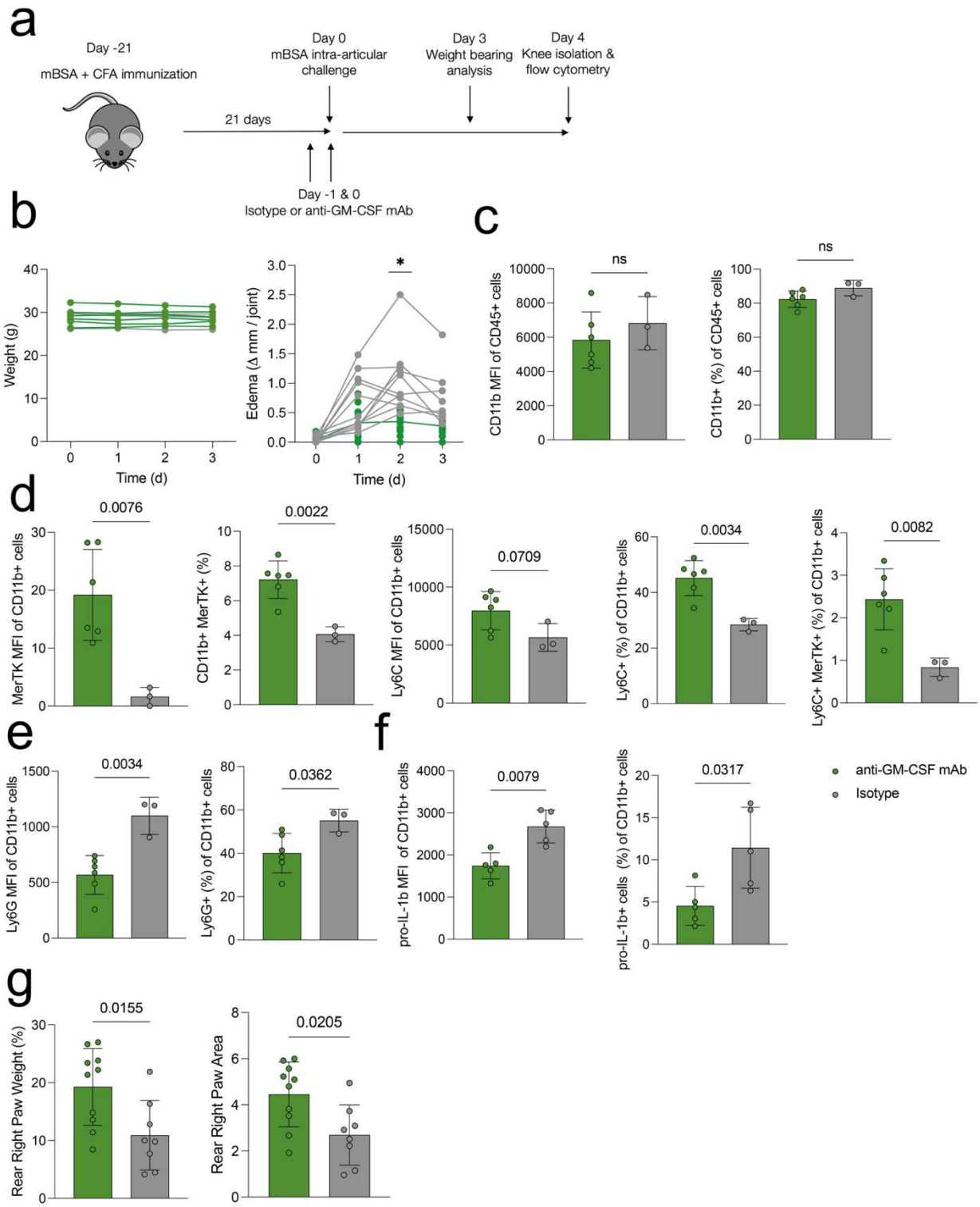

Figure 23 | Anti-GM-CSF blockade reduces synovial macrophage inflammatory profile, pro-IL-1β levels, disease severity, and pain in AIA. a) Schematic of *in vivo* experimental timeline. Mice were immunized on D-21 with mBSA + CFA and challenged with an intra-articular mBSA injection on D0. Anti-GM-CSF antibody was given intraperitoneally on D-1 and D0 (n=6 anti-GM-CSF, n=3 isotype control in two independent experiments). Synovium was digested and stained for flow cytometry. b) Weight and joint oedema of individual mice plotted through time. c) CD11b expression on CD45+ cells in the isolated murine arthritic synovium 4 days after intra-articular injection of mBSA. d) F4/80 and MerTK expression and positivity on CD11b+ myeloid cells 4 days after intra-articular injection of mBSA. e) Ly6G and Ly6C expression on CD11b+ myeloid cells 4 days after intra-articular injection. f) pro-IL-1β expression and positivity in CD11b+ myeloid cells 2 days after intra-articular mBSA injection. g) Pain measurements of rear right paw weight bearing/area bearing 3 days after intra-articular mBSA injection. Data are shown as mean ± SEM with single datapoints representing individual mice. anti-GM-CSF mAb (green), isotype control (grey).

8.3.3 GM-CSF blockade reduces inflammation and correlates with improved pain outcomes

To measure pain, we used the non-invasive BioSeb Dynamic Weight Bearing test, where mice are placed in a cage equipped with a camera on top to monitor movement and sensors on the bottom to monitor the weight/force put on each of their legs and the area covered by that leg as mice move. Less weight and less area covered by the affected, arthritic leg indicate more pain. Anti-GM-CSF-treated mice distributed more body weight through the arthritic right rear leg compared to isotype-treated controls, indicating reduced pain (Figure 23g). Thus, GM-CSF blockade mitigates mechanical pain in AIA by limiting inflammatory macrophage and neutrophil infiltration and pro-IL-1β expression in the synovium. Given IL-1β's hypothesized role in arthritic pain, I correlated pro-IL-1β expression with pain outcomes. Higher pro-IL-1β levels were associated with reduced weight bearing on the affected limb (Figure 24a,b), confirming a positive correlation between IL-1β and pain. Additionally, pro-IL-

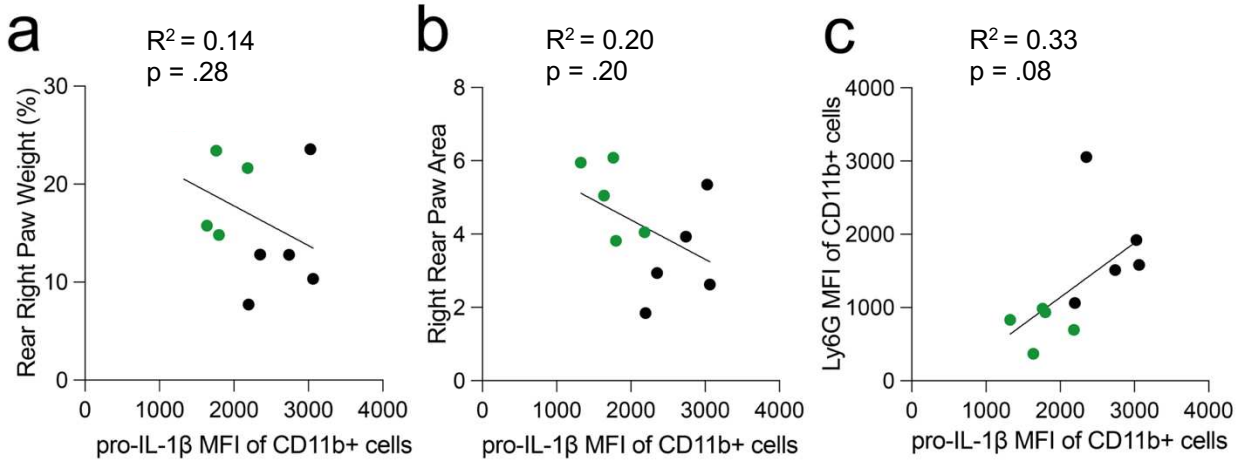

Figure 24 | Pro-IL-1β levels in the synovium positively correlate with neutrophil recruitment and pain in AIA. Pro-IL-1β expression (MFI) in live CD11b+ gated cells correlated with pain measurements a) rear right paw weight bearing (% of body weight) b) rear right paw weight area c) Ly6G MFI of CD11b+ gated cells on day 2 after intra-articular mBSA injection. Single datapoints representing individual mice. anti-GM-CSF mAb (green), isotype control (black).

1β expression correlated with increased Ly6G+ neutrophil recruitment in the synovium (Figure 24c).

8.4 Discussion

In this chapter, my data demonstrate systemic GM-CSF neutralization in the AIA model reduced synovial macrophage pro-inflammatory phenotypes, pro-IL-1β expression, neutrophil recruitment, synovitis, and pain. Consistent with foundational work by John Hamilton, I confirmed that GM-CSF blockade attenuates AIA severity, as evidenced by decreased joint swelling and inflammatory cell infiltration (Figure 19b,e,f). Extending these findings, my data suggests that GM-CSF blockade prior to disease induction upregulates the homeostatic marker MerTK on total CD11b+ myeloid cells and incoming Ly6C+ monocytes in the synovium (Figure 19d), suggesting a shift toward tissue-resident, anti-inflammatory phenotypes.

My data also highlight that GM-CSF blockade reduces synovial pro-IL-1β, which strongly correlates with improved weight bearing, a proxy for reduced pain (Figure 19f,g; Figure 20a,b). Recent studies indicate that specific synovial macrophage subsets localize near nociceptor neurons, potentially activating IL-1R+ neurons via IL-1β secretion, and neuronal IL-1R signalling has been linked to pain in a murine RA model[26,27]. The observed correlation between pro-IL-1β and neutrophil recruitment (Figure 20c) further aligns with IL-1β's role in amplifying inflammation. However, the relevance to human RA remains uncertain. Despite promising preclinical results, clinical trials of GM-CSF and IL-1R blockade in RA have yielded mixed outcomes, possibly due to patient heterogeneity. Stratifying RA patients with high inflammasome signatures (elevated IL-1β or NLRP3 activity) and establishing better timing of GM-CSF and IL-1R blockade (between flares, or at the initiation of the flare,

or in patients with high risk), could identify responders to GM-CSF, IL-1R, or inflammasome targeted therapies (Chapter 5)[28].

Model-specific limitations, such AIA's monoarticular nature, suggest the need for further studies in polyarticular models like K/BxN STIA to fully elucidate GM-CSF's therapeutic potential in rheumatoid arthritis.

8.5 Limitations

The AIA model using mBSA is a valuable tool for studying inflammatory arthritis, but has several limitations that impact its applicability and translation to human disease, such as RA. The primary limitation of the AIA model is that it relies on a single, well-characterized antigen to trigger arthritis, which oversimplifies the complex, multifactorial etiology of human RA. RA involves a combination of genetic and environmental factors and autoantibody production proceeds clinical disease onset by years. The artificial nature of mBSA as a foreign antigen further distances the model from RA's autoantibodies including rheumatoid factor (RF) and anti-citrullinated peptide antibodies (ACPA). AIA is a localized hypersensitivity reaction to an exogenous antigen rather than a systemic breach of immunological tolerance to endogenous autoantigen.

Another limitation of AIA is that it is induced by intra-articular injection of mBSA, resulting in monoarticular inflammation. In contrast, human RA is a systemic, polyarticular disease affecting multiple joints. This localized response limits the model's ability to mimic the systemic nature of RA, including extra-articular manifestations like cardiovascular or pulmonary involvement. Additionally, intra-articular injection itself may cause physical injury and activate mechano-sensing

pathways in the joint, contributing to inflammation independently of the antigen-specific response.

The AIA model is also self-resolving and does not recapitulate the persistence and flaring nature of RA. As the disease peaks within days of mBSA intra-articular injection, the therapeutic window is narrow, and biologic intervention is often given as a prophylaxis rather than treatment. In our model, we administered an anti-GM-CSF mAb one day prior to disease induction. These limitations impact the therapeutic predictability of the AIA model to RA, where biologic treatment is often reserved for patients with established, and often MTX-resistant disease.

However, combining multiple murine models across various strains can mitigate bias from individual murine models. For example, C57BL/6 mice are susceptible to AIA (used in this study), while CBA mice are resistant to this model. CBA mice are susceptible to CIA, K/BxN STIA, and *Streptococcal* cell wall-induced arthritis.

Technically, synovial analysis in AIA is challenging. Dissecting synovium without contamination from cartilage, bone, or periarticular tissue requires expertise, particularly in arthritic joints where inflammation blurs tissue boundaries. The monoarticular model yields limited tissue (one joint per mouse), constraining cell numbers for flow cytometry. Homogenization for soluble proteins, as required for ELISA, destroys tissue, precluding further analyses, unlike flow cytometry, which I prioritized for single-cell resolution of intracellular/extracellular markers. Obtaining synovial supernatants for ELISA is feasible but technically demanding due to low yields (~100–200 µL from one knee) and risks of blood or cartilage contamination, which can skew cytokine measurements. However, staining synovial tissue for ASC specks or measuring cleaved IL-18 or IL-1β would provide more supportive evidence

that GM-CSF blockade reduces NLRP3 activity *in vivo*. These constraints highlight the need for optimized protocols or complementary models like K/BxN STIA, which offers polyarticular inflammation and higher synovial yields.

8.6 Conclusions

In vitro, I demonstrated that GM-CSF drives pro-IL-1β transcription and production in response to sterile priming signals. *In vivo*, I evaluated GM-CSF blockade in the AIA model and found that it significantly reduced joint oedema, pain, neutrophil recruitment, and pro-IL-1β expression in the affected knee compared to isotype controls. These findings underscore GM-CSF's role in amplifying synovial inflammation and pain via inflammasome activation, suggesting its potential as a therapeutic target in inflammatory arthritis, pending further validation in systemic models and human studies.

8.7 References

1. Chu, C. Q. *et al.* Detection of Cytokines at the Cartilage/Pannus Junction in Patients with Rheumatoid Arthritis: Implications for the Role of Cytokines in Cartilage Destruction and Repair. *Rheumatology* **31**, 653–661 (1992).
2. Torres, R. *et al.* Hyperalgesia, synovitis and multiple biomarkers of inflammation are suppressed by interleukin 1 inhibition in a novel animal model of gouty arthritis. *Annals of the Rheumatic Diseases* **68**, 1602–1608 (2009).
3. Janssen, C. A. *et al.* Anakinra for the treatment of acute gout flares: a randomized, double-blind, placebo-controlled, active-comparator, non-inferiority trial. *Rheumatology* **58**, 1344–1352 (2019).

4. Saag, K. G. *et al.* A Randomized, Phase II Study Evaluating the Efficacy and Safety of Anakinra in the Treatment of Gout Flares. *Arthritis & Rheumatology* **73**, 1533–1542 (2021).
5. Hazenberg, B., Van Leeuwen, M., Van Rijswijk, M., Stern, A. & Vellenga, E. Correction of granulocytopenia in Felty's syndrome by granulocyte- macrophage colony-stimulating factor. Simultaneous induction of interleukin-6 release and flare-up of the arthritis. *Blood* **74**, 2769–2770 (1989).
6. Thwaites, R. S. *et al.* Inflammatory profiles across the spectrum of disease reveal a distinct role for GM-CSF in severe COVID-19. *Sci. Immunol.* **6**, eabg9873 (2021).
7. Temesgen, Z. *et al.* Lenzilumab in hospitalised patients with COVID-19 pneumonia (LIVE-AIR): a phase 3, randomised, placebo-controlled trial. *The Lancet Respiratory Medicine* **10**, 237–246 (2022).
8. Temesgen, Z. *et al.* C reactive protein utilisation, a biomarker for early COVID-19 treatment, improves lenzilumab efficacy: results from the randomised phase 3 'LIVE-AIR' trial. *Thorax* thoraxjnl-2022-218744 (2022) doi:10.1136/thoraxjnl-2022-218744.
9. Stock, A. T., Hansen, J. A., Sleeman, M. A., McKenzie, B. S. & Wicks, I. P. GM-CSF primes cardiac inflammation in a mouse model of Kawasaki disease. *Journal of Experimental Medicine* **213**, 1983–1998 (2016).
10. Croxford, A. L. *et al.* The Cytokine GM-CSF Drives the Inflammatory Signature of CCR2+ Monocytes and Licenses Autoimmunity. *Immunity* **43**, 502–514 (2015).
11. Ifergan, I. *et al.* Targeting the GM-CSF receptor for the treatment of CNS autoimmunity. *Journal of Autoimmunity* **84**, 1–11 (2017).

12. Amorim, A. *et al.* IFNγ and GM-CSF control complementary differentiation programs in the monocyte-to-phagocyte transition during neuroinflammation. *Nat Immunol* **23**, 217–228 (2022).

13. Inoue, M., Williams, K. L., Gunn, M. D. & Shinohara, M. L. NLRP3 inflammasome induces chemotactic immune cell migration to the CNS in experimental autoimmune encephalomyelitis. *Proc. Natl. Acad. Sci. U.S.A.* **109**, 10480–10485 (2012).

14. Campbell, I. K., Bendele, A., Smith, D. A. & Hamilton, J. A. Granulocyte-macrophage colony stimulating factor exacerbates collagen induced arthritis in mice. *Annals of the Rheumatic Diseases* **56**, 364–368 (1997).

15. Campbell, I. K. *et al.* Protection from collagen-induced arthritis in granulocyte-macrophage colony-stimulating factor-deficient mice. *J Immunol* **161**, 3639–3644 (1998).

16. Cook, A. D. *et al.* Granulocyte macrophage colony-stimulating factor receptor α expression and its targeting in antigen-induced arthritis and inflammation. *Arthritis Res Ther* **18**, 287 (2016).

17. Bischof, R. J., Zafiropoulos, D., Hamilton, J. A. & Campbell, I. K. Exacerbation of acute inflammatory arthritis by the colony-stimulating factors CSF-1 and granulocyte macrophage (GM)-CSF: evidence of macrophage infiltration and local proliferation. *Clinical and Experimental Immunology* **119**, 361–367 (2001).

18. Joosten, L. A. *et al.* IL-1 alpha beta blockade prevents cartilage and bone destruction in murine type II collagen-induced arthritis, whereas TNF-alpha blockade only ameliorates joint inflammation. *J Immunol* **163**, 5049–5055 (1999).

19. van de Loo, A. A. *et al.* Role of interleukin 1 in antigen-induced exacerbations of murine arthritis. *Am J Pathol* **146**, 239–249 (1995).

20. Louis, C. *et al.* NK cell–derived GM-CSF potentiates inflammatory arthritis and is negatively regulated by CIS. *Journal of Experimental Medicine* **217**, e20191421 (2020).

21. Ji, H. *et al.* Critical Roles for Interleukin 1 and Tumor Necrosis Factor α in Antibody-induced Arthritis. *The Journal of Experimental Medicine* **196**, 77–85 (2002).

22. Choe, J.-Y., Crain, B., Wu, S. R. & Corr, M. Interleukin 1 Receptor Dependence of Serum Transferred Arthritis Can be Circumvented by Toll-like Receptor 4 Signaling. *The Journal of Experimental Medicine* **197**, 537–542 (2003).

23. Plater-Zyberk, C. *et al.* GM-CSF neutralisation suppresses inflammation and protects cartilage in acute streptococcal cell wall arthritis of mice. *Annals of the Rheumatic Diseases* **66**, 452–457 (2007).

24. Martinon, F., Pétrilli, V., Mayor, A., Tardivel, A. & Tschopp, J. Gout-associated uric acid crystals activate the NALP3 inflammasome. *Nature* **440**, 237–241 (2006).

25. Shaw, O. M., Steiger, S., Liu, X., Hamilton, J. A. & Harper, J. L. Brief Report: Granulocyte–Macrophage Colony-Stimulating Factor Drives Monosodium Urate Monohydrate Crystal–Induced Inflammatory Macrophage Differentiation and NLRP3 Inflammasome Up-Regulation in an In Vivo Mouse Model. *Arthritis & Rheumatology* **66**, 2423–2428 (2014).

26. Hasegawa, T. *et al.* Macrophages and nociceptor neurons form a sentinel unit around fenestrated capillaries to defend the synovium from circulating immune challenge. *Nat Immunol* **25**, 2270–2283 (2024).

27. Mailhot, B. *et al.* Neuronal interleukin-1 receptors mediate pain in chronic inflammatory diseases. *Journal of Experimental Medicine* **217**, e20191430 (2020).

28. Mertens, M. & Singh, J. A. Anakinra for Rheumatoid Arthritis: A Systematic Review. *J Rheumatol* **36**, 1118–1125 (2009).

9. Chapter 4 | Recognition of apoptotic cells lowers NLRP3 inflammasome activity in macrophages

9.1 Introduction

This thesis has primarily explored mechanisms that enhance NLRP3 expression and activity in recruited myeloid populations during active disease. However, understanding mechanisms that maintain joint homeostasis is equally critical to elucidate how systemic loss of tolerance manifests as synovial inflammation and cartilage destruction in conditions like rheumatoid arthritis (RA). Current therapeutics predominantly target active inflammatory pathways, potentially overlooking opportunities to leverage endogenous pathways that promote joint health.

Tissue-resident synovial macrophages highly express efferocytosis receptors, including MerTK, TIMD-4, and VSIG4 (Chapter 1). Notably, MerTK+ macrophage populations strongly correlate with synovial health and RA remission in humans, sparking significant interest in MerTK's role in joint homeostasis[1,2]. In agreement, when we blocked GM-CSF in a mouse model of AIA, this reduced disease and pain scores, while restoring MerTK expression on synovial macrophages. MerTK belongs to the TAM receptor tyrosine kinase family, alongside Tyro3 and Axl. The concept that TAM receptors and efferocytosis broadly dampen inflammation is well-established, with foundational studies dating back to the early 2000s.

In 1999, MerTK knockout mice exhibited exacerbated responses to endotoxic shock, characterized by increased NF-κB nuclear translocation and elevated serum TNF-α levels[3]. MerTK contributes to tissue health through three primary mechanisms: (1) efferocytosis, the phagocytic clearance of apoptotic cells; (2) induction of soluble

anti-inflammatory and pro-resolving mediators; and (3) endogenous inhibition of inflammatory signalling pathways.

Estimating daily cell death in a healthy human is complex due to variability across tissues and individuals, but studies estimate that 50–70 billion cells undergo apoptosis daily[4]. Inefficient clearance of apoptotic cells can lead to secondary necrosis and the release of damage-associated molecular patterns (DAMPs), triggering immune responses and chronic inflammation, which may exacerbate autoimmune diseases or tissue damage[5].

MerTK-deficient mice develop rapid, progressive blindness within eight weeks of birth due to defective phagocytosis of retinal pigment epithelium and shed photoreceptor outer segment fragments[6]. Recent studies suggest that defective phagocytosis alone is insufficient to cause this phenotype; rather, MerTK ablation triggers inflammation, leading to rapid photoreceptor degeneration[7]. *In vivo* models of TAM receptor deficiencies indicate that MerTK is the primary efferocytosis receptor in murine macrophages, although Axl and Tyro3 can partially compensate[8]. A seminal 2007 study demonstrated that TAM triple-knockout mice exhibit hyperresponsiveness to Toll-like receptor (TLR) activation[9]. Mechanistically, TAM receptor activation induces SOCS1 and SOCS3 expression and inhibits TRAF3/6 ubiquitination, attenuating NF-κB signalling and downstream cytokine release[9].

MerTK's phagocytic and anti-inflammatory functions are mediated by distinct signalling pathways. The autophosphorylation site Tyr-867 is essential for efferocytosis but dispensable for inhibiting NF-κB activation, highlighting the separation of these roles[10]. Soluble factors downstream of TAM receptors, such as IL-10 and TGF-β, further dampen inflammation in contexts like cancer and pregnancy[11,12]. IL-10, a potent inhibitor of NLRP3 and IL-1β production, is both

induced by and induces MerTK in human macrophages, establishing a feedback loop[13,14]. In a vesicular stomatitis virus (VSV) infection model, apoptotic cell recognition via MerTK promoted innate immune anergy through IL-10 and TGF-β synthesis[15].

MerTK signalling in human macrophages also promotes the release of specialized pro-resolving mediators (SPMs), which drive inflammation resolution *in vitro* and *in vivo*[16]. In a zymosan-induced peritonitis model, MerTK deficiency reduced SPM production and increased neutrophil infiltration, suggesting a broader role for MerTK in tissue repair beyond IL-10 and TGF-β[16]. In pregnancy, MerTK inhibition in *ex vivo* foetal membrane models and *in vivo* models led to NLRP3 activation and IL-1β release, indicating MerTK's role as a brake on NLRP3 activity[17]. Additionally, MerTK inhibits NLRP3 protein levels via autophagy in a subarachnoid haemorrhage model[18], while NLRP3 activation reciprocally inhibits MerTK-dependent efferocytosis[19].

9.2 Aims

The overarching goal of this chapter is to test whether high MerTK signalling can lower the expression or activity of the NLRP3 inflammasome in macrophages. The specific aims are to:

1) Characterize the dynamic regulation of MerTK expression under inflammatory conditions *in vitro* and correlate with inflammasome activity in macrophages.
2) Determine the impact of apoptotic cell recognition via MerTK on NLRP3 inflammasome expression and activity

9.3 Results

9.3.1 High MerTK expression in synovial macrophages correlates with low NLRP3 expression

Our scRNAseq analysis revealed high expression of efferocytosis receptor such as *MERTK* on tissue-resident macrophages in healthy synovium in mice, which agrees with previous reports describing synovium of healthy people, and those in disease remission[1]. Notably, high MerTK expression inversely correlated with NLRP3 expression in macrophages from both mouse and human synovium. As MerTK recognizes phosphatidylserine on apoptotic cells via bridging molecules Protein S (ProS) and Gas6, and is a known inducer of the NLRP3 suppressor IL-10, I hypothesized that apoptotic cell recognition by MerTK-high macrophages inhibits NLRP3 expression and activity. To test this, I used *in vitro* models of MerTK-high (M-CSF-derived) and MerTK-low (GM-CSF-derived) bone marrow-derived macrophages (BMDMs).

In vitro, M-CSF BMDMs express both MerTK and basal levels of NLRP3. As M-CSF BMDMs have peak NLRP3 responses 4 h after LPS priming and induce tolerance within 24 h, I investigated transcript levels of *Mertk*, *Nlrp3*, and *Il1b* in M-CSF BMDMs at 4 h post LPS. LPS treatment resulted in significant upregulation in NLRP3 inflammasome components *Nlrp3*, *Il1b*, and *Gsdmd. Mertk*, *Socs3*, and *Il10* were also significantly upregulated after 4h LPS, suggesting negative regulators of NLRP3 are expressed well-before endotoxin tolerance is observed (Figure 25a-f).

I reproduced work from Gurung *et al*., demonstrating that IL-10R mAb blockade prolongs NLRP3 responses (Figure 26a-d)[13].

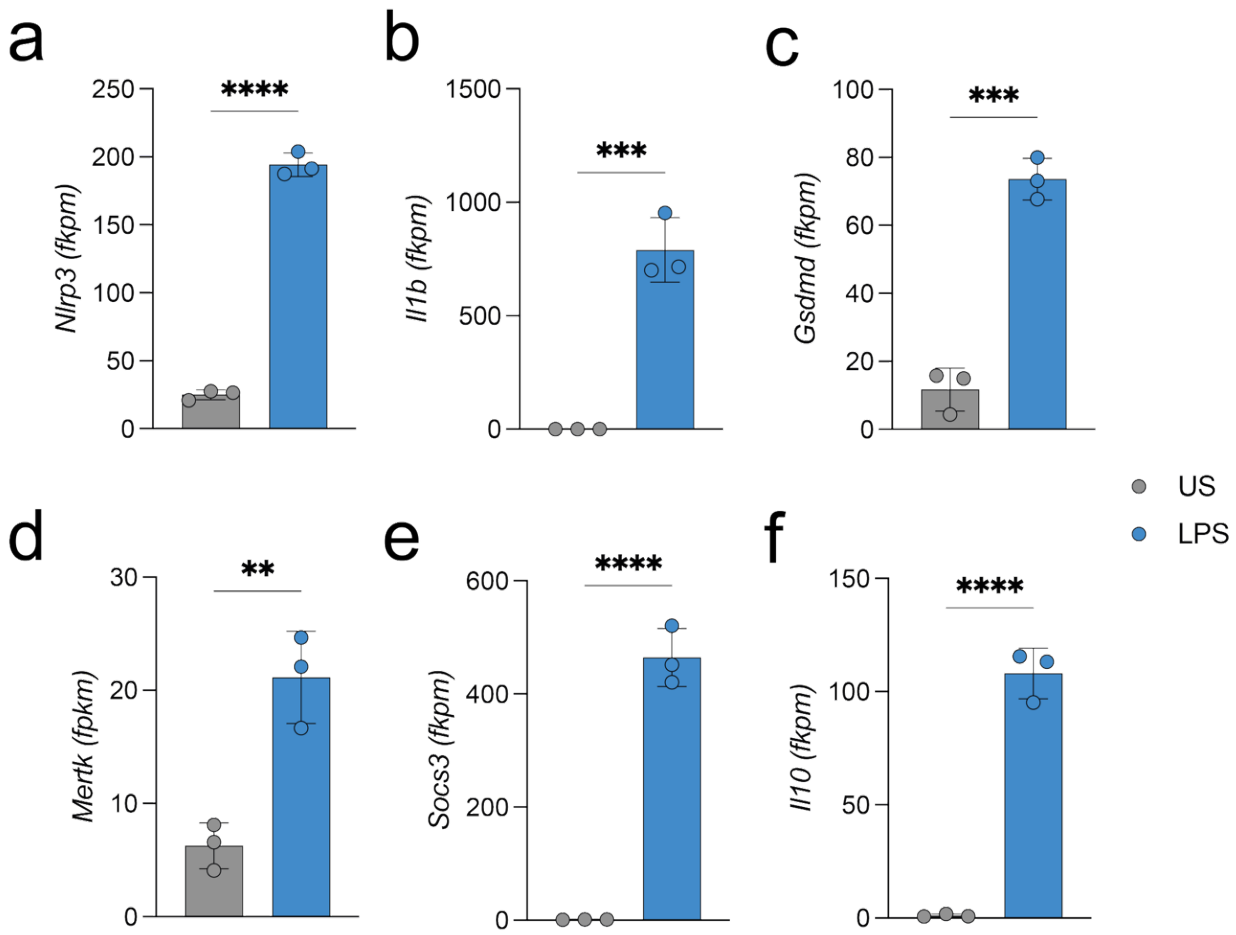

Figure 25 | *Mertk*, *Socs3*, and *Il10* are upregulated after LPS priming at peak inflammation *in vitro*.
M-CSF differentiated BMDMs were lysed in RLT buffer and RNA was isolated and sent for bulk sequencing a-f) mRNA expression measured by bulk RNA sequencing of indicated DEGs. Data shown as mean ± SEM, points representing independent biological replicates. Unstimulated BMDMs (grey), LPS treated BMDMs (blue).

9.3.2 MerTK expression is dynamically regulated by LPS and high MerTK levels inversely correlate with NLRP3 responses

As I found *Mertk* was upregulated following LPS treatment, I aimed to quantify surface MerTK expression in a time course following LPS treatment. To assess MerTK regulation under inflammatory conditions, I exposed M-CSF BMDMs to LPS (100 ng/mL) and monitored MerTK expression over time. MerTK was transiently downregulated within 1 hour of LPS exposure but returned to baseline levels by 6

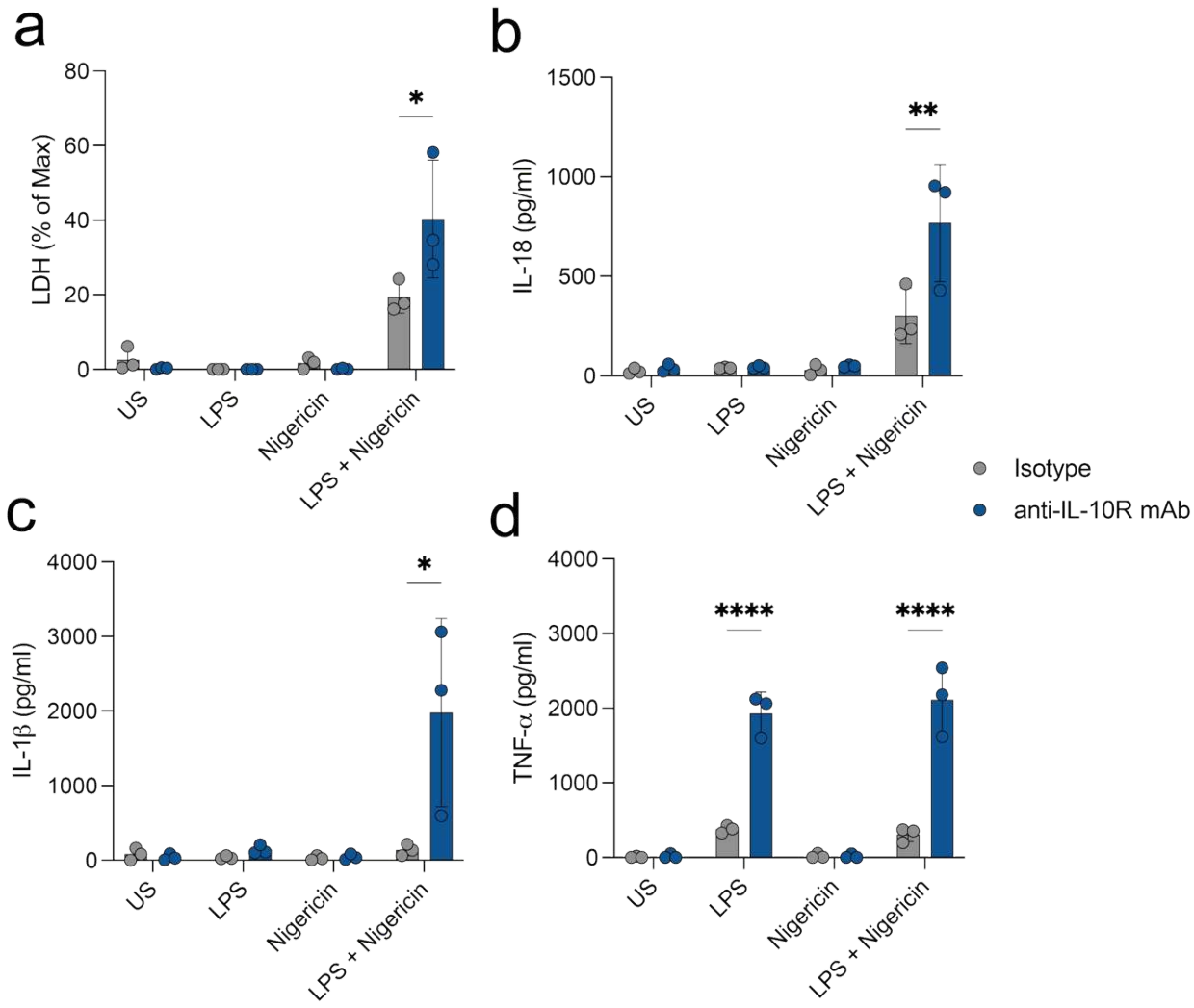

Figure 26 | IL-10R blockade increases NLRP3 responses.
WT BMDMs differentiated in M-CSF were primed with 100 ng/mL ultrapure LPS for 24 h ± 7.5μM nigericin (1 h). Supernatants and lysates collected post-stimulation. a) Inflammasome-dependent LDH release. b) IL-18, c) IL-1β, and d) TNF secretion measured by ELISA. Data shown as mean ± SEM, points representing three independent biological replicates. M-CSF BMDMs + isotype (grey), M-CSF BMDMs + anti-IL-10R (CD210) mAb (dark blue).

hours and was upregulated by 24 hours (Figure 27a). This kinetic aligns with endotoxin tolerance in M-CSF BMDMs, which is IL-10-dependent and associated with increased MerTK expression[13]. To investigate MerTK's role in NLRP3 regulation, I used $CX_3CR1^{CreER/+}MerTK^{fl/fl}$ BMDMs (bone marrow kindly provided by Prof Mariola Kurowska-Stolarska) treated with 4-OH-tamoxifen *in vitro* to induce partial MerTK knockdown, with wild-type (WT) BMDMs as controls (Figure 27b). In WT BMDMs, 4-OH-tamoxifen markedly suppressed NLRP3 responses (LDH and IL-1β secretion)

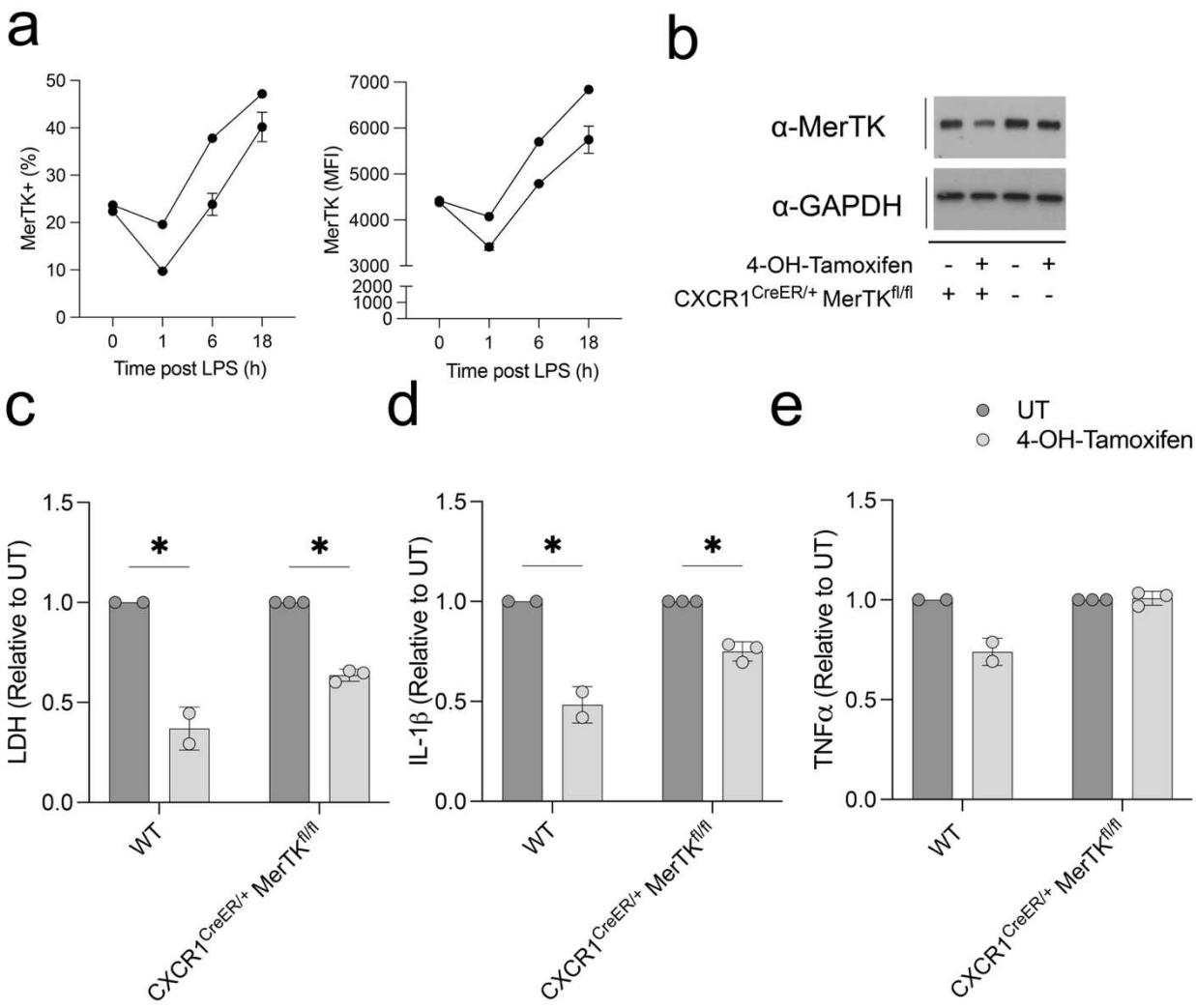

Figure 27 | *In vitro* 4-OH-Tamoxifen induced deletion of MerTK results in a modest increase in NLRP3 responses relative to 4-OH-Tamoxifen WT. a) Cell surface expression of MerTK+ (%) and MFI measured by flow cytometry 0, 1, 6, and 18h after LPS exposure in M-CSF BMDMs. b) MerTK expression in the whole cell lysate (WCL) of WT or $CX_3CR1^{CreER/+}MerTK^{fl/fl}$ ± 4-OH-Tamoxifen interrogated by Western blot. c) NLRP3-dependent cell death after 24h 100ng/mL LPS + 1h 10um nigericin measured by LDH normalized relative to untreated. d) IL-1β release and e) TNF release after 24h 100ng/mL LPS + 1h 10um nigericin measured by ELISA normalized relative to untreated.

(Figure 27c), suggesting a general influence of 4-OH-tamoxifen on inflammasome signalling, somewhat lowering the robustness of this experimental approach. Nonetheless, even very partial MerTK knockdown achieved in $CX_3CR1^{CreER/+}MerTK^{fl/fl}$ BMDMs increased NLRP3 responses (Figure 27c), when compared to control, 4-OH-tamoxifen-treated cells. Data suggest that MerTK suppresses NLRP3 activity,

however, the overall suppressive effect of 4-OH-tamoxifen limits definitive conclusions about MerTK's specific contribution in this system.

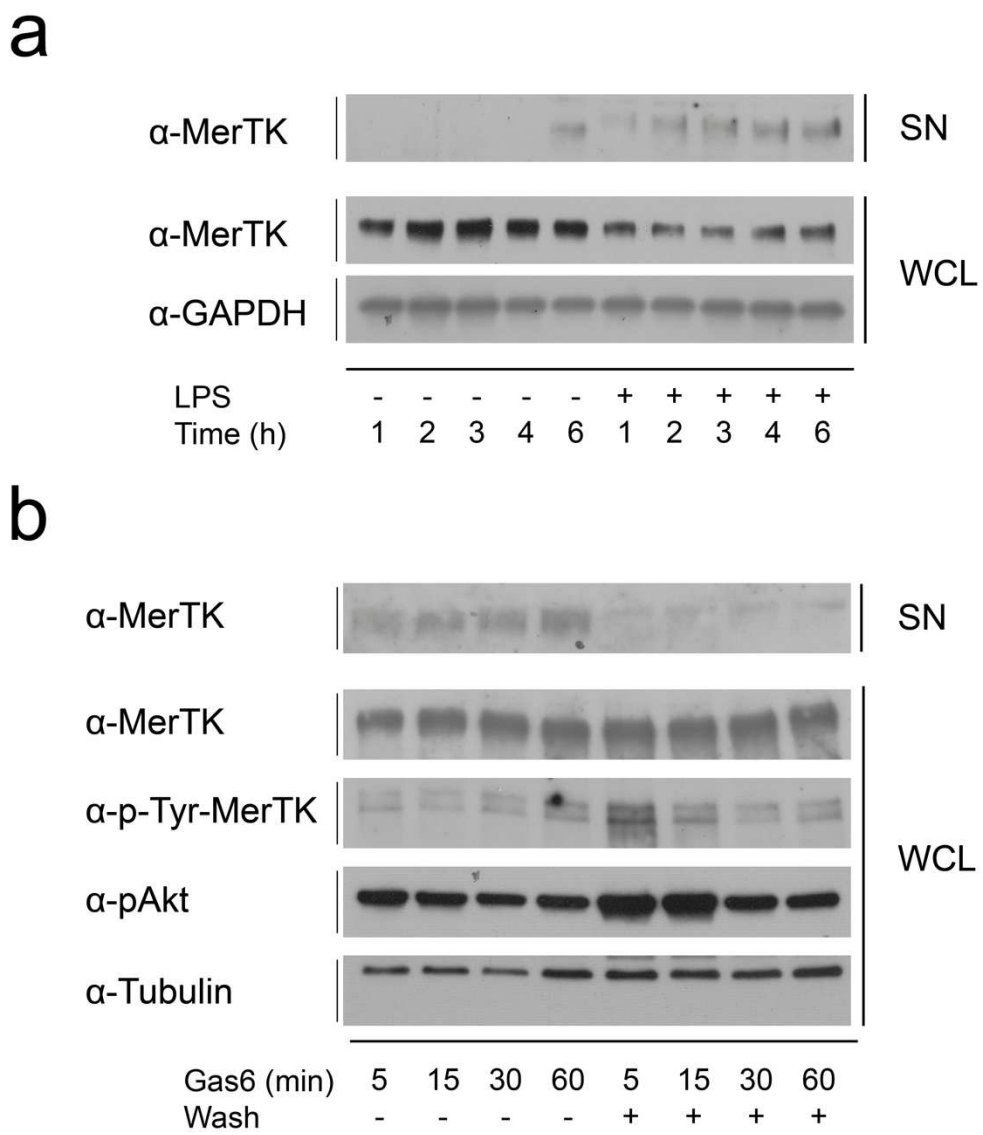

Figure 28 | MerTK is shed from the membrane during macrophage activation and its ectodomain acts as a physiological dominant negative to inhibit Gas6 ligand binding. a) MerTK and GAPDH levels in whole cell lysate (WCL) and supernatant (SN) of M-CSF BMDMs over 6h ± 100ng/mL LPS. b) MerTK (WCL and SN), p-Tyr-MerTK, p-Akt, and GAPDH (WCL) in M-CSF BMDMs over 60min + 250ng/mL Gas6 ± a pre-wash of supernatant to remove shed MerTK ectodomain.

9.3.3 MerTK ectodomain shedding inhibits Gas6-mediated signalling

We next tested whether enhancing MerTK signalling with Gas6, a bridging ligand, could suppress NLRP3 activity. M-CSF BMDMs were pre-treated with Gas6

before LPS priming, but no significant effect on NLRP3 responses was observed across multiple time points (data not shown). As MerTK ectodomain is shed from macrophages under inflammatory conditions, I hypothesized that MerTK ectodomain shedding, which occurs in our system within 1 h of LPS challenge and under homeostatic conditions after 6 h in culture (Figure 27a, Figure 28a), might act as a dominant-negative inhibitor of MerTK signalling. To test this, I washed BMDMs after overnight culture to remove shed MerTK ectodomain before adding Gas6. This wash significantly enhanced Gas6-induced MerTK signalling, as evidenced by increased phosphorylation of MerTK and downstream Akt (Figure 28b). These findings indicate that MerTK ectodomain shedding limits ligand-dependent signalling, potentially attenuating efferocytosis-mediated NLRP3 suppression.

9.3.4 Small molecule TAM inhibition increases NLRP3 activity

As direct stimulation of MerTK with Gas6 presented technical challenges, I used a small molecule inhibitor, RU-301, to inhibit TAM receptors. Work from Carla Rothlin's group demonstrated that normal BMDM cultures have steady state apoptosis and blockade of apoptotic cell recognition with Annexin V reduced transcripts of genes associated with tissue repair[20]. To this end, I pre-treated steady state BMDMs with a TAM inhibitor for 16 h and performed an acute NLRP3 inflammasome stimulation. I found LDH release and IL-18 processing were increased with TAM inhibition (Figure 29a,b). Protein levels of the NLRP3 sensor did not appear to change with TAM inhibition. However, pathway activity measured by IL-18 release and capase-1 cleavage was increased, suggesting that steady state TAM receptor engagement by apoptotic cells lowers NLRP3 activity in macrophages (Figure 29c).

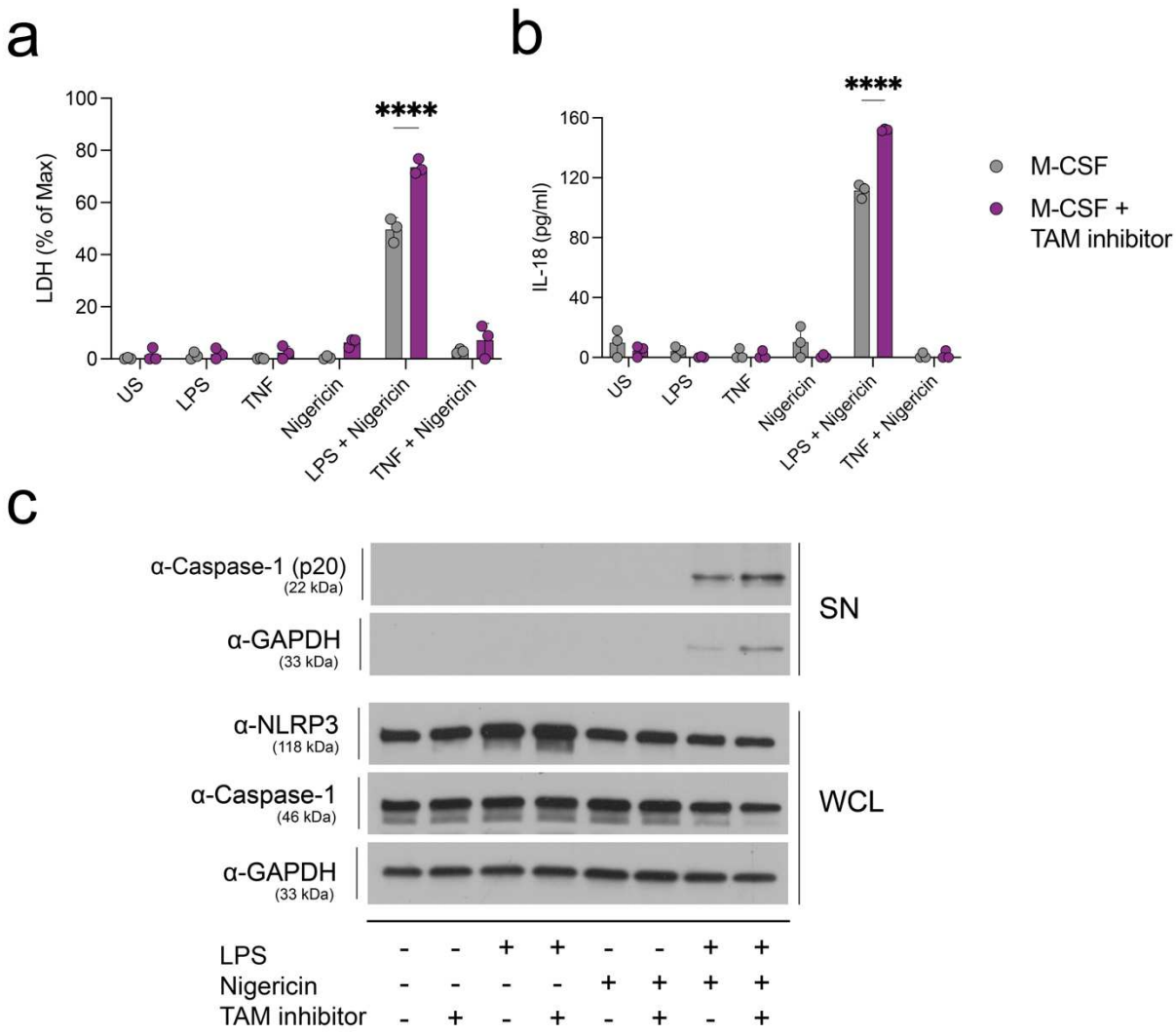

Figure 29 | Small molecule TAM inhibition increases NLRP3 activity.
WT BMDMs differentiated in M-CSF were pre-treated for 16h with the 10 μM RU-301 (small molecule TAM inhibitor) primed with 100 ng/mL ultrapure LPS for 30min ± 7.5 μM nigericin (1 h). Supernatants and lysates collected post-stimulation. a) Inflammasome-dependent LDH release. Data shown as mean ± SEM, points representing three independent biological replicates. b) IL-18 secretion measured by ELISA. c) Western blot of NLRP3, Caspase-1, and GAPDH in lysates and supernatants after acute activation (30 min LPS + 1 h nigericin). Data shown as mean ± SEM, points representing technical replicates from a representative experiment of two independent biological replicates for IL-18 and Western blot. M-CSF BMDMs + vehicle (grey), M-CSF BMDMs + RU-301 (purple).

9.3.5 Apoptotic cell recognition inhibits NLRP3 activation in MerTK^{high} macrophages

To directly assess the role of efferocytosis, I treated BMDMs with apoptotic neutrophils induced by ABT737 (250 nM) and MCL1i (250 nM) (Figure 30). I used

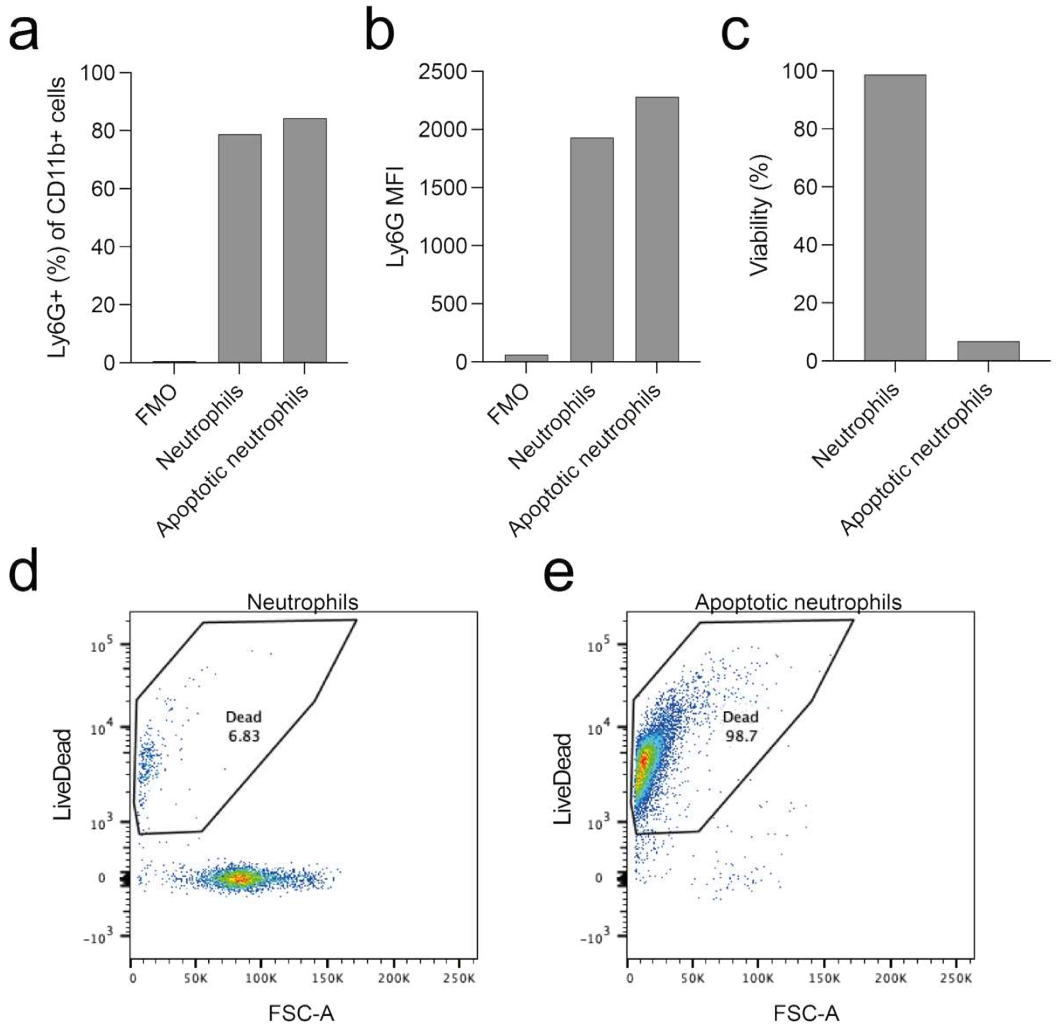

Figure 30 | Chemotherapeutic drugs ABT737 and MCLi reliably induce apoptosis in primary bone marrow neutrophils. Primary neutrophils were isolated from murine bone marrow via negative selection and treated with 250nM ABT727 and MCLi. a,b) Cell surface expression of Ly6G in isolated bone marrow neutorphils as a) percent Ly6G positive of CD11b+ cells and b) Ly6G MFI. c-e) Viability measured by LiveDead staining. Data are presented as representative gating and histograms from two independent biological replicates.

apoptotic primary neutrophils isolated from murine bone marrow as work by Carla Rothlin and others has demonstrated apoptotic cell identity is sensed by macrophages, and apoptotic neutrophils specifically promote tissue-repair and anti-inflammatory phenotypes[20]. I also used neutrophils as they robustly infiltrate synovium at peak or RA and need to be removed during resolution. I used apoptotic drugs to ensure a consistent and reliable induction of apoptosis (Figure 30). Apoptotic drugs

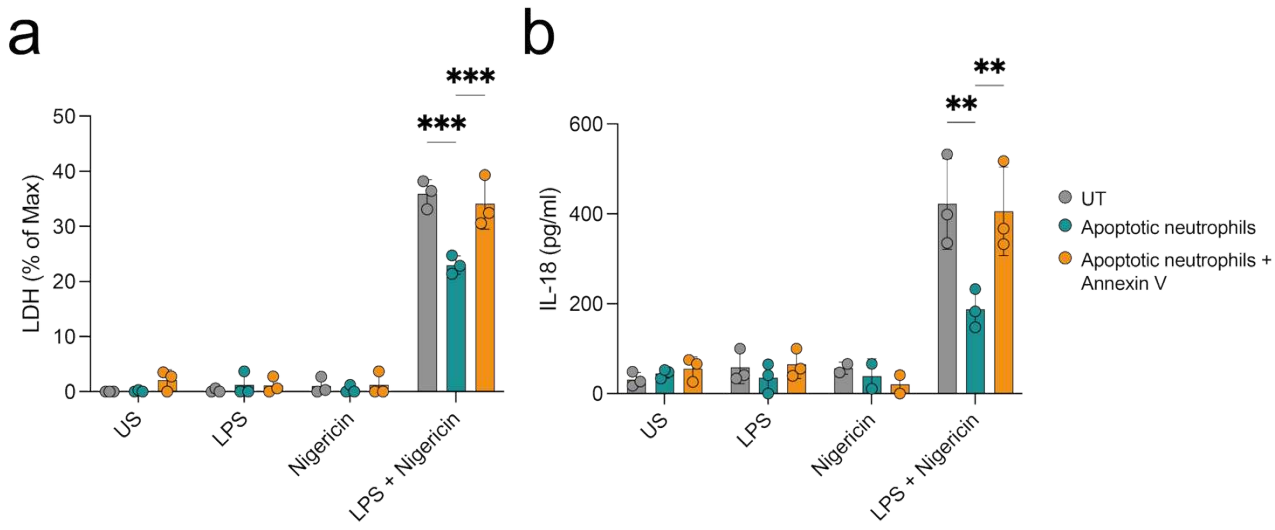

Figure 31 | Apoptotic neutrophil recognition reduces NLRP3 activity in MerTK^{high} M-CSF BMDMs. Apoptotic neutrophils were generated as described previously. Apoptotic neutrophils were pelleted and the media containing apoptotic drugs was washed away. Apoptotic neutrophils were counted and resuspended ± Annexin V (10ug/ml) to block phosphatidyl serine. BMDMs were co-cultured with apoptotic cells at a ratio of 1.5:1 for 2.5 h, apoptotic cells were washed away and BMDMs were rested for 16 h before acute inflammasome assay (30 min priming with 100ng/ml LPS before 1h of 7.5 uM nigericin). After stimulation, cell supernatants were collected, and cells were lysed. a,b) Inflammasome-dependent cell death and IL-18 processing was measured by a) LDH release and b) IL-18 ELISA. Data are shown as mean ± SEM with points representing three independent biological replicates.

were washed away before apoptotic neutrophils were added to BMDMs for 2.5 h, followed by washing to prevent secondary necrosis of unengulfed cells. BMDMs were then rested for 16 hours, to allow induction of any MerTK-driven anti-inflammatory programmes, before inflammasome activation. I used an acute inflammasome protocol with 30 min of LPS (100 ng/mL) priming and 1 h of nigericin (10 uM) stimulation to focus on immediate NLRP3 signalling, rather than transcriptional reprogramming. In MerTK^{high} M-CSF BMDMs, apoptotic cell exposure significantly reduced NLRP3 activation, as measured by reduced LDH release and IL-18 release (Figure 31a,b). This inhibition was completely reversed by Annexin V (100 µg/mL), which blocks phosphatidylserine recognition by TAM receptors (Figure 31a,b). These results suggest that phosphatidyl serine-dependent recognition of apoptotic cells may

inhibit NLRP3 inflammasome activity in healthy synovium, where MerTK^{high} macrophages predominate.

9.4 Discussion

Our findings demonstrate that phosphatidyl-serine-dependent efferocytosis of apoptotic cells suppresses NLRP3 inflammasome activity *in vitro*. Efferocytosis may similarly dampen NLRP3 expression and activity in tissue-resident macrophages, particularly in the healthy synovium, but this remains to be tested *in vivo* (for example, in mice lacking MerTK in macrophages, or over-expressing cleavage-resistant MerTK). The inverse correlation between high MerTK expression and low NLRP3 expression in synovial macrophages, as revealed by scRNAseq, aligns with prior reports describing elevated MerTK in healthy human synovium and patients in disease remission, suggesting a role for MerTK in maintaining joint homeostatsis[1].

The dynamic regulation of MerTK expression in response to LPS provides insight into the balance between inflammatory and anti-inflammatory signalling in macrophages *in vitro*. The transient downregulation of MerTK within 1 hour of LPS exposure, followed by its recovery and upregulation between 4-6h (Figure 25, Figure 27a), mirrors the kinetics of endotoxin tolerance, a state characterized by IL-10-dependent suppression of pro-inflammatory responses (Figure 26)[13]. In agreement, previous reports suggest that at the time IL-10 suppression is established *in vitro*, inflammasome signalling is terminated in M-CSF BMDMs[13]. Our finding that partial MerTK knockdown modestly enhances NLRP3-dependent cell death and cytokine release (Figure 27b-e) supports the hypothesis that MerTK may act as a negative regulator of NLRP3 activity. However, the overall suppressive effect of 4-OH-tamoxifen on NLRP3 responses in both wild-type and $CX_3CR1^{CreER/+}MerTK^{fl/fl}$ BMDMs

(Figure 27c–e) complicates interpretation. This limitation highlights the need for alternative models, such as CRISPR-based MerTK knockouts or small-molecule inhibitors, to precisely dissect MerTK's role without off-target effects.

The shedding of the MerTK ectodomain emerged as a key regulatory mechanism limiting efferocytosis signalling. The detection of shed MerTK in culture supernatants within 1 hour of LPS challenge and under homeostatic conditions after 6 hours (Figure 28a) suggests that ectodomain cleavage serves as a physiological brake on MerTK activity. This is further supported by our observation that removing shed ectodomain enhanced Gas6-induced MerTK phosphorylation and downstream Akt signaling (Figure 28b). These findings are consistent with studies showing that MerTK shedding, mediated by metalloproteinases such as ADAM17, inhibits efferocytosis in inflammatory contexts[21]. The failure of exogenous Gas6 to suppress NLRP3 activity in our experiments may reflect this dominant-negative effect of shed ectodomain, underscoring the complexity of MerTK signalling *in vitro*. Future studies should explore whether stabilizing cell-surface MerTK or inhibiting ectodomain shedding can enhance efferocytosis-mediated NLRP3 suppression.

The most compelling evidence for efferocytosis as a regulator of NLRP3 activity came from our apoptotic cell transfer experiments. In MerTK^{high} M-CSF BMDMs, recognition of apoptotic cells significantly reduced NLRP3 activation, as evidenced by decreased IL-18 maturation and LDH release (Figure 31a,b). This effect was entirely dependent on phosphatidylserine recognition, as annexin V reversed the suppression (Figure 31a,b). These findings align with reports that efferocytosis induces anti-inflammatory cytokines, such as IL-10 and TGF-β, which downregulate NLRP3 priming[9,15].

Our results suggest that recognition of normal apoptotic cells via efferocytosis receptors such as MerTK reduces NLRP3 activity, possibly explaining low *NLRP3* level in health and during arthritis resolution, where MerTK^{high} cells are the dominant synovial macrophage subset[22]. Loss of the *MERTK*+ population correlates with active disease and predicts poor treatment response[1]. MerTK belongs to a family of TAM (Tyro3, Axl, MerTK) receptors, which recognise apoptotic cells. *Axl*$^{-/-}$ and *MerTK*$^{-/-}$ mice develop more severe arthritis and deletion of all three TAM receptors (*Tyro3*$^{-/-}$*/Axl*$^{-/-}$*/MerTK*$^{-/-}$) results in spontaneous bone-marrow oedema and poly-arthritis[23,24]. All TAM family members promote IL-10 synthesis, the best-known negative regulator of NLRP3 and IL-1β protein expression[9,13,15]. MerTK has also been shown to limit NLRP3 activity in an experimental neuroinflammation model, where the mechanism suggests induction of autophagy, a pathway known to degrade active NLRP3 complexes[18]. Hence, tissue-resident macrophages in many tissues may use efferocytosis of apoptotic cells as homeostatic signals that suppress NLRP3 expression and activity in health and during the resolution of inflammation.

9.5 Limitations

Despite these insights, several limitations warrant consideration. First, the *in vitro* nature of our experiments, using M-CSF BMDMs, may not fully recapitulate the heterogeneity of synovial macrophages *in vivo*, which are influenced by diverse local cues such as cytokines and stromal interactions. Our focus on MerTK overlooks the potential contributions of other efferocytosis receptors, such as Axl or TIM-4, which may compensate or synergize with MerTK to regulate NLRP3 activity. Third, the use of bone marrow neutrophils as a model for apoptotic cells may not reflect the diversity

of apoptotic cell types in the synovium, such as lymphocytes or fibroblasts, which could elicit distinct macrophage responses[20].

The dominant suppressive effect of 4-OH-tamoxifen in our knockdown experiments, and off target effects in siRNA knockdown (data not shown) limit definitive conclusions about MerTK's specific role, necessitating alternative genetic or pharmacological approaches.

Our experiments focused on acute inflammasome activation following short-term apoptotic cell exposure, potentially missing chronic or repeated efferocytosis dynamics that could alter macrophage polarization or NLRP3 priming over time.

Future studies should address these limitations by employing *in vivo* models, such as STM-specific MerTK knockouts, to validate the role of efferocytosis in NLRP3 regulation. Additionally, investigating the contributions of other efferocytosis receptors and diverse apoptotic cell types could provide a more comprehensive understanding of inflammasome suppression. Therapeutically, strategies to enhance MerTK signalling, stabilize cell-surface MerTK, or promote efferocytosis could restore immune homeostasis in NLRP3-driven inflammatory diseases.

9.6 Conclusion

In conclusion, our data establish MerTK-mediated efferocytosis as a suppressor of NLRP3 inflammasome activity in MerTK^{high} M-CSF BMDMs, with implications for health and disease. The dynamic regulation of MerTK expression and signalling, coupled with the physiological clearance of apoptotic cells, maintains an anti-inflammatory state in healthy tissues. Disruption of this mechanism in disease states

underscores the therapeutic potential of targeting MerTK or efferocytosis pathways to mitigate NLRP3-driven inflammation.

9.7 References

1. Alivernini, S. *et al.* Distinct synovial tissue macrophage subsets regulate inflammation and remission in rheumatoid arthritis. *Nat Med* **26**, 1295–1306 (2020).
2. MacDonald, L. *et al. COVID-19 and Rheumatoid Arthritis Share Myeloid Pathogenic and Resolving Pathways*. http://biorxiv.org/lookup/doi/10.1101/2020.07.26.221572 (2020) doi:10.1101/2020.07.26.221572.
3. Camenisch, T. D., Koller, B. H., Earp, H. S. & Matsushima, G. K. A novel receptor tyrosine kinase, Mer, inhibits TNF-alpha production and lipopolysaccharide-induced endotoxic shock. *J Immunol* **162**, 3498–3503 (1999).
4. Reed, J. C. Mechanisms of Apoptosis. *The American Journal of Pathology* **157**, 1415–1430 (2000).
5. Poon, I. K. H., Lucas, C. D., Rossi, A. G. & Ravichandran, K. S. Apoptotic cell clearance: basic biology and therapeutic potential. *Nat Rev Immunol* **14**, 166–180 (2014).
6. Nandrot, E. F., Silva, K. E., Scelfo, C. & Finnemann, S. C. Retinal pigment epithelial cells use a MerTK-dependent mechanism to limit the phagocytic particle binding activity of αvβ5 integrin. *Biology of the Cell* **104**, 326–341 (2012).
7. Mercau, M. E. *et al.* Inflammation of the retinal pigment epithelium drives early-onset photoreceptor degeneration in Mertk-associated retinitis pigmentosa. *Sci Adv* **9**, eade9459 (2023).

8. Seitz, H. M., Camenisch, T. D., Lemke, G., Earp, H. S. & Matsushima, G. K. Macrophages and Dendritic Cells Use Different Axl/Mertk/Tyro3 Receptors in Clearance of Apoptotic Cells. *The Journal of Immunology* **178**, 5635–5642 (2007).
9. Rothlin, C. V., Ghosh, S., Zuniga, E. I., Oldstone, M. B. A. & Lemke, G. TAM Receptors Are Pleiotropic Inhibitors of the Innate Immune Response. *Cell* **131**, 1124–1136 (2007).
10. Tibrewal, N. *et al.* Autophosphorylation Docking Site Tyr-867 in Mer Receptor Tyrosine Kinase Allows for Dissociation of Multiple Signaling Pathways for Phagocytosis of Apoptotic Cells and Down-modulation of Lipopolysaccharide-inducible NF-κB Transcriptional Activation. *Journal of Biological Chemistry* **283**, 3618–3627 (2008).
11. Cook, R. S. *et al.* MerTK inhibition in tumor leukocytes decreases tumor growth and metastasis. *J. Clin. Invest.* **123**, 3231–3242 (2013).
12. Zhou, C., Zhu, Y., Zhang, L., Zhao, M. & Zhang, C. Axl deficiency promotes preeclampsia and vascular malformations in mice. *Molecular Therapy Nucleic Acids* **36**, 102408 (2025).
13. Gurung, P. *et al.* Chronic TLR Stimulation Controls NLRP3 Inflammasome Activation through IL-10 Mediated Regulation of NLRP3 Expression and Caspase-8 Activation. *Sci Rep* **5**, 14488 (2015).
14. Zizzo, G., Hilliard, B. A., Monestier, M. & Cohen, P. L. Efficient Clearance of Early Apoptotic Cells by Human Macrophages Requires M2c Polarization and MerTK Induction. *J.I.* **189**, 3508–3520 (2012).
15. Adomati, T. *et al.* Dead Cells Induce Innate Anergy via Mertk after Acute Viral Infection. *Cell Reports* **30**, 3671-3681.e5 (2020).

16. Cai, B. *et al.* MerTK signaling in macrophages promotes the synthesis of inflammation resolution mediators by suppressing CaMKII activity. *Sci. Signal.* **11**, eaar3721 (2018).

17. Cross, S. N. *et al.* Viral Infection Sensitizes Human Fetal Membranes to Bacterial Lipopolysaccharide by MERTK Inhibition and Inflammasome Activation. *J.I.* **199**, 2885–2895 (2017).

18. Du, Y. *et al.* MerTK inhibits the activation of the NLRP3 inflammasome after subarachnoid hemorrhage by inducing autophagy. *Brain Research* **1766**, 147525 (2021).

19. Wei, S. *et al.* NLRP3 inflammasome constrains liver regeneration through impairing MerTK-mediated macrophage efferocytosis. *Sci. Adv.* **11**, eadq5786 (2025).

20. Liebold, I. *et al.* Apoptotic cell identity induces distinct functional responses to IL-4 in efferocytic macrophages. *Science* **384**, eabo7027 (2024).

21. Cai, B. *et al.* MerTK cleavage limits proresolving mediator biosynthesis and exacerbates tissue inflammation. *Proc Natl Acad Sci USA* **113**, 6526–6531 (2016).

22. Culemann, S. *et al.* Locally renewing resident synovial macrophages provide a protective barrier for the joint. *Nature* **572**, 670–675 (2019).

23. Waterborg, C. E. J., Koenders, M. I., van Lent, P. L. E. M., van der Kraan, P. M. & van de Loo, F. A. J. Tyro3/Axl/Mertk-deficient mice develop bone marrow edema which is an early pathological marker in rheumatoid arthritis. *PLoS ONE* **13**, e0205902 (2018).

24. Waterborg, C. E. J. *et al.* Protective Role of the MER Tyrosine Kinase via Efferocytosis in Rheumatoid Arthritis Models. *Front. Immunol.* **9**, 742 (2018).

10. Appendix Data Chapter 5 | Seronegative RA: a novel cohort for inflammasome targeting and GM-CSF blockade

10.1 Introduction

10.1.1 Seronegative RA

This thesis has demonstrated that GM-CSF enhances NLRP3 inflammasome activity and IL-1β production *in vitro*. *In vivo*, GM-CSF blockade reduces synovial pro-IL-1β levels and pain in AIA. Early clinical trials of anti-GM-CSF mAbs showed promising reductions in disease activity and pain in RA patients. However, these findings have not been consistently replicated in large Phase III randomized controlled trials. I hypothesize that anti-GM-CSF therapy may remain effective, but its success depends on identifying the appropriate patient cohort and optimal treatment timing. This chapter explores seronegative RA as a compelling patient subset with suboptimal responses to current therapies and a potential molecular mechanism that suggests a high likelihood of responding to anti-GM-CSF or inflammasome-targeted therapies. Specifically, patients with clonal haematopoiesis mutations are overrepresented in seronegative RA. Clonal haematopoiesis happens when somatic mutations are acquired later in life, often in myeloid cells, which leads to the expansion of myeloid clones and myeloid-driven inflammation. This inflammation is associated with strong GM-CSF and NLRP3 signatures. This appendix data chapter reviews the literature on seronegative RA and presents preliminary *in vitro* data generated toward the end of my DPhil.

Seronegative RA is defined by the absence of rheumatoid factor (RF) and anti-citrullinated protein antibodies (ACPA) in the blood, distinguishing it from seropositive RA, where these autoantibodies are present[1]. Despite lacking these serological

markers, seronegative RA shares clinical features with seropositive RA, including joint inflammation, synovial damage, and systemic symptoms, but it exhibits distinct diagnostic, prognostic, and therapeutic considerations[2]. Diagnosed in patients meeting the 2010 ACR/EULAR classification criteria for RA but testing negative for RF and ACPA, seronegative RA is a diagnosis of exclusion, necessitating the exclusion of other inflammatory arthritic conditions, such as psoriatic arthritis, spondyloarthropathies, or crystal arthropathies. Estimates suggest seronegative RA accounts for approximately 20–30% of RA cases and this estimate is consistent across large Phase III clinical trials[2].

Clinical studies indicate that seronegative RA may present with less severe small joint involvement and a higher prevalence of large joint (e.g., knees, shoulders) or asymmetrical patterns, resembling spondyloarthropathies[2]. The absence of RF and ACPA suggests a distinct pathophysiological mechanism, which may underlie the observed poor response to biologics targeting TNF-α or CD20 (e.g., rituximab) in some seronegative RA patients[3,4].

10.1.2 The link between clonal haematopoiesis, myeloid neoplasms, and innate immune dysfunction in seronegative RA

Seronegative RA represents an underserved patient population within RA, with limited therapeutic options and poorly understood molecular drivers. Toward the end of my DPhil, I became interested in a newly identified association between isocitrate dehydrogenase 1 (IDH1) mutations, clonal haematopoiesis, and seronegative RA.

A 2024 study reported a high prevalence of IDH1 mutations in seronegative RA patients with myeloid neoplasms, accompanied by elevated levels of the

oncometabolite D-2-hydroxyglutarate (2-HG) and evidence of innate immune activation[5,6]. This study suggested a causative role for IDH1 mutations in seronegative RA. Notably, 44.4% of seronegative RA patients with myeloid neoplasms harboured IDH1/2 mutations, compared to 0% in seropositive RA patients[5]. Among seronegative RA cases, 75% of IDH mutations were IDH1, while IDH2 mutations predominated in other autoimmune inflammatory diseases[5].

A compelling temporal relationship exists between IDH1 mutations and arthritis onset. In 84% of cases, the myeloid neoplasm diagnosis follows the RA diagnosis, but the interval is significantly shorter in seronegative RA (34.6 months vs. 135.4 months for seropositive RA) and even shorter in IDH1/2-mutant cases (44.4 months vs. 106.3 months for wild-type)[5]. IDH1-mutant cases exhibited the shortest latency (12.9 months vs. 85.6 months for IDH2), suggesting that IDH1 mutations may accelerate RA onset[5]. Patients with IDH mutations also displayed elevated serum levels of pro-inflammatory cytokines, including IL-18, IL-1β, and GM-CSF[5,6].

10.1.3 IDH1 and TET2 coordinate to restrain innate immune activation

How does a single somatic mutation lead to systemic inflammation? In healthy cells, IDH1 is a cytoplasmic enzyme that catalyses the oxidative decarboxylation of isocitrate to α-ketoglutarate (α-KG) as part of the citric acid cycle (Figure 32). There are three IDH enzymes in humans, but IDH2 and IDH3 are restricted to mitochondria, while IDH1 is in the cytoplasm and peroxisomes.

In the cytoplasm, α-KG is critical for protecting against oxidative stress and is a cofactor for the enzymatic activity of tet methylcytosine dioxygenase 2 (TET2)[7]. TET2, a DNA demethylase, oxidizes 5-methylcytosine (5mC) to 5-hydroxymethylcytosine (5hmC), promoting DNA demethylation and regulating gene expression in

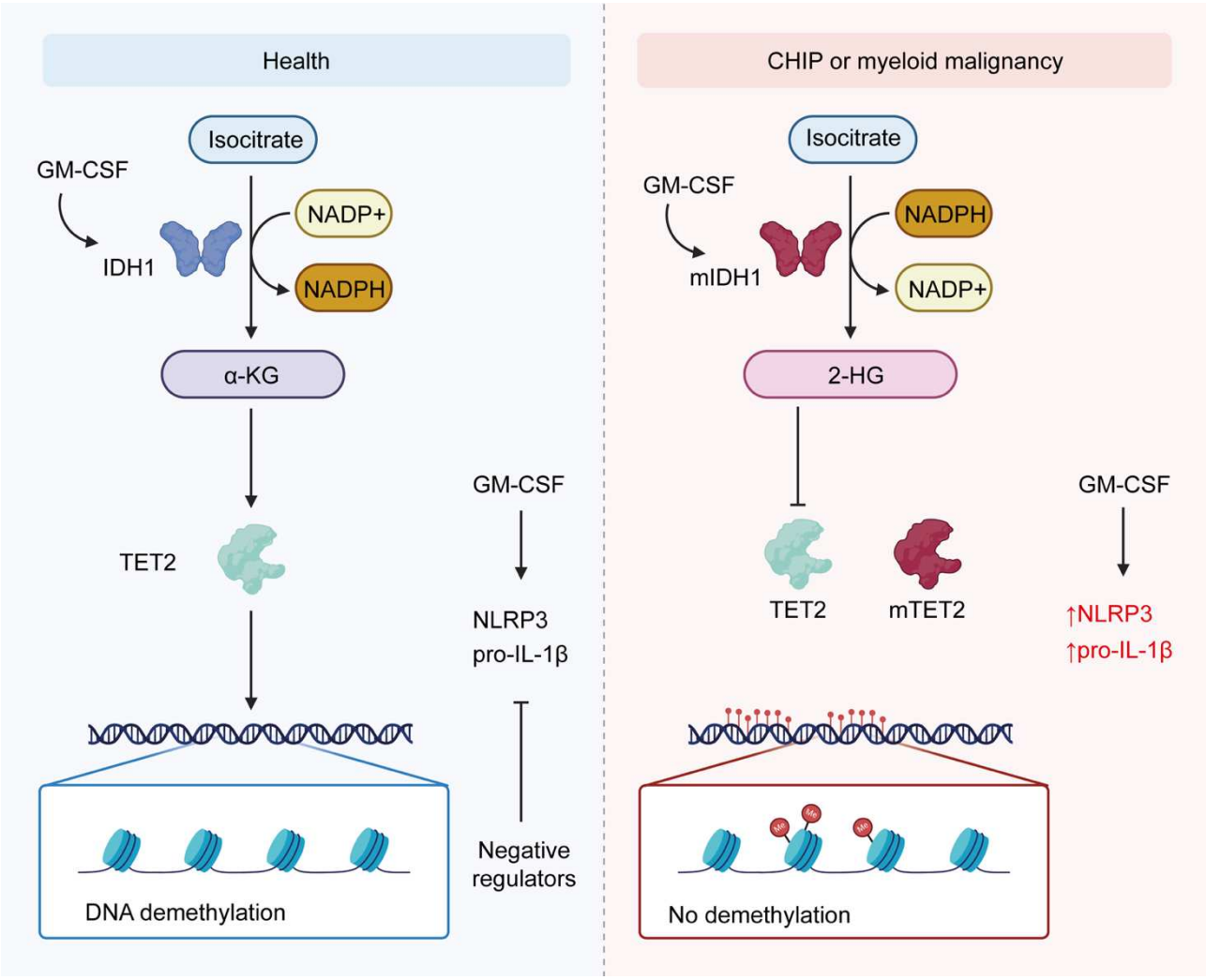

Figure 32 | TET2 restrains NLRP3 expression in GM-CSF macrophages via IDH1-dependent α-KG production in health, but mutations in IDH1/TET2 Drive NLRP3 dysregulation in inflammatory diseases. In healthy states, GM-CSF induces IDH1 expression in macrophages, promoting the production of α-ketoglutarate (α-KG), a critical co-factor for TET2. TET2 mediates DNA demethylation, upregulating negative regulators of NLRP3, such as IL-10, to suppress excessive NLRP3 expression and activity. This maintains immune homeostasis. In clonal hematopoiesis of indeterminate potential (CHIP) or myeloid malignancies, mutant IDH1 acts as a dominant-negative, consuming isocitrate to produce 2-hydroxyglutarate (2-HG), which inhibits TET2 activity. Similarly, loss-of-function TET2 mutations impair DNA demethylation, leading to unchecked NLRP3 and IL-1β expression.

macrophages (Figure 32)[7]. Furthermore, in macrophages, TET2 normally restrains inflammatory gene expression through histone deacetylation at specific promoters (*IL-6*, *IL-1b*), rather than direct DNA demethylation[8,9]

Mutations in IDH1 confer a neomorphic function, producing 2-HG instead of α-KG. 2-HG competitively inhibits α-KG-dependent enzymes, including TET2, resulting in reduced 5hmC levels and DNA hypermethylation (Figure 32)[7]. This epigenetic

dysregulation disrupts macrophage differentiation and function, skewing macrophages toward pro-inflammatory states. In clonal haematopoiesis of indeterminate potential (CHIP) or myeloid malignancies, IDH1 mutations drive 2-HG production and inhibit TET2 activity, leading to increased expression of inflammatory genes, such as IL-1β and IL-6, in macrophages (Figure 32) [5,6].

TET2-deficient macrophages, which exhibit increased IL-1β and IL-6 production[8,10], resemble a GM-CSF-driven inflammatory signature in models like atherosclerosis[7,11]. Clinically, somatic TET2 mutations are associated with over a two-fold increased risk of giant cell arteritis, a vasculitis driven by innate immune activation[12].

10.1.4 Are mutant IDH1 or TET2 myeloid cells highly sensitive to GM-CSF-driven inflammatory gene expression?

IDH1 and TET2 are functionally interlinked, and emerging evidence suggests that both IDH1 and TET2 mutations are associated with inflammatory arthritis and enhanced NLRP3 inflammasome activity.

As previously discussed, patients with IDH-mutant CHIP or myeloid malignancies exhibit elevated serum IL-1β and GM-CSF levels[5]. TET2-mutant clonal haematopoiesis is linked to an increased risk of incident gout, an NLRP3-driven inflammatory arthritis[13]. *In vivo*, MSU crystal treatment enhanced Nlrp3-dependent IL-1β secretion in Tet2-knockout mice[13]. Analysis of the FINRISK database revealed that RA patients with TET2 variants were more likely to have seronegative RA compared to those with wild-type TET2[14].

No studies have directly examined the interaction between GM-CSF and IDH1/TET2 mutations in macrophages. However, Hamilton and colleagues showed that GM-CSF increases IDH1 expression and activity, increasing α-KG levels[16]. As GM-CSF promotes IDH1 mRNA expression, and the accumulation of α-KG, mutant of IDH function may have altered GM-CSF signalling. Similarly, the heightened levels of α-KG may suggest GM-CSF macrophages are more reliant on TET2 to restrain pro-inflammatory programs. Based on increased GM-CSF and inflammasome signature in patients with IDH1 or TET2 mutations, I hypothesize that IDH1- or TET2- mutant macrophages may be hypersensitive to GM-CSF-driven inflammatory gene expression and inflammasome signalling, potentially exacerbating seronegative RA pathology.

10.2 Aims

The overarching goal of this appendix data chapter is to explore seronegative RA, particularly those with IDH1 and TET2 mutations, as a novel patient cohort for targeted therapies, focusing on GM-CSF blockade and NLRP3 inflammasome inhibition. The specific aims for this early work are:

1. Characterize the expression of IDH1 and TET2 in M-CSF versus GM-CSF macrophages *in vitro*.
2. Evaluate the NLRP3 responses of M-CSF versus GM-CSF macrophages in the context of TET2 inhibition.

10.3 Results

We first investigated wild-type *Idh1* and *Tet2* expression in our *in vitro* BMDM model. Murine M-CSF and GM-CSF BMDMs were differentiated as previously described and exposed to LPS or TNF-α to assess the expression of wild-type *Idh1* and *Tet2*. Both M-CSF- and GM-CSF-differentiated BMDMs exhibited similar kinetics of *Idh1* and *Tet2* expression following LPS exposure (Figure 33a). GM-CSF-polarized BMDMs displayed significantly higher baseline *Idh1* expression and elevated levels at 30 min post-LPS and post-TNF-α exposure compared to M-CSF BMDMs (Figure 33a).

Notably, both M-CSF and GM-CSF BMDMs reduced *Idh1* expression 4 h post-LPS treatment, coinciding with peak inflammatory responses. In contrast, *Tet2* expression peaked 4 h after LPS exposure, with GM-CSF BMDMs showing significantly higher *Tet2* levels at this time point and at 24 h following TNF-α treatment compared to M-CSF BMDMs (Figure 33b). These findings suggest that GM-CSF polarization enhances *Tet2* expression during inflammatory stimuli.

As IDH1 is a metabolic enzyme involved in several processes including lipid synthesis, oxidative stress protection, and redox balance maintenance, modulating TET2 provided more specificity to our *in vitro* study. To evaluate the functional consequence of inhibited TET2 (mimicking people with TET2 mutation) on inflammasome signalling in M-CSF and GM-CSF BMDMs I pre-treated both with the TET2 inhibitor Bobcat339 before LPS priming, followed by inflammasome activation. GM-CSF-polarized BMDMs, which express a higher level of TET2 post LPS (Figure 33b) exhibited significantly enhanced NLRP3-dependent cell death (pyroptosis) and IL-1β release upon TET2 inhibition, whereas M-CSF BMDMs which express a lower level of TET2 post LPS (Figure 33b) showed no significant changes in inflammasome

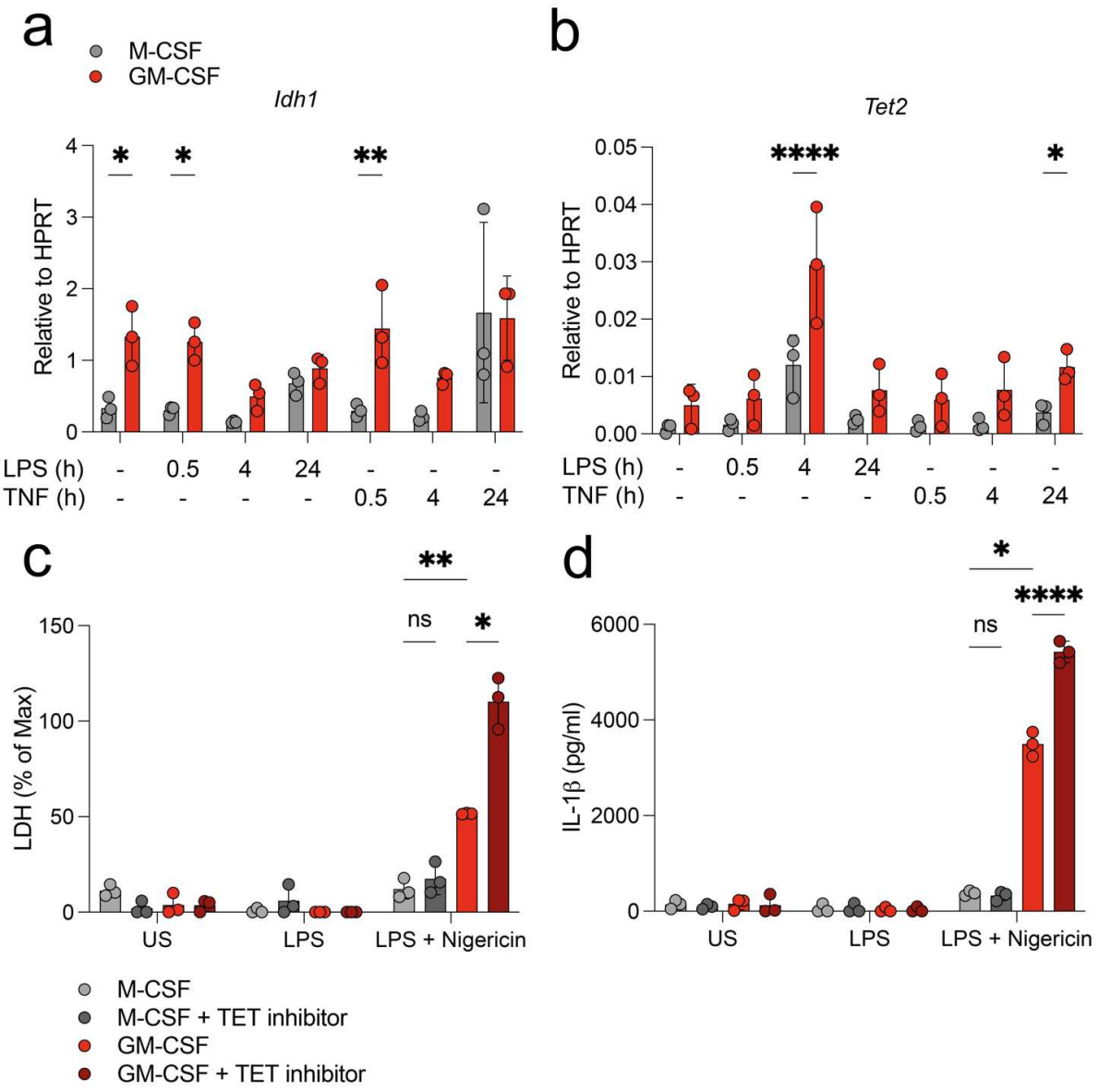

Figure 33 | TET2 specifically restrains NLRP3 responses GM-CSF BMDMs. M-CSF and GM-CSF BMDMs were primed for 30 min, 4 h, or 24 h with 100 ng/ml ultrapure LPS or 100 ng/ml TNF. After stimulation, cells were lysed with RLT lysis buffer a) *Idh1* b) *Tet2* mRNA expression measured relative to HPRT by qPCR. NLRP3 inflammasome activation of M-CSF and GM-CSF derived BMDMs with TET2 small molecular inhibition. M-CSF and GM-CSF BMDMs were pre-treated with the TET2 inhibitor Bobcat339 overnight and primed with 100ng/mL ultrapure LPS for 24 h ± 1h 10 uM nigericin. After stimulation, cell supernatants were collected, and cells were lysed. c) Inflammasome-dependent cell death was measured by LDH release and d) IL-1β secretion was measured by ELISA. Data shown as mean ± SEM, points representing independent biological replicates. M-CSF BMDMs (grey), M-CSF BMDMs + TET inhibitor (dark grey), GM-CSF BMDMs (red), and GM-CSF BMDMs + TET2 inhibitor (dark red).

signalling upon TET2 inhibition (Figure 33c,d). These results indicate that TET2 restrains NLRP3 inflammasome responses in GM-CSF-polarised macrophages, as its

inhibition specifically heightened and prolonged NLRP3 responses in GM-CSF BMDMs.

10.4 Discussion

The results presented in this chapter provide novel insights into the role of TET2 in restraining inflammatory responses in GM-CSF-polarized macrophages, with implications for seronegative RA, particularly in patients with IDH1/TET2 clonal haematopoiesis mutations and myeloid neoplasms. Our *in vitro* findings demonstrate that GM-CSF-polarized BMDMs exhibit heightened *Tet2* expression during inflammatory stimuli (LPS and TNF). Inhibition of TET2 with Bobcat339 selectively enhanced NLRP3-dependent pyroptosis and IL-1β production in GM-CSF-polarized BMDMs, underscoring TET2's critical role in modulating GM-CSF-driven inflammation. These findings align with the hypothesis that seronegative RA, characterized by innate immune activation, may be a promising cohort for therapies targeting GM-CSF or the NLRP3 inflammasome, especially in the context of IDH1-driven epigenetic dysregulation.

We found elevated baseline *Idh1* expression in GM-CSF-polarized BMDMs, suggesting that IDH1, through its production of α-KG, may support TET2's epigenetic regulatory functions under homeostatic conditions. The suppression of *Idh1* expression at peak inflammation (4 h post-LPS) may reflect a temporary shift toward pro-inflammatory states, which *Tet2* counteracts by peaking at the same time point. This dynamic interplay is particularly relevant in seronegative RA patients with IDH1 mutations, where production of 2-HG inhibits TET2, leading to DNA hypermethylation and increased expression of IL-1β in macrophages[5,6]. Our results support the notion that IDH1-mutant macrophages may be hypersensitive to GM-CSF-

driven inflammation, as 2-HG exacerbates the loss of TET2's anti-inflammatory restraint, amplifying NLRP3 activity and IL-1β production.

The selective enhancement of NLRP3 responses in GM-CSF-polarized BMDMs upon TET2 inhibition highlights a specific role for TET2 in GM-CSF-driven macrophage activation. Our findings suggest TET2 may modulate inflammasome expression in GM-CSF-polarized macrophages, potentially through epigenetic regulation of NLRP3 or its upstream regulators. This is consistent with reports of increased IL-1β secretion in TET2-deficient macrophages in models of atherosclerosis and gout, where NLRP3-driven inflammation is prominent[7,13].

The relevance of these findings to seronegative RA is further supported by clinical and genomic data. The high prevalence of IDH1 mutations seronegative RA patients with myeloid neoplasms, with elevated serum IL-1β, IL-18, and GM-CSF, and a short latency to myeloid neoplasm diagnosis, suggesting a causative role for IDH1-driven inflammation[5]. Similarly, analysis of the FINRISK database indicated that TET2 variants are associated with RA[14]. Our results provide a mechanistic basis for these observations, demonstrating that TET2 restrains GM-CSF-driven NLRP3 responses. I hypothesize IDH1-mutant macrophages via 2-HG inhibit TET2 and this may mimic the TET2 inhibition I see *in vitro*. In seronegative RA with IDH1 mutations, this amplification of IL-1β could exacerbate synovial inflammation, supporting the rationale for GM-CSF blockade to reduce both cytokine and chemokine-driven pathology.

10.5 Limitations

This appendix data chapter discusses known clinical data and offers preliminary evidence supporting the role of TET2 in restraining GM-CSF-driven NLRP3 inflammasome responses in macrophages, with implications for seronegative

rheumatoid arthritis (RA) in patients with IDH1 mutations and myeloid neoplasms. However, several limitations must be acknowledged due to the preliminary nature of the findings and the experimental design.

Firstly, as described in previous chapters, mRNA expression does not equate to protein level expression or function. As IDH1 expression and TET2 expression are inversely correlated in BMDMs, it suggests multiple layers of regulation control downstream genetic expression including: IDH1/TET2 expression, IDH1's activity and broader metabolic functions, and TET2 co-factor availability.

Our functional data blocking TET2 with Bobcat339 is limited by the nature of it being a minimalist *in vitro* system and potential off-target effects of the small molecular inhibitor. This preliminary evidence does not show that mutations in IDH1 or TET2 confer increased sensitivity to GM-CSF. The next proposed experiment would be to retrovirally express mutant IDH1 or TET2 into murine BMDM progenitors, differentiate these progenitors into M-CSF or GM-CSF macrophages, and examine their NLRP3 responses. TET2 knockdown or knockout models could also be used to confirm specificity.

This chapter also lacks *in vivo* validation. Further work could examine the incidence and severity of murine arthritis models in mice expressing mutant IDH1 of TET2, particularly in models where exogenous GM-CSF is known to increase severity of disease such as CIA and AIA[17,18].

From a clinical perspective, our study does not address whether seronegative RA patients with IDH1 mutations exhibit distinct responses to GM-CSF blockade. Post-hoc analysis of Phase III GM-CSF clinical trials could identify demographic or molecular biomarkers predicting response, particularly in the 20–30% of trial participants with seronegative RA. The AMP Consortium's Cell Type-Specific Analysis

Program (CTAP) study offers a framework for identifying such signatures, but no such analysis was performed here.

This chapter does not explore undifferentiated polyarthritis (UPA), noting that 20–40% of UPA patients progress to RA within 1–3 years, with RF/ACPA positivity as strong predictors. However, our study does not investigate whether GM-CSF-driven NLRP3 activation contributes to UPA progression to RA. Prospective studies examining early biologic intervention in UPA could clarify these mechanisms, but such data are beyond the scope of this work.

10.6 Conclusions

In conclusion, this work provides preliminary evidence that TET2 restrains GM-CSF-driven inflammation in macrophages, with implications for seronegative RA in IDH1/TET2 mutant patients. Future studies should validate these findings in preclinical and clinical settings, focusing on the therapeutic potential of GM-CSF blockade to address the unmet needs of this unique RA subset. By targeting the interplay of GM-CSF, NLRP3, and epigenetic dysregulation, we may unlock personalized treatment strategies for seronegative RA and prevent RA progression in at-risk populations.

10.7 References

1. Paroli, M. & Sirinian, M. I. When Autoantibodies Are Missing: The Challenge of Seronegative Rheumatoid Arthritis. *Antibodies* **12**, 69 (2023).
2. Bugatti, S., De Stefano, L., Gandolfo, S., Ciccia, F. & Montecucco, C. Autoantibody-negative rheumatoid arthritis: still a challenge for the rheumatologist. *The Lancet Rheumatology* **5**, e743–e755 (2023).

3. Iannone, F. *et al.* Effectiveness of biological targeted therapies may discriminate seronegative from seropositive rheumatoid arthritis. *Rheumatology* **63**, 3442–3448 (2024).
4. Bird, P. *et al.* Treatment outcomes in patients with seropositive versus seronegative rheumatoid arthritis in Phase III randomised clinical trials of tofacitinib. *RMD Open* **5**, e000742 (2019).
5. Hong, L. E. *et al. IDH* -mutant myeloid neoplasms are associated with seronegative rheumatoid arthritis and innate immune activation. *Blood* **143**, 1873–1877 (2024).
6. Hong, L. E. *et al.* High Prevalence of *IDH* Mutation in Myeloid Neoplasm with Concomitant Autoimmune Rheumatic Disorders. *Blood* **142**, 4621–4621 (2023).
7. Fuster, J. J. *et al.* Clonal hematopoiesis associated with TET2 deficiency accelerates atherosclerosis development in mice. *Science* **355**, 842–847 (2017).
8. Cull, A. H., Snetsinger, B., Buckstein, R., Wells, R. A. & Rauh, M. J. Tet2 restrains inflammatory gene expression in macrophages. *Experimental Hematology* **55**, 56-70.e13 (2017).
9. Jiang, S., Yan, W., Wang, S. E. & Baltimore, D. Dual mechanisms of posttranscriptional regulation of Tet2 by Let-7 microRNA in macrophages. *Proc. Natl. Acad. Sci. U.S.A.* **116**, 12416–12421 (2019).
10. Qin, W. *et al.* Role of Myeloid Tet Methylcytosine Dioxygenase 2 in Pulmonary and Peritoneal Inflammation Induced by Lipopolysaccharide and Peritonitis Induced by Escherichia coli. *Cells* **11**, 82 (2021).
11. Peng, J. *et al.* Tet methylcytosine dioxygenase 2 inhibits atherosclerosis via upregulation of autophagy in ApoE−/− mice. *Oncotarget* **7**, 76423–76436 (2016).
12. Robinette, M. L. *et al.* Association of Somatic TET2 Mutations With Giant Cell Arteritis. *Arthritis Rheumatol* **76**, 438–443 (2024).

13. Agrawal, M. *et al. TET2* -mutant clonal hematopoiesis and risk of gout. *Blood* **140**, 1094–1103 (2022).

14. Hiitola, E. *et al.* Clonal Hematopoiesis Associated with Rheumatoid Arthritis. *Blood* **142**, 2698–2698 (2023).

15. Quin, C. *et al.* Chronic TNF in the Aging Microenvironment Exacerbates *TET2*-loss-of-Function Myeloid Expansion. *Blood* **142**, 938–938 (2023).

16. Ming-Chin Lee, K. *et al.* Type I interferon antagonism of the JMJD3-IRF4 pathway modulates macrophage activation and polarization. *Cell Reports* **39**, 110719 (2022).

17. Campbell, I. K., Bendele, A., Smith, D. A. & Hamilton, J. A. Granulocyte-macrophage colony stimulating factor exacerbates collagen induced arthritis in mice. *Annals of the Rheumatic Diseases* **56**, 364–368 (1997).

18. Bischof, R. J., Zafiropoulos, D., Hamilton, J. A. & Campbell, I. K. Exacerbation of acute inflammatory arthritis by the colony-stimulating factors CSF-1 and granulocyte macrophage (GM)-CSF: evidence of macrophage infiltration and local proliferation. *Clinical and Experimental Immunology* **119**, 361–367 (2001).

11. Appendix Data Chapter 6 | Inflammasome pathway activation in rational vaccine design

11.1 Introduction

11.1.1 Mechanistically informed vaccine adjuvants: insights from a collaborative study

This chapter draws on my second-author publication in *Cell Reports Medicine* (2023), which delineates the molecular mechanisms of action for globally accessible vaccine adjuvants[1]. Here, I present only the data I generated during my DPhil, while discussing these findings in the context of the broader results reported in our collaborative manuscript with the Jenner Institute at the University of Oxford and the Vaccine Formulation Institute (VFI) in Lausanne, Switzerland.

The field of vaccinology is evolving from empirical discoveries to sophisticated, rationally designed products that enhance pathogen-specificity responses. The term ‘adjuvant’ comes from the Latin *adjuvare*, meaning "to help" and refers to substances added to vaccines to boost immunogenicity and improve antigen-specific immune responses.

The discovery of the first adjuvant in 1926, aluminium salts (alum) was serendipitous. Alexander Glenny and colleagues were developing a Diphtheria toxoid vaccine and were using aluminium potassium sulphate as a precipitating agent to purify diphtheria toxoid. Alum-precipitated toxoid elicited robust immune responses *in vivo* compared to toxoid alone and induced higher antibody titres[2]. Despite the empirical observation made in the 1920s, insights into the mechanisms of alum beyond its ‘depot effect’ came much later, with NLRP3 activation and IL-1β production

critical to alum's immunogenicity revealed in 2008[3]. Later in the 20th century lipid-based emulsions were discovered, with the TLR-4 agonist monophosphoryl lipid A (MPL) and QS-21 saponin following.

Adjuvanted vaccines have superior protection in several infectious disease contexts, including malaria[4,5]. In protein-subunit vaccines, simply injecting a foreign protein *in vivo* does not generate a substantial immune reaction or immune memory. An adjuvant is required to stimulate immune activation, drive antigen presentation, and promote durable long-term immune memory.

In the UK childhood vaccine schedule there are eleven vaccines, five of which are protein-subunit vaccines. The remaining six are live-attenuated, conjugate, or inactivated whole-virus. The adjuvants in these scheduled protein-subunit vaccines are still based on early discoveries from the 20th century, alum and AS04 (a combination of aluminium hydroxide and MPL). Hence, understanding the molecular mechanisms of adjuvants may drive a new era of vaccine design.

11.1.2 Global open access vaccine adjuvants

Rational vaccine design represents a paradigm shift from the empirical approaches of the 18th–20th centuries, pioneered by Edward Jenner and Louis Pasteur, to a data-driven, mechanistic strategy enabled by technological revolutions. Currently, 21st century vaccine design is leveraging advances in immunology, structural biology, genomics, and systems vaccinology to optimize pathogenic-specific immune responses.

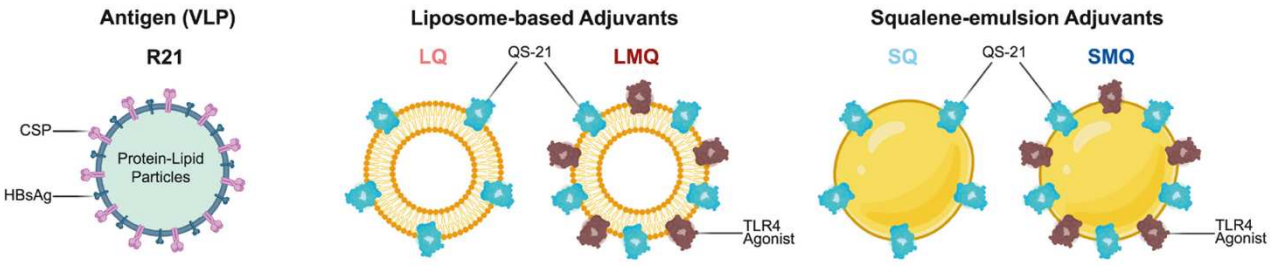

Figure 34 | Schematic of R21 antigen and adjuvants LQ, LMQ, SQ and SMQ. R21 antigen was combined with liposomal (L) or squalene (S) emulsion formulations with saponin QS-21 (Q). These were studied with and without the TL4 agonist 3D-6-acyl-PHAD (M). Figure from Reinke, S. *et al.* (2023)[1].

The VFI is a not-for-profit organization dedicated to advancing vaccine adjuvant and formulation technologies, particularly for global health challenges. Founded in 2012 by Dr. Nicolas Collin, a veterinarian and virologist with experience at the World Health Organization (WHO) and the University of Lausanne, the VFI bridges the gap between academic research and industrial vaccine production. Its mission is to make vaccines accessible to low- and middle-income countries by developing cost-effective, stable formulations and transferring technology to local manufacturers.

To accelerate access to vaccine adjuvants, the VFI have developed a modular approach to vaccine production. They have generated four open access adjuvants: two liposomal (L) and two squalene (S) emulsion-based adjuvants with QS-21 saponin (Q). These are formulations are supplemented with or without the synthetic TLR4 agonist (M). This plug-and-play modular approach yields the following combination of adjuvants: LQ, LMQ, SQ, and SMQ (Figure 34).

11.1.3 Malaria vaccines: novel methods for prevention

As of April 2025, two WHO-recommended malaria vaccines, RTS,S/AS01 (Mosquirix) and R21/Matrix-M, are available for children in areas with moderate to high

malaria transmission, primarily in sub-Saharan Africa targeting *Plasmodium falciparum*. RTS,S, developed by GSK, reduces malaria cases by about 39% with a 4-dose schedule, while R21, from Oxford and the Serum Institute, shows up to 77% efficacy with a 3-dose plus booster regimen. Despite their impact, limited supply, vaccine hesitancy, and the need for complementary measures like bed nets remain challenges.

This study investigated the immune responses elicited by the R21 malaria vaccine when formulated with global open access VFI adjuvants: the liposome based (LQ and LMQ) and emulsion based (SQ and SMQ). In preclinical models, we found two adjuvants with distinct formulations, LMQ and SQ, protect against *Plasmodium falciparum* malaria through different mechanisms. Due to its ability to activate TLR4 and NLRP3, LMQ, which contains TLR ligand MPL-1 and QS-21 saponin, induced Th1 skewed responses *in vivo*. SQ, which does not contain a TLR ligand, just QS-21 saponin caused cell death but no TLR4 or NLRP3 activation and induced Th2 skewed responses *in vivo*. These findings highlight the importance of adjuvant choice in optimizing malaria vaccine performance and inform future vaccine design.

11.2 Aims

Collaborating with Anita Milicic's group at the Jenner Institute, I compared the *in vivo* efficacy of four adjuvants in a malaria model with their *in vitro* innate immune activation. My aims and role in this study were to:

1) Characterise the *in vitro* NLRP3 and cell death responses of human monocyte derived macrophages (HMDMs) to LQ, LMQ, SQ, and SMQ

2) Investigate if R21 antigen augments *in vitro* HMDM responses to LQ, LMQ, SQ, and SMQ

11.3 Results

11.3.1 Protective adjuvants LMQ and SQ trigger different innate immune pathways *in vitro* in HMDMs

Given the stark differences in adjuvant efficacy among the four tested adjuvants and the distinct adaptive immune responses elicited by the two efficacious adjuvants, I sought to elucidate the inflammatory pathways activated in HMDMs *in vitro* to provide a molecular basis for the *in vivo* results.

We isolated peripheral blood mononuclear cells (PBMCs) from healthy human donors at the Oxford Blood Bank, performed CD14+ positive selection to obtain monocytes, and differentiated them into HMDMs over 7 days in complete RPMI supplemented with recombinant human macrophage colony-stimulating factor (rh-M-CSF) (Figure 35a). I then evaluated cell death and NLRP3 inflammasome activation triggered by the adjuvants *in vitro*, assessing NLRP3 dependence using the small-molecule inhibitor MCC950.

The two protective malaria vaccine adjuvants, LMQ and SQ, activated distinct innate immune pathways in HMDMs. LMQ primed and activated the NLRP3 inflammasome, leading to caspase-1 activation and IL-1β release (Figure 35b). LMQ induced the highest levels of caspase-1 activity and IL-1β release among the adjuvants, alongside moderate cell death, as measured by LDH release (Figure 35b,c). Compared to a positive control for NLRP3 activation (4 h 100 ng/mL LPS + 2 h 10 μM nigericin), LMQ was a relatively weak activator (Figure 35b,c). Both caspase-1 activation and IL-1β release by LMQ were NLRP3-dependent, as they were

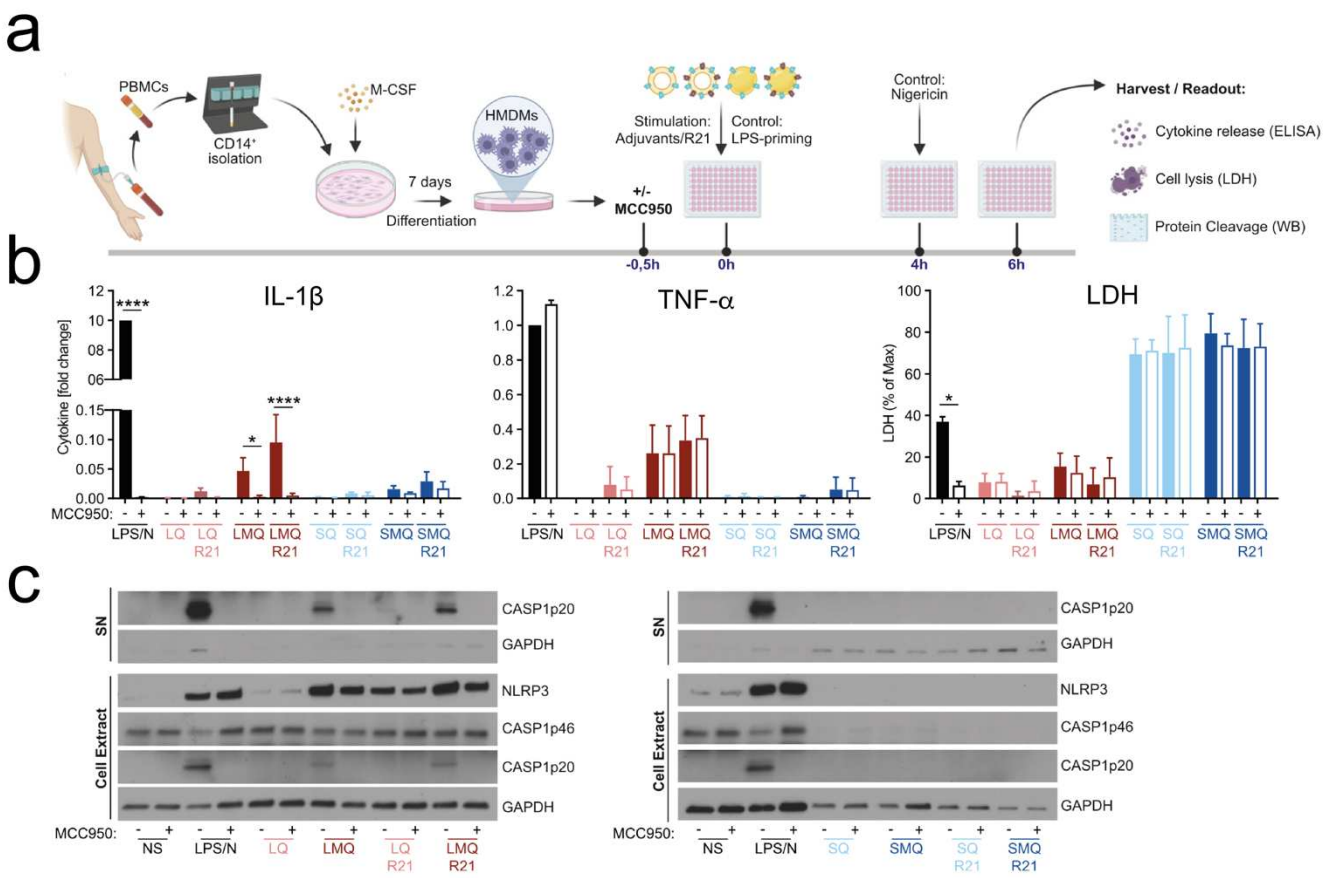

Figure 35 | Protective adjuvants LMQ and SQ in murine malaria model trigger different innate pathways in HMDMs *in vitro.* a) HMDMs were stimulated for 6 h with adjuvants (1:20 dil.) in the presence or absence of R21 antigen (given at 1/5 of mouse dose to preserve the ratio of antigen:adjuvant given *in vivo*), in the presence or absence of NLRP3 inhibitor MCC950 (10 mM) added 0.5 h before the adjuvants. b) IL-1b and TNF-a secretion in supernatants was measured by ELISA. LDH release was measured using a colorimetric assay. LPS/nigericin served as a positive control (100 ng/mL LPS for 6 h with 10 mM nigericin for the last 2 h) (pooled data from three independent experiments/donors for IL-1b and LDH and two independent experiments/donors for TNF-a; cells are stimulated in triplicates; cytokines were normalized to LPS/nigericin control set to 1; cell death/LDH was normalized to maximal cell death lysis control, set to 100%; mean ± SEM are shown). (c) Representative western blots for pro-caspase-1 (p46), cleaved caspase-1 (p20), NLRP3, and GAPDH in cell lysates and supernatants from HMDMs stimulation as described above (representative data from two independent experiments/donors are shown). All statistical analyses were done using two-way ANOVA with Bonferroni's correction for multiple comparisons; *p < 0.05, **p < 0.01, ***p < 0.001, ****p < 0.0001. Figure from Reinke, S. *et al.* (2023)[1].

completely abolished by MCC950 (Figure 35b,c). LMQ also stimulated TNF-α release in HMDMs, which was independent of NLRP3.

In contrast, the other effective adjuvant, SQ, induced high levels of cell death (Figure 35b), confirmed by detecting GAPDH in the supernatant of SQ-treated HMDMs (Figure 35c). However, SQ did not promote caspase-1 activity or IL-1β release. These

results demonstrate that LMQ and SQ trigger distinct innate immune pathways in HMDMs *in vitro*.

Among the adjuvants that failed to provide robust malaria protection, LQ neither activated NLRP3 nor induced cell death (Figure 35b). SMQ triggered cell death comparable to SQ and a small amount of IL-1β release (Figure 35b). Surprisingly, despite containing a TLR4 agonist (M) and effectively inducing cell death, SMQ elicited only weak NLRP3 responses (Figure 35b,c). This was likely due to the stronger cell death response caused by SMQ (compared to LMQ), which prematurely terminated pathway activity and cytokine secretion.

We also investigated the effect of adjuvants in the presence of the R21 antigen to explore potential synergistic effects. The presence of R21 did not enhance the innate immune pathways triggered by any of the four adjuvants (Figure 35b). While IL-1β release from LMQ-treated HMDMs appeared slightly increased with R21, this effect was not statistically significant across multiple donors, and caspase-1 activation (p20 band detection) was not visibly enhanced (Figure 35b,c). Thus, as expected, the addition of antigen did not significantly boost the adjuvants' *in vitro* immunogenicity but likely contributes to antigen-specific responses *in vivo.*

11.4 Discussion

This study revealed that two protective malaria vaccine adjuvants, LMQ and SQ, activate distinct innate immune pathways in HMDMs *in vitro*. LMQ promoted NLRP3 inflammasome activation, resulting in moderate cell death and release of IL-1β and TNF-α. In contrast, SQ induced significant cell death and DAMP release but no cytokine production.

When correlated with our *in vivo* findings, these adjuvants elicited markedly different adaptive immune responses despite comparable efficacy. LMQ skewed responses toward type 1 immunity, while SQ favoured type 2 immunity. Although total antigen-specific IgM, IgG, and IgA levels were similar between LMQ and SQ, IgG subclass profiles differed[1]. R21 antigen alone or with SQ promoted IgG1, associated with Th2 responses. LMQ, however, robustly induced Th1 responses, with higher proportions of IgG2 and IgG3[1].

T-helper cell skewing was assessed by stimulating splenocytes with R21 peptide and measuring IFN-γ and TNF-α double-positive CD4+ T cells via flow cytometry. LMQ induced significantly more IFN-γ+ TNF-α+ CD4+ T cells, and greater IFN-γ was detected in the supernatant of splenocytes from mice vaccinated with LMQ-R21[1]. This Th1 skewing was partially NLRP3-dependent, as double-positive CD4+ T cells and secreted IFN-γ were reduced in *Nlrp3*-deficient mice but not significant. However, the overall antibody profile and IgG subclasses remained unchanged in *Nlrp3*-deficient mice. In contrast, SQ-stimulated splenocytes secreted IL-13, and responses were unaffected by *Nlrp3* deficiency.

Historically, type 2 immunity was considered most protective against *Plasmodium falciparum*, a parasitic infection. These data challenge this notion, demonstrating that efficacious malaria vaccines can achieve protection through diverse immune mechanisms.

11.5 Limitations

These *in vitro* findings have limitations. HMDMs may not fully represent tissue-resident innate immune cells exposed to adjuvants during intramuscular vaccination. While I focused on macrophages as key sentinels and pathogen sensors, our study

did not investigate pathways activated in dendritic cells (DCs), which are critical antigen-presenting cells bridging innate and adaptive immunity. To better understand how these adjuvants drive adaptive immunity and IgG subclass switching, future studies should examine DC activation *in vitro* and *in vivo*.

Additionally, *in vivo* vaccine efficacy in murine models may not directly correlate with clinical protection against *Plasmodium falciparum* malaria in humans. Future research should evaluate these open-access adjuvants in other pathogen-specific models, including bacterial and viral infections, to determine the adaptive immune profiles required for protection against diverse infectious agents.

11.6 Conclusions

Activation of distinct innate immune pathways can yield equally effective protection against malaria. We identified two protective, globally accessible vaccine adjuvants that provide comparable protection to the WHO-recommended R21/Matrix-M vaccine in a murine model. LMQ activates TLR4 and the NLRP3 inflammasome to drive type 1-skewed immunity, while SQ induces cell death and alarmin release to promote type 2-skewed immunity.

11.7 References

1. Reinke, S. *et al.* Emulsion and liposome-based adjuvanted R21 vaccine formulations mediate protection against malaria through distinct immune mechanisms. *Cell Reports Medicine* **4**, 101245 (2023).
2. Parish, H. J. Immunization against Diphtheria with Alum-precipitated Toxoid. *BMJ* **1**, 209–210 (1936).

3. Eisenbarth, S. C., Colegio, O. R., O'Connor, W., Sutterwala, F. S. & Flavell, R. A. Crucial role for the Nalp3 inflammasome in the immunostimulatory properties of aluminium adjuvants. *Nature* **453**, 1122–1126 (2008).
4. Tiono, A. B. *et al.* First field efficacy trial of the ChAd63 MVA ME-TRAP vectored malaria vaccine candidate in 5-17 months old infants and children. *PLoS ONE* **13**, e0208328 (2018).
5. Nielsen, C. M. *et al.* Protein/AS01B vaccination elicits stronger, more Th2-skewed antigen-specific human T follicular helper cell responses than heterologous viral vectors. *Cell Reports Medicine* **2**, 100207 (2021).

12. Concluding Remarks

This thesis has utilized inflammatory arthritis as a model to elucidate the tissue biology of inflammasomes. Through an integrative approach combining publicly available and in-house scRNA-seq of mouse STIA and human RA, bulk RNA sequencing, as well as *in vitro* and *in vivo* models, I investigated the expression patterns of inflammasomes, specifically their localization, timing, and cellular specificity in the synovium during health and disease.

Our findings establish that NLRP3 is the primary inflammasome sensor expressed in the joint, with its expression confined to myeloid cells, particularly inflammatory monocyte-derived macrophages recruited to the synovium during joint inflammation in both mice and humans (Chapter 1). These recruited macrophages, absent in healthy joints, infiltrate during disease and are characterized by expression of CCR2+, the GM-CSF receptor, adhesion molecules, and NLRP3 inflammasome components (Figure 36, Chapter 1). Spatial transcriptomic analysis suggests these inflammasome-enriched recruited macrophages localise to the lining layer, adjacent to lining layer fibroblasts which have a heightened IL-1 response gene signature in RA (Chapter 1). I observed that *Nlrp3* expression at the transcript level increases during the initiation of inflammatory arthritis, peaks with disease severity, and declines during remission, though levels remain elevated compared to healthy joints. Remission is further marked by increased expression of negative regulators of NLRP3, including *Mertk*, *Socs3*, and *Il10* (Chapter 1).

In contrast, synovial tissue-resident macrophages (MerTK+ TREM2+) do not express detectable levels of *Nlrp3* at any disease stage. I hypothesized that apoptotic cell turnover in the steady state may suppress NLRP3 expression and activity of

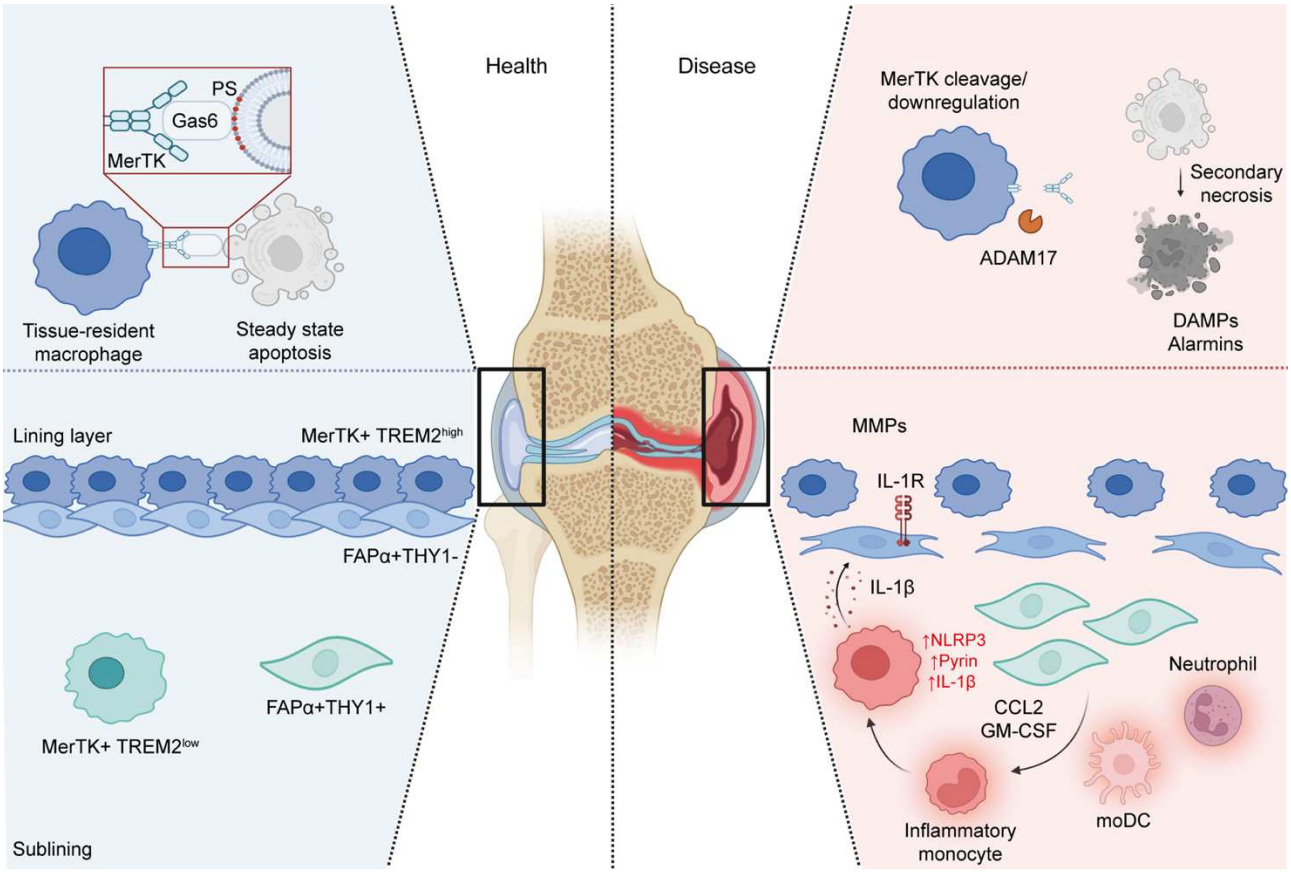

Figure 36 | Inflammasome expression is low in tissue-Resident macrophages in health but elevated in inflammatory arthritis due to recruited monocyte-derived macrophages. In healthy joints, tissue-resident macrophages in the synovial lining and sublining maintain homeostasis through efferocytosis, a process mediated by receptors including MerTK. During steady-state conditions, these macrophages efficiently clear apoptotic cells, remaining quiescent and preventing inflammation. The synovial lining is primarily composed of MerTK+ TREM2^{high} macrophages, which form a protective barrier shielding the intra-articular space. Interstitial MerTK+ TREM2low (CSF1R+) macrophages support the maintenance of this lining layer as needed. In inflammatory arthritis, disruptions in this balance lead to disease. Loss of MerTK expression is a key predictor of disease flares. Impaired efferocytosis results in apoptotic cells undergoing secondary necrosis, releasing damage-associated molecular patterns (DAMPs) and alarmins that trigger tissue inflammation and damage. This is compounded by the breakdown of the synovial lining layer and the expansion of sublining fibroblasts, which produce pro-inflammatory cytokines and chemokines. These signals drive emergency myelopoiesis, recruiting inflammatory monocytes into the tissue. These monocytes differentiate into macrophages with elevated expression of NLRP3, pyrin, and IL-1β, localizing to the compromised lining layer. Spatial transcriptomic analysis reveals that lining layer fibroblasts, which express IL-1R, exhibit the strongest IL-1 response gene signature in the synovium.

macrophages in tissue, potentially via IL-10 induction (Figure 36, Chapter 4). Our *in vitro* studies demonstrated that blockade of TAM receptors, which are involved in apoptotic cell recognition, increases NLRP3 activity, while recognition of apoptotic

neutrophils via phosphatidylserine reduces NLRP3 activity (Chapter 4). These findings suggest a regulatory mechanism that warrants further exploration, particularly the direct linkage between MerTK-mediated apoptotic cell recognition and IL-10 synthesis.

I have also demonstrated that GM-CSF BMDMs upregulate pro-IL-1β in response to sterile TNF-α priming and release mature IL-1β in an NLRP3-dependent manner when a second signal is provided (Chapter 2). Notably, GM-CSF BMDMs exhibit heightened NLRP3 pathway activity within 30 minutes of priming, despite no differences in NLRP3 sensor or caspase-1 levels. Compared to M-CSF BMDMs, GM-CSF BMDMs produce significantly more TNF-α and IL-1β, with higher steady-state *Il1b* transcript levels, while M-CSF BMDMs exhibit higher *Il10* transcripts and rapid IL-10 production following LPS exposure (Chapter 2). In the AIA model, where NLRP3 deficiency is protective, GM-CSF monoclonal antibody blockade reduces pro-IL-1β, neutrophil recruitment, and pain, with a linear correlation observed between pain, neutrophil recruitment, and pro-IL-1β levels in the synovium (Chapter 3).

In summary, this thesis demonstrates that inflammasomes, particularly NLRP3, are lowly expressed in tissue-resident macrophages within healthy joints and are predominantly enriched in GM-CSFR+ inflammatory macrophages recruited during disease. Our findings underscore the critical role of GM-CSF and NLRP3 in driving inflammatory arthritis, highlight their potential as therapeutic targets, and suggest seronegative RA as therapeutic area where inflammasome blockade may be efficacious (Chapter 5). By delineating the cellular and molecular dynamics of NLRP3 in the synovium, this work contributes to the foundation for developing targeted therapies to alleviate the burden of inflammatory joint diseases.

13. Appendix

13.1 List of Figures

Figure 36 | Inflammasome expression is low in tissue-Resident macrophages in health but elevated in inflammatory arthritis due to recruited monocyte-derived macrophages.

13.2 List of Publications

- Reinke, S., Pantazi, E., **Chappell, GR.**, … Milicic, A., (2023) Emulsion and liposome-based adjuvanted R21 vaccine formulations mediate protection against malaria through distinct immune mechanisms. Cell Reports Medicine.
- Yow, SJ., … **Chappell, GR**… Bezbradica, JS., Boucher, D., Chen, KW. Threat assessment shapes neutrophil cell fate upon inflammasome activation. Manuscript prepared for submission.
- **Chappell, GR.**, … Bezbradica, JS. Tissue-recruited inflammatory GM-CSFR+ macrophages drive inflammasome activity and pain in arthritis. In revision.

13.3 List of Presentations and Awards

- 2024 Abstract selected for oral presentation: Oxford Immunology Symposium (Oxford, UK)
- 2023 Abstract selected for oral presentation: European Network of Immunology Institutes School (Sardinia, IT)
- 2023 Poster Award: Kennedy Trust Networking Event (Manchester, UK)
- 2022 Poster Award: Ox-Berlin Summer School (Berlin, GER)

“You may not find what you were looking for, but you find something else equally important.”

-Robert Noyce

“To live is to risk it all, otherwise you’re just an inert chunk of randomly assembled molecules drifting wherever the universe blows you”

-Rick Sanchez

“Nothing in life is to be feared, it is only to be understood. Now is the time to understand more so that we may fear less.”

-Marie Curie

“The hardest thing to do is to be true to yourself, especially when everybody is watching.”

-Dave Chappelle

“And here, poor fool! with all my lore, I stand no wiser than before.”

-Johann Wolfgang von Goethe

“Last but not least, I wanna thank me
I wanna thank me for believing in me
I wanna thank me for doing all this hard work
I wanna thank me for having no days off
I wanna thank me for, for never quitting
I wanna thank me for always being a giver
And tryna give more than I receive
I wanna thank me for tryna do more right than wrong
I wanna thank me for just being me at all times
Snoop Dogg, you a bad motherfucker”

-Snoop Dogg